Investigating the Role of the 3'UTR of Claudin-5 and Circadian Rhythms at Tight Junctions in the Blood-Brain Barrier

A thesis submitted to The University of Dublin for the degree of Master of Science 2020

By Nirmala Ramanath

Supervisor: Dr. Matthew Campbell

Department of Genetics

Trinity College Dublin

Trinity College Dublin
Coláiste na Tríonóide, Baile Átha Cliath
The University of Dublin

Declaration:

I declare that this thesis has not been submitted as an exercise for a degree at this or any other university and it is entirely my own work.

I agree to deposit this thesis in the University's open access institutional repository or allow the library to do so on my behalf, subject to Irish Copyright Legislation and Trinity College Library conditions of use and acknowledgement.

Nirmala Ramanath

September 2020

Summary:

The blood-brain barrier (BBB) is comprised of the vasculature surrounding the central nervous system (CNS), and most importantly consists of endothelial cells. These brain endothelial cells have unique properties that protect the neurons which are integral for CNS function. These specialized endothelial cell functions allow for modulation of the flow of solutes from the bloodstream to the CNS, and include reduced flow across endothelial cells mediated via transporters (transcellular pathway), and reduced flow between cells (paracellular transport), which is mediated by specialized tight junctions (TJs). While this is beneficial for protecting the neurons from harmful blood-borne pathogens, this also poses a problem for drug delivery across the barrier, as neurotherapeutics which are large and hydrophilic in nature are not able to pass through the TJs through paracellular transport. Other cell types such as pericytes, microglia, astrocytes, etc. form crosstalk interactions with the endothelial cells at the BBB, creating an overarching neurovascular unit that maintains proper BBB function. However, the focus of this investigation is on endothelial cells, with respect to tight junctions and their associated mediation of BBB integrity. As the BBB is dynamic, variations in TJ expression mechanisms can affect BBB permeability through various regulatory pathways which we are interested in studying in this investigation, namely circadian mediated regulation, and 3'UTR mediated post-transcriptional and post-translational regulation of the key TJ component claudin-5.

It was previously shown by Hudson *et al.,* 2019, that claudin-5 (which is the most enriched tight junction component) is associated with Bmal1 (a circadian clock component), and cycles in tissues in a circadian manner, with other tight junction proteins such as ZO-1 and occludin cycling in a temporal manner. Serum shock studies as shown by Balsalobre *et al.,* 1998 can recapitulate a circadian rhythm in cell lines, and these experiments were done for a short period of time in Hudson *et al.,* 2019. The goal of this investigation was to model the circadian rhythm in endothelial cell lines for an extended period of time (72 hours), and characterize protein and transcript expression patterns, as this could have an impact on BBB integrity. Temporal changes were observed for all TJ components and clock components analyzed (claudin-5, occludin, ZO-1, Bmal1). In the future, changes in BBB permeability should be looked at, with particular focus on points when claudin-5 expression is high and low. These changes can be taken advantage of, and drug delivery could be designed for administration at points when BBB permeability is higher, as revealed by TJ protein expression patterns.

The 3'UTR is a non-coding region on the mRNA transcript that has been known to mediate RNA-protein interactions via *cis* elements, about which not much is known. This has an effect on post-transcriptional and post-translational modifications for the overall protein. It was found that a 3'UTR single nucleotide polymorphisms (SNP) on claudin-5, rs10314, was associated with schizophrenia in certain populations, and a study by Greene *et al.,* 2018 showed that rs10314 results in a 50% downregulation of claudin-5, and up to 75% of claudin-5 is downregulated in patients with both the 22q11 deletion syndrome as well as presence of this SNP. This has a significant effect on tight junction formation and BBB integrity. Our study focused on expanding these findings, and assessing the effect that various other SNPs in the 3'UTR of claudin-5 have on its overall expression. Various plasmid constructs were made using site-directed mutagenesis to express various SNPs in the 3'UTR, and were assayed for claudin-5 expression levels. Several 3'UTR claudin-5 SNPs resulted in abrogated protein expression, which indicates that the 3'UTR plays a significant role in the overall protein structure and function, and should be explored further, particularly with relation to the associated RNA-binding protein (RBP) interactions, that impact post-transcriptional and post-translational outcomes. Overall, the results are consistent with the general findings in the field that suggest that tight junction expression at the BBB is not static, but rather constantly changing through various regulatory mechanisms in order to maintain homeostasis and protect the CNS. As BBB breakdown is a hallmark of neurological diseases, it is important to understand these phenomena.

Acknowledgements:

I would like to thank my supervisor Dr. Matthew Campbell, for his tremendous support throughout my research, and for his guidance regarding the direction of this project. My deepest gratitude to all of the members in the lab for your advice, guidance, and support—Dr. Yosuke Hashimoto, Conor Delaney, Dr. Chris Greene, and Dr. Natalie Hudson, Nicole Hanley, and Claire O'Connor.

Specifically, I'd like to thank Nicole Hanley and for your friendship and encouragement and moral support, and to Claire O'Connor with whom I joined the lab together with, for your great support.

Thanks to the Irish Research Council for supporting my project.

Finally, thank you to my parents.

Table of Contents:

CHAPTER 1: Introduction

1.1. Blood-brain Barrier and the Neurovascular Unit:

The central nervous system (CNS) is comprised of the brain and spinal cord and contains neurons, which are integral to carrying out key functions of regulating metabolism, cognition, and coordinating function of peripheral organs (Keaney and Campbell, 2015). The brain accounts for about 20% of the body's total energy and O_2 consumption, and in children can be as high as 50%, despite constituting only 2% of overall body mass (Clark and Sokoloff, 1999; Kennedy and Sokoloff, 1957). In order to protect these critical functions, the blood-brain barrier (BBB) which is situated along the blood vessels of the CNS, forms a tightly regulated and protective barrier with unique properties in order to maintain a balanced microenvironment; essentially, the BBB separates the brain from harmful substances at the microvasculature surrounding CNS (Daneman and Prat, 2015). It is important that a homeostatic environment is maintained that is amenable to the function of the neuron, which is a non-regenerating terminally differentiated cell, and requires regulated electrophysiological and chemical signals to function proficiently (Nowakowski, 2006; Greene and Campbell, 2016).

Owing to this need for protection, the BBB associated vasculature is structurally and functionally distinct from the vasculature of the rest of the body (Abbot *et al*., 2010; Engelhardt and Liebner, 2014). The BBB is important in protecting neural tissue from damaging pathogens, anaphylatoxins, and immune cells that circulate in the blood, and regulating exchange of nutrients between the blood and the brain (Abbot *et al*., 2010; Kealy *et al*., 2018); it has been generally assessed that each neuron is intimately linked with its own capillary, indicating the close relationship between the blood-supply and CNS function (Begley and Brightman, 2003; Zlokovic, 2005; Cipolla, 2009).

Endothelial cells in the BBB have evolved specialized properties, compared to that of endothelial cells in other tissues, in order to help maintain homeostasis within the CNS. These specializations include an intricate network of tight junction proteins, which comprise the paracellular pathway between adjacent cells and limit the flow of material (Yang *et al*., 2017; Kealy *et al.*, 2018); TEER measurements first introduced by Crone and Christensen (1981) as a parameter to assess integrity of the BBB, can go as high as 5900 Ohm*cm^2 *in vivo* for tight junctions in endothelial cells of the BBB, which is often higher than what can currently be replicated *in vitro* (Srinivasan *et al*., 2015; Butt *et al.,* 1990). As the paracellular route is highly resistant to entry of most molecules, requiring that they enter the cells through the transcellular route, there are specialized proteins that regulate transcytosis at the BBB on the luminal and abluminal membranes through adsorptive mediated vesicular transport—this occurs at low

rates to limit most large hydrophilic molecules crossing the BBB (Ayloo and Gu, 2019; Abbot *et al*., 2010; Hervé *et al.*, 2008; Pardridge *et al.*, 1990); there are other transcytotic pathways for regulated entry of larger molecular weight peptides and molecules across cells such as receptor mediated and carrier mediated transport (Jones and Shusta, 2007; Abbot *et al.,* 2010) which has implications for use in drug delivery across the BBB; other specializations of brain endothelial cells include increased presence of functioning mitochondria to enable the higher energy requirement of the brain's metabolism (Kim *et al.*, 2017; Oldendorf *et al.*, 1977), and finally absence of fenestrations, or pores that allow exchange of molecules between blood and tissue among endothelial cells (Coomber and Stewart, 1985; Kealy *et al.*, 2018). It is due to these aforementioned unique properties that brain endothelial cells (BEC) in the BBB are the primary focus of our study due to their involvement in several mechanistic and regulatory process of homeostasis at the BBB. Understanding the physiology of BECs and tight junctions is important for furthering research in the BBB field.

Apart from the endothelial cells at the BBB, other cells and components also participate in crosstalk with the BBB, and surround and interact with the BBB vasculature, such as pericytes, and astrocytic end-feet, neurons, microglia, interneurons, and the non-cellular basement membrane, all of which forms the neurovascular unit (NVU) (McConnell *et al.*, 2017). The NVU pictured in Fig. 1.1.1, along with a depiction of tight junctions associated with BBB endothelial cells. As these various components interact as a unit to protect the CNS, dysfunction in any one unit can leads to adverse physiological consequences. Pericytes normally contribute to stability of microvessels, and release signals that promote BEC differentiation and quiescence (Zlokovic, 2008; von Tell *et al.*, 2006; Armulik *et al.*, 2005). Astrocytes sheath either neuronal processes or blood vessels (Abbot *et al.*, 2006), and certainly provide a cellular link between the two, thus enabling astrocytes to provide signals that regulate blood-flow in response to neuronal activity (Attwell *et al.*, 2010; Gordon *et al.*, 2011; Daneman and Prat, 2015). These features highlight the fact that there are many cellular components that comprise the NVU, and that brain endothelial cells in the BBB have unique features that are interesting to study that protect the CNS from the external environment.

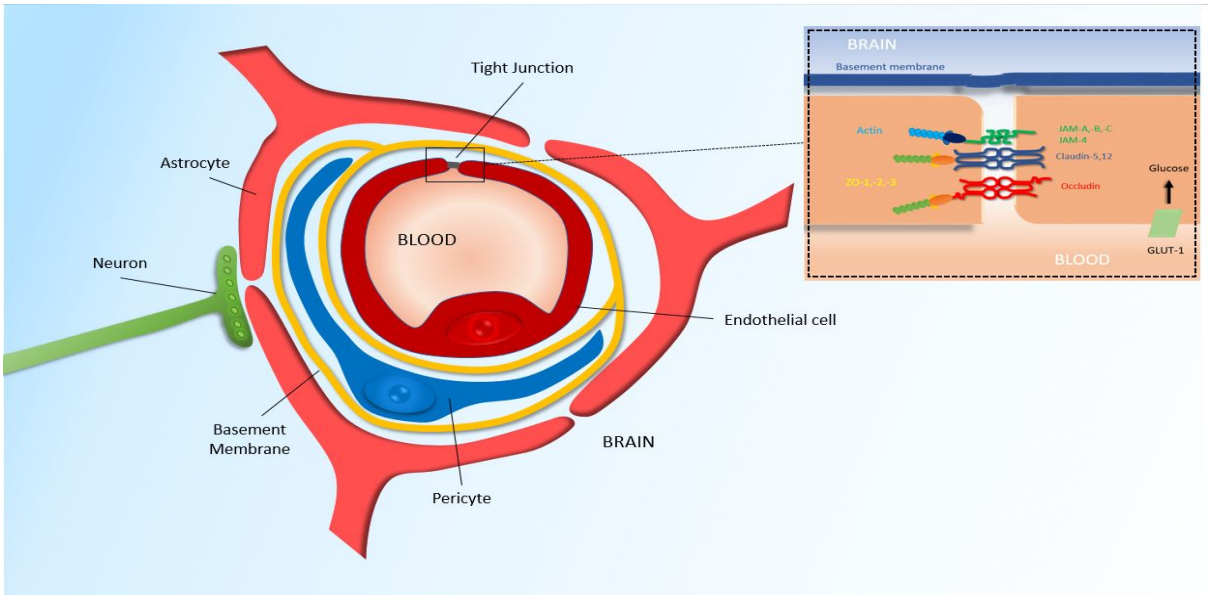

Figure 1.1.1. Endothelial cells, pericytes, astrocytes, microglia, interneurons, and neurons and non-cellular basement membrane are various components that interact closely to form the neurovascular unit. Inset: Tight junction components create a paracellular barrier between adjacent endothelial cells, separating the blood and brain microenvironment. (Image and description taken from O'Connor *et al.*, 2019).

1.1.1 Brief History of BBB Research:

Much work has been done to contribute to our current understanding of the dynamic nature and components of the BBB as described previously. In 1900, Lewandowsky conducted an experiment where the pharmacological effect of bile acids or ferrocyanide, when intravenously administered, was absent in the CNS, and it was suggested that this could be due to a mechanical membrane separating the blood and the brain, which would later be known as the BBB (Lewandowsky, 1900; Zlokovic, 2008). As a pharmacological effect was observed when compounds were directly injected into the brain, Lewandowsky postulated that the cerebral capillary walls may have properties that prevented the passage of certain compounds (Lewandowsky, 1900; Liddelow, 2011). This phenomenon involving the concept of a mechanical barrier was confirmed by Goldmann in 1909, when trypan blue dye administered intravenously into the blood stream failed to stain the brain and spinal cord tissue (Goldmann, 1909; Zlokovic, 2008). In 1913, Goldmann conducted an experiment, injecting trypan blue dye directly into the cerebrospinal fluid, which did produce staining in the brain and spinal cord, which were the seminal experiments indicating the presence of a barrier between the blood and the CNS (Goldmann, 1913; Zlokovic, 2008). At the time, it was thought that this barrier was impenetrable, but later physiological studies in the 1950s-60s have since shown that the barrier is highly regulated and semi-permeable (Zlokovic, 2008). Electron microscopy studies involving ferritin and horseradish peroxidase contributed to the knowledge that the site of BBB permeability and regulation is highly localized to the tight junctions between adjacent brain

endothelial cells (Reese and Karnovsky, 1967; Brightman and Reese, 1969; Zlokovic, 2008). Also, the seminal quail-chick transplantation experiment by Stewart and Wiley (1981) demonstrated that the specialized endothelial cell properties of brain endothelial cells are not intrinsic, and rather develop as a result of their neural environment, highlighting the importance of NVU crosstalk between the BBB endothelial cells, and that it is a dynamic environment, and not static in nature as previously thought in the early days of BBB research. The focus of this research will highlight the importance of these specialized tight junctions and their physiology.

1.2 Junctional Complexes in BBB Endothelial Cells:

Junctional complexes such as adherens junctions, and tight junctions, exist between endothelial cells that contain the aforementioned specialized properties unique to the BBB.

1.2.1 Adherens Junctions:

Adherens junctions are present in endothelial cells of all tissue types, and not just at the BBB. They are abluminal to tight junctions and are comprised of VE-cadherin (vascular endothelial cadherin) dimers that bind to the actin-cytoskeleton via catenins and are able to link cells together and mediate cell contacts (Blanchette and Daneman, 2015; Wolburg and Lippoldt, 2002). Their entire comprehensive functions have not yet been elucidated, however it is believed that adherens junctions are involved in maintaining cell polarity, stability, and responding to stimuli and promoting endothelial cell survival through interactions with the actin cytoskeleton (Kealy *et al.*, 2018; Bazzoni and Dejana, 2004). Much of the adherens junctions physiology and expression is mediated through cadherins (Kowalczyk and Nanes, 2012). Cadherins homotypically interact to form dimers when Ca^{2+} is present, and much of the functions of these junctions like adhesion are dependent on presence of Ca^{2+}, and lack of this metabolic component can lead to a reduction in cell permeability, cell proliferation, and migration (Chen and Liu, 2012; Cook *et al.*, 2008). Upregulation of ß-catenin it thought to be important for the maintenance of tight junction protein assembly and barrier function (Vorbrodt *et al.*, 2008; Chen and Liu, 2012).

1.2.2 Tight Junctions and Key Proteins (Claudins, Occludin, ZOs, etc.):

Tight junctions are the core interest of a lot of current research in the BBB field. Tight junctions are cited in research more often as they contribute to a higher TEER value, resulting in more electrically resistant protein complexes which contribute increased barrier integrity, and a lower rate of paracellular diffusion (Blanchette and Daneman, 2015). Tight junctions form zones of association between close cell-cell contacts that are joined and form strands that

seal off the intercellular space at these regions (Anderson and Van Itallie, 2009); the structure of these TJs viewed through electron microscopy, in combination with physiological studies suggest that TJs constitute a barrier that regulates passage of solutes through size and charge selectivity and can restrict flow across the barrier (Simionescu *et al.*, 1975; Furuse, 2010; Tsukita *et al.*, 2001). Understanding the physiology of the tight junctions is important for furthering our understanding of the BBB and the unique properties of its endothelial cells. A schematic of tight junctions is shown in Fig 1.1.1.

So far, 27 members of the claudin family of proteins have been identified (Mineta *et al.*, 2011). Claudins form a major component of tight junctions. They are all homologous, as they are integral proteins that have four transmembrane helical domains (Morita *et al.*, 1999), but differ in the lengths of their N and C terminus, and also have two extracellular loops, with extracellular loop 1 having the most conserved sites (Heinemann and Schuetz, 2019; Suzuki *et al.*, 2017). Mutations in non-conserved residues in extracellular loop 2 resulted in improper formation of claudin-5 and claudin-3 into tight junctions (Rossa *et al.*, 2014). The C terminus also has a PDZ motif which allows for claudins to bind to scaffolding proteins (Krause et al, 2009; Greene and Campbell, 2016). Claudins interact through homotypic and heterotypic interactions via their extracellular loops in order to form tight junctions (Furuse *et al.*, 1999; Krause *et al.*, 2008; Piontek *et al.*, 2008; Rossa *et al.*, 2014), and claudins are also integral in the initial strand formations that make up tight junctions and their complex meshwork formation (Gonschior *et al.*, 2020; Furuse, *et al.*, 1998). Claudin-5, claudin-3 and claudin-12 are present at the BBB (Daneman *et al.*, 2010; Winger *et al.*, 2014; Dias *et al.*, 2019; Ohtsuki *et al.*, 2007). A number of key studies involving genetic knock-out and knock-in genetic and *in vitro* models respectively has highlighted the importance of claudin-5 as a primary area of focus. For example, claudin-5 knockout mice have shown to have an impaired BBB, that is permeable to molecules up to 800 Da in size, which is much larger than what would typically be able to enter the BBB, and that complete homozygous knockout of claudin-5 is lethal and that mice die within hours (Nitta *et al.*, 2003). Over-expression of claudin-5 in cultured brain endothelial cells increases paracellular tightness of TJs and reduces BBB permeability (Ohtsuki *et al.*, 2007). In comparison, claudin-12 is not required for BBB tight junction function (Dias *et al.*, 2019). Claudin-5 is the dominant and most highly expressed protein at tight junctions in endothelial cells (Ohtsuki *et al.*, 2007). These results highlight the importance of claudin-5 and its integral role in maintaining the proper function of tight junctions at the BBB, and regulating barrier permeability, and why it is an important topic of study in the field in general and certainly in this study.

Occludin is also an integral membrane protein, and like claudin-5, has four membrane spanning domains and two extracellular loops (Hartsock and Nelson, 2008); it was the first identified integral protein to localize at tight junctions and was discovered in novel experiments using avian sourced membrane preparations by the Tsukita group (Furuse *et al.*, 1993; Schneeberger and Lynch, 2004). Occludin localized to tight junctions (Hirase *et al.*, 1997), but transfection of occludin cDNA into insect cells only induced formation of multilamellar bodies, but did not result in formation of formal tight junction strands (Furuse *et al.*, 1996; Schneeberger and Lynch, 2004). A deletion lacking the N terminus and extracellular domain of occludin negatively impacts the integrity of tight junctions (Bamforth *et al.*, 1999; Zlokovic, 2008). In another experiment, occludin was knocked out of embryonic stem cells, which resulted in differentiation into polarized epithelial cells that were impermeable to a low molecular weight tracer molecule and also freeze-fracture images showed the presence of tight junction networks, indicating that occludin, though present at TJs, is not integral for TJ formation (Saitou *et al.*, 1998; Schneeberger and Lynch, 2004). However, in *in vivo* studies, occludin knockout mice still form tight junctions, but have an abnormal phenotype involving post-natal growth retardation, brain calcification, thinning of compact bone, testicular atrophy, inflammation, and other complex phenotypes which suggest occludin could have a role in other pathways (Saitou *et al.*, 2000; Chiba *et al.*, 2008; Greene and Campbell, 2016). Therefore, the role of claudin-5 is heavily emphasized over other TJ components with respect to TJ formation and maintenance. Occludin deficient mice result in downregulation of MAPK and Akt signaling pathways, as well as several other studies indicate that occludin may be involved in mediating signaling pathways at tight junctions (Chiba *et al.*, 2008; Murata *et al.*, 2005). Occludin also undergoes alternative splicing resulting in several structural polymorphisms, which could potentially be a reason why occludin has various effects in different pathways (Cummins, 2012; Heinemann and Schuetz, 2019). Tricellulin is another protein that co-localized with occludin at tight junctions in epithelial and endothelial tight junctions (Cummins, 2012; Steed *et al,.* 2009).

Scaffolding proteins such as zonula occludins proteins (ZO-1, ZO-2, and ZO-3) are also present in tight junctions (Hartsock and Nelson, 2008) and are members of the membrane-associated guanylate-kinase (MAGUK) protein family (Anderson *et al.*, 1995). Integral membrane proteins at the TJs are linked to the actin cytoskeleton via ZO proteins as ZO proteins interact with claudins, occludin and many others (Bauer *et al.*, 2010; Zlokovic, 2008; Hawkins and Davis, 2005; Greene and Campbell, 2016). ZO-1 is important for barrier formation in primary endothelial cells, and ZO-1 depletion leads to tight junction disruption and redistribution of active myosin II from junctions to stress fibers, and impaired tension on VE-cadherin junctions (Tornavaca *et al.*, 2015). As ZO proteins belong to the MAGUK family

of proteins, they have PDZ domains, SH3, and guanylate kinase homologous domains (Umeda *et al.*, 2006; Hartsock and Nelson, 2008; Fanning *et al.*, 2007). The PDZ domain of ZO-1 has been shown to interact with the carboxyl terminus of claudins and are recruited at TJs (Itoh *et al.*, 1999). ZO-1 knockout mice result in an embryonic lethal phenotype that caused defective vascular development in the yolk sac, and improper localization of endothelial junctional molecules (Katsuno *et al.*, 2008). In ZO-1 knockout/ZO-2 knockdown cell line, restoration of ZO-1 or ZO-2 restored claudin localization to TJs (Umeda *et al.*, 2006; Hartsock and Nelson, 2008). This protein is highly relevant to our understanding of physiology at the BBB, and is pertinent to our interest in the claudins, particularly claudin-5.

Finally, other proteins are also present at tight junctions in the BBB such as junctional adhesion molecules (JAMs) like JAM-A which is a member of the immunoglobulin supergene family (Zlokovic, 2008; Bazzoni *et al.*, 2005). It has been suggested that altered JAM-A expression can affect the integrity of tight junctions and may affect leukocyte trafficking (Padden *et al.*, 2007). Essentially, evidence suggests that alteration of endothelial TJ component expression can affect overall BBB integrity and permeability (Luissint *et al.*, 2012).

1.3 BBB Dysfunction and Disease in CNS with Respect to Tight Junctions

BBB dysfunction has been shown to be a hallmark of many neurological diseases (Sweeney *et al.,* 2019). A common phenomenon of these various disease pathologies involves breakdown of the BBB at tight junctions, which is why TJs and protein complexes in these regions are of huge interest in furthering BBB research. For example, in Alzheimer's Disease, deficiencies in the GLUT1 transporter reduce glucose transport into the brain, which requires a large energy input to function, and when modelled in *Glut1*+/- mice results in loss of tight junctions and loss of neurons (Winkler *et al.*, 2015; Sweeney *et al.*, 2019). In Huntington's Disease, histological analysis of brain tissues reveals decreased levels of endothelial tight junction proteins claudin-5 and occludin (Drouin-Ouellet *et al.*, 2015; Sweeney *et al.*, 2019). In Multiple Sclerosis, tight junction associated protein ZO-1 was examined in relation to BBB leakage, and it was found that disruption of TJs contributes to BBB leakage and disease pathogenesis (Kirk *et al.*, 2003). In traumatic brain injuries (TBI), tissue damage in rats leads to injury of cerebral blood vessels, and impacts BBB integrity and causes a biphasic opening of the barrier (Başkaya *et al.*, 1997), and a study done in mice showed changes in BBB permeability to small and large molecules after TBI (Habgood *et al,.* 2007). Abnormal BBB integrity in schizophrenia has also been reported, as elevated S100ß levels are present in the blood, which is indicative of a disrupted BBB (Najjar *et al.*, 2013; Najjar *et al.*, 2017). Also, studies have shown that age related disruption in claudin-5 distribution results in a constitutive loss in barrier integrity, which has been suggested to be caused by a loss of TJ proteins in

endothelial junctions (Bake *et al.*, 2009). This atypical physiology with respect to tight junctions is a key area of research interest, as abnormal TJs clearly are implicated in several disease pathologies, as is a disruption of BBB homeostasis. Understanding the role of BBB dysfunction with respect to its breakdown at tight junctions is important.

1.4 Role of Transcellular and Paracellular Transport in Drug Delivery Across the BBB

It has previously been discussed that due to the properties of transcellular and paracellular transport at the BBB that are designed to maintain homeostasis for CNS function (Pardridge, 2005; Hersh *et al.*, 2016), permeability across the BBB is limited to small, electrically charged, lipophilic molecules that are generally less than 500 Da in size, through diffusion across paracellular pathways comprised of tight junctions (Pardridge, 2012). Larger, less lipophilic molecules enter the barrier through transcellular pathways described in section 1.1, however this is still not amenable for passage of many therapeutics drugs which tend to be large and hydrophilic, as 100% of large therapeutics and 98% of small therapeutic drugs are not able to cross the BBB (Pardridge, 2005). This is important for our understanding, as we study BBB dysfunction in disease, and also aim to deliver therapies to treat these diseases. It has been established in previous sections that tight junctions are often more permeable in disease conditions, and this can be taken advantage of for delivery of therapeutics to the CNS.

1.4.1 Select Methods of Drug Delivery Across the BBB

Peptidomimetics, or "peptide mimics" refer to synthetic peptides that mimic natural peptides and can be designed to target key proteins of interest, and can result in degradation or altered function of the target (Vagner *et al.*, 2008). To deliver therapeutics across the BBB in endothelial cells, tight junctions would be of imminent interest to target with peptidomimetics and modulate BBB opening. C1C2 is a peptide that targets the C-terminus of extracellular loop 1 of claudin-1, and when administered at >100μM concentration, results in redistribution of claudins and occludin from junctions to the cytosol, and increased permeability of the BBB to molecules of various sizes (Staat *et al.*, 2015). Similarly, peptidomimetic C5C2 targeting the extracellular loop of claudin-5, after administration resulted in redistribution of claudin-5 to the cytosol from tight junctions, and increased permeability of the BBB (Dithmer *et al.*, 2017). RNAi is another method which can aid in drug delivery and temporarily open the BBB, as siRNA mediated targeting of claudin-5 at endothelial tight junctions have shown transient, increased permeability of the BBB in mice of molecules up to 742 Da (Campbell *et al.*, 2008). Focused ultrasound is another method of transient opening of the BBB through targeted sonication in certain brain regions, that increases permeability of molecules that normally cannot pass through the barrier, which can occur within minutes of treatment (Wang *et al.*, 2009).

While the aforementioned techniques can be used to manipulate TJ protein expression, and aid drug delivery through paracellular pathways, molecular trojan horse (MTH) methods of drug delivery tend to use endogenous transport mechanisms in the BBB that can deliver larger drugs through transcellular pathways (Pardridge, 2006). MTH methods can allow for uptake of ligands such as engineered antibodies like human insulin receptor monoclonal antibody (HIRMAb) or OX-26 which can be fused to therapeutics, and delivered to the brain through receptor-mediated transcytosis using the transferrin receptor or insulin receptor respectively, on endothelial cells (Pardridge, 2012; Chen and Liu, 2012).

Finally, viral vectors such as lentivirus, herpes simplex virus, adenovirus, and adeno-associated virus (AAV) vectors can naturally transduce cells with nucleic acids, and can be engineered to deliver therapeutics of choice and have a high transduction efficiency, however some forms of viral vectors can have an adverse health outcome on patients in clinical trials (Dong, 2018). AAV therapies are still being tested to determine how best to target tight junction proteins and modulate BBB integrity, but the AAV9 serotype is revealed to be more effective at crossing the BBB (Merkel *et al.*, 2016). The goal is to develop clinical therapies that deliver therapeutics through targeted manipulation of components of the BBB, particularly tight junction proteins (Bors and Erdő, 2019).

1.5 Circadian Rhythms and the BBB

The role of the sleep-wake cycle and the effect that it has on BBB physiology is critical for our research interests, and forms the basis of our initial experiments. Chronic sleep restriction (CSR) is a common phenomenon in modern life, associated with a number of lifestyle changes and behaviours such as longer commute times, work hours and distractions, and has adverse effects on health outcomes and can trigger mortality through cardiovascular disease, depression, diabetes, etc. (He *et al.*, 2014; Krueger and Friedman, 2009). Studies have shown that CSR modelled in C57 mice using artificial light cycles, result in decreased tight junction protein expression of key components like claudin-5, occludin, and ZO-2, downregulated glucose transporters in cerebral microvessels at the BBB as well as decreased metabolite uptake by the brain, and increased permeability of the BBB to sodium fluorescein and biotin tracer molecules (He *et al.*, 2014). Promisingly, it was found that 24 hour sleep recovery after 6 days of sleep restriction resulted in a return of paracellular permeability at the BBB to baseline values (He *et al.*, 2014). The expression of claudin-5 and actin also decreased after CSR, and is found to impact inter-endothelial tight junctions and BBB permeability in the hippocampus (Hurtado-Alvarado *et al,.* 2017). This is a critical public health issue, and is an important aspect of studying BBB physiology with respect to tight junctions.

While sleep-wake cycles can be irregular and alter BBB physiology, circadian rhythms are endogenous oscillations of biological processes that are regulated by a molecular clock (Zhang *et al.*, 2018). Sleep-wake cycles can be modulated by circadian rhythms (He *et al.*, 2014; Zisapel, 2018), and the intersection of sleep restriction and circadian rhythms is an interesting area of research, particularly with respect to the impact that this has on BBB physiology; it was found that a circadian clock in the BBB is responsible for regulation of BBB mediated efflux (Zhang *et al.*, 2018). Many hormonal secretions also come under the control of circadian rhythms (Pan and Kastin, 2016).

In humans and mammals, circadian rhythms are controlled by superchiasmatic nuclei (SCN), which is a cluster of 10,000 neurons, located 3 cm behind the eyes, on either side of the midline above the optic chiasma (Hastings, 1998; Hastings, 1997; Klein *et al.*, 1991). Without the SCN, the ability to express circadian rhythms is destroyed (Hastings, 1998). Circadian rhythms are controlled by a circadian clock, which consists of a feedback loop—essentially, in human brain and eye regions controlled by the circadian clock, the *Clock* and *Bmal1* genes form a heterodimer, which encodes a transcription factor that binds to E-box elements, and positively induces rhythmic transcription of *per* genes, which negatively regulate the Clock/Bmal1 complex in an oscillatory pattern throughout the 24 hour circadian cycle (Gekakis *et al.,* 1998; Hastings, 1998).

Recent findings (Hudson *et al.*, 2019) provided intriguing results linking TJ components of the BBB and circadian rhythms, which was further explored in this study. It has been shown from open-sourced data available on http://cirgrdb.biols.ac.cn/ (Li *et al.*, 2018), that claudin-5 transcript cycles in a circadian manner in various mouse tissues such as the heart, white fat, liver, adrenal glands, muscle, brown fat, aorta, lung, as well as in the cerebellum, hypothalamus, and brainstem regions of the brain (Hudson *et al.*, 2019). The study revealed Bmal1 regulates claudin-5 levels in mouse and human endothelial retinal cells, which causes shifts in permeability at the blood retina barrier (Hudson et al, 2019). The study also showed that claudin-5 can cycle in a circadian dependent manner in mouse brain endothelial cells (bEnd.3), for just over 24 hours, while ZO-1 and occludin appear to cycle depending on time of day, but not in a circadian-dependent manner like claudin-5 (Hudson *et al,.* 2019). Thus, for this study, these findings serve as a reason to expand on research on the circadian cycling of claudin-5, and cycling patterns of other tight junction associated proteins at the BBB.

The goal of this investigation was to recapitulate and expand on these results and study the physiology of tight junctions with respect to circadian and temporal expression patterns. We wanted to explore if characterizing expression of tight junction proteins and certain clock components in *in vitro* conditions for an extended period of time of up to 72 hours is possible,

and what this physiology might look like. The protocol described in (Balsalobre *et al.*, 1998), and that was also used in Hudson *et al.*, 2019, called "serum shock" can be used to reset circadian rhythms *in vitro* in bEnd.3 cell lines which model the BBB endothelial tight junctions. Implications of these longer term studies with respect to circadian rhythms can have significance for our understanding of BBB permeability, regarding expression of tight junction proteins. As the nature of the BBB is dynamic, knowledge of expression patterns of tight junction proteins can be used when designing therapies to deliver across the BBB as discussed in section 1.4.1 in a time-dependent manner. Sleep cycles, and circadian and time-dependent disruption of tight junction protein expression can have an impact of BBB integrity.

1.6 Background on the 3'UTR

The established central dogma states that genetic information follows a pathway of genetic code being established in DNA, becomes transcribed to mRNA, and translated into proteins which then perform necessary functions required for proper operation of an organism (Crick, 1958). However, mRNA also contains the 3'UTR (untranslated region) sequence, which is not translated in the final protein structure, but are thought to regulate a variety of functions such as mRNA processing, transport, stability, and translation (Zhao *et al.*, 2011). Much is still not known about this region, but it has been recently found that genetic information stored in the 3'UTRs can be transmitted to proteins, not through translation of these 3'UTR sequences, but through formation of 3'UTR mediated protein-protein interactions (Berkovits and Mayr, 2015; Mayr, 2018). These findings suggest that 3'UTRs play an important role in regulating biological complexity (Mayr, 2018). *Cis*-elements in the 3'UTR mediate binding with *trans*-elements, also known as RNA-binding proteins (RBPs), which can contribute to post-transcriptional and post-translational modifications that impact protein physiology (Brown *et al.*, 2015; Mayr, 2018). The concept of post-transcriptional/translational modifications having an effect on protein expression is certainly an interesting topic, and will be explored in this study. RBPs bind to motifs on the 3'UTR and participate in signal transduction pathways, and certain regulatory motifs in the 3'UTR can be subject to single nucleotide polymorphisms or mutations that result in loss of function that disrupt RNA-binding motifs, that affect association with RBPs (Brown *et al.*, 2015). These can have drastic effects on overall function of proteins. There are gaps in our understanding of how TJ proteins are regulated, especially with regard to the 3'UTR region, and the impact that this has on BBB physiology.

1.6.1 3'UTR Associated Polymorphisms in Claudin-5

Previously, a single nucleotide polymorphism (SNP) located in the 3'UTR of claudin-5, identified as rs10314, has been shown to be associated with schizophrenia in Iranian populations through linkage disequilibrium studies (Omidinia *et al.*, 2014); however, two other SNPs found on the claudin-5 locus, but that were not located on its 3'UTR, were not found to be associated with schizophrenia, which suggests that the role of the 3'UTR for claudin-5 has a critical effect on proper function of the claudin-5 protein and its physiology (Omidinia *et al.*, 2014). The rs10314 polymorphism associated with the 3'UTR region of claudin-5 was also found to be associated with schizophrenia in a Han Chinese population (Sun *et al.*, 2004).

22q11 deletion syndrome is a condition that causes up to 1.5 to 3 megabase sized deletions in chromosome 22q11.2, and affects psychological and cognitive abilities, and studies have showed that this condition is associated with schizophrenia (Karayiorgou *et al.*, 2010; Karayiorgou *et al.*, 1995; Xu *et al.*, 2008). Claudin-5 happens to be located in this region, and it was recently found that the 3'UTR polymorphism in rs10314 in claudin-5 results in up to 50% abrogation of claudin-5 expression and up to 75% reduction in claudin-5 expression in patients with both the rs10314 polymorphism, as well as 22q11 deletion syndrome (Greene *et al.*, 2018). Schizophrenia is a disorder that is characterized by impaired BBB integrity (Najjar *et al.*, 2013; Najjar *et al.*, 2017), and we have previously described that many neurological diseases are characterized by BBB dysfunction with respect to tight junctions. In order to study BBB physiology which is affected by improper tight junction expression, particular emphasis was placed on claudin-5 as it is the most abundant TJ protein at the BBB (Ohtsuki *et al.*, 2007). That is why this significant 3'UTR claudin-5 link of certain polymorphisms causing abnormal function is insightful to explore.

It will be pertinent to screen various polymorphisms in the 3'UTR of claudin-5 to determine the effect that this has, if any, on overall claudn-5 expression, regulation, localization, and BBB physiology. Looking at post-transcriptional and post-translational modifications governed by 3'UTR function and its interaction with RBPs will also be important.

1.7 Objectives

As previously discussed, the BBB is highly dynamic, and its integrity is strongly mediated by expression of tight junction proteins at endothelial TJ complexes, in order to protect CNS neural function, and that BBB dysfunction is a hallmark of many neurological diseases. The circadian and time-dependent rhythms are relevant to BBB integrity studies, and

the 3'UTR is a key mediator of RNA/protein interactions and can impact the overall function of a protein through post-transcriptional and post-translational modifications. We are interested in studying the regulation of key tight junction proteins and the role that circadian, and 3'UTR mediated regulation has on overall TJ protein expression, and BBB physiology, with particular emphasis on claudin-5.

One objective of this investigation is to **1)** expand upon previous work by (Hudson *et al.*, 2019) and characterize tight junction protein expression of critical TJ proteins and clock components such as claudin-5, ZO-1, occludin, and Bmal1 over an extended period of time (72 hours), in *in vitro* conditions (bEnd.3 endothelial cell lines) that mimic circadian rhythms through serum shock experiments. It is hypothesized that there will be changes in TJ and clock component expression, as levels increase and decrease in a temporal manner over an extended period of time due to the dynamic nature of the BBB.

The other objective is to **2)** study whether various other 3'UTR claudin-5 polymorphisms affect claudin-5 phenotypes in *in vitro* conditions. To do this, certain claudin-5 3'UTR SNPs were selected, and plasmid constructs expressing these polymorphisms were created and screened for claudin-5 protein expression and localization. It is hypothesized that there will be changes in claudin-5 protein expression for at least some SNPs in the 3'UTR of claudin-5, compared to that of native levels, as the rs10314 3'UTR variant of claudin-5 has a significant impact on protein expression. We wanted to explore effect that other SNPs in the 3'UTR of claudin-5 may have, as 3'UTR mediated regulation is critical for proper protein function.

Chapter 2: Methods and Materials

2.1 Circadian Experimental Procedures

2.1.1 bEnd.3 Cell Culture

The mouse brain endothelial cell line bEnd.3 (American Type Culture Collection, [ATCC] CRL-2299), was maintained in a humidified sterile cycle CO_2 incubator (Hepa Class 100, Thermo Scientific™) at 37°C with 5% CO_2, and cell culture was performed in a laminar flow cabinet (Holten LaminAir Model 1.2, Thermo Electron Corporation). Cells were visualized periodically using a light microscope (Olympus CK30). Cells were subcultured in t-75 flasks in growth media consisting of DMEM(1X) GlutaMAX™ media (Gibco™), supplemented with 10% FBS. For plating cells for experiments, cells were washed with 1X PBS and gently aspirated, trypsinized with 0.25% trypsin-EDTA (Gibco™) in the incubator at 37°C with 5% CO_2 for several minutes until cells detached from the flask, then neutralized in growth media, centrifuged at 1000 rpm for 5 minutes, and resuspended in 1 mL fresh growth media. Cell counting was done using a Luna™ Automated Cell Counter, where a 10 µL aliquot was diluted 1:2 in trypan blue solution, and 10 µL of this was loaded into the cell counter slide—the cell counter provides the number of viable cells/mL.

2.1.2 Serum Shock

The serum shock procedure used to mimic circadian rhythms in bEnd.3 cells in order to study TJ protein expression patterns was adapted from Balsalobre *et al.*, 1998, which has been shown to recapitulate cycling of cells, comparable to circadian rhythms in *in vitro* conditions. Briefly, bEnd.3 cells were grown to confluent monolayers in 12-well plates in order to form tight junctions that mimic the BBB, in normal growth media described in 2.1.1. Cells were then cultured for 2 hours at 37°C with 5% CO_2 in the incubator, in serum- rich media (50% FBS in DMEM(1X) GlutaMAX™ media (Gibco™), which constitutes a “shock”, then the serum-rich media was discarded and then cells were washed 2X with 1X PBS and cultured in serum-free media (DMEM(1X) GlutaMAX™ only), to be assayed at various points for the remainder of the experiment. Once cultured in serum free media, RNA and protein samples were extracted from cells every 4 hours for 72 hours, as well as at 0 hours post serum shock, as well as from pre-serum shock (PS) control cells that had been cultured in normal growth media. RNA and protein extraction procedures will be detailed in future sections.

2.1.3 Protein Extraction

In order to extract protein from cells, cells of interest were washed with 1X PBS and then scraped off the plate surface and resuspended in 100 µL of 1X RIPA buffer supplemented with 1 cOmplete™ Mini Protease Inhibitor cocktail tablet (Roche) in 1.5 mL Eppendorf tubes. 10X RIPA buffer includes 50 mM Tris, 150 mM NaCl, 0.5% w/v Sodium Deoxycholate, 1% Triton X-100, and 0.1% w/v SDS. Samples were centrifuged at 12,000 rpm for 15 minutes, until a pellet settled at the bottom, and the supernatant was transferred to a fresh tube and stored at -20°C until needed. Protein concentration estimation was performed using the Pierce® BCA Assay Kit, according to the manufacturer's instructions. Briefly, reagent A and B were mixed at a ratio of 50:1, and 5 µL of each protein sample and standard was added in duplicate in wells of a 96 well plate, with 200 µL of this solution. The standard curve was made from BSA, and the concentrations used were 0, 125, 250, 500, 750, 1000, 1500, 2000 µg/mL. The plate was covered with film, and protected from light, and incubated at 37°C in an incubator for 30 minutes, cooled to room temperature, and then absorbances were read on a MultiSkan FC plate reader (Thermo Scientific) at 595 nm. The standard curve was graphed in excel by plotting averaged absorbances vs concentrations (µg/mL), which were then subtracted by the averaged blank absorbance values. This blank corrected standard curve, was then used to calculate the concentrations (µg/mL) of the unknown protein samples, using their blank corrected, averaged absorbance values.

2.1.4 Western Blotting

After protein estimation through BCA Assays described in section 2.1.3, protein lysates were prepared, using 10 µg of protein lysates, , 1X sample buffer, and dH_20 in a total volume of 20 µL, and denatured at 95°C for 10 minutes.

Resolving gels and stacking gels were prepared at the following concentrations: **12% resolving gel**-6.6 mL dH_20, 5 mL 1.5M Tris (pH=8.8), 8 mL 30% Acrylamide/Bis-acrylamide solution 37.5:1 (Sigma Aldrich), 200 µL 10% w/v SDS, 200 µL 10% w/v APS, 20 µL TEMED (Sigma-Aldrich): **9% resolving gel**- 8.58mL dH_20, 5 mL 1.5M Tris (pH=8.8), 6 mL 30% Acrylamide/Bis-acrylamide solution 37.5:1 (Sigma Aldrich), 200 µL 10% w/v SDS, 200 µl 10% w/v APS, 20 µl TEMED (Sigma-Aldrich): **4% stacking gel**- 6.8 mL dH_20, 1.67 mL 0.5M Tris (pH=6.8), 1.33 mL 30% Acrylamide/Bis-acrylamide solution 37.5:1 (Sigma Aldrich), 100 µL 10% w/v SDS, 100 µL 10% w/v APS, 10 µL TEMED (Sigma-Aldrich). For visualizing ZO-1 and Occludin, 9% resolving gel was used, and to visualize claudin-5 and Bmal1, a 12% resolving gel was used, and ß-actin can visualized as a loading control for both gels. The resolving gels were then topped off with a 4% stacking gel poured on top.

To prepare the gels for SDS-PAGE, the resolving gel mixture of desired percentage was poured into a two glass plates separated by a rubber gasket and held together with clamps, leaving enough room for a gel comb to be inserted into the stacking gel on top of this resolving gel. The resolving gel was then left to harden. 70% Ethanol in dH_20 was poured on top of the resolving gel to ensure that it sets evenly. Once hard, the 70% ethanol solution was poured off, and the gel was rinsed with dH20, and the 4% stacking gel was added to fill up the remaining space, and a gel comb was inserted and left to harden. Once the gel was completely hard, the clamps, rubber gasket, and comb were gently removed. The balanced prepared gels were loaded into a gel electrophoresis rig with 1X running buffer [1 L of 10X running buffer includes 30.3 g Tris, 144.2 g glycine, 10 g SDS, dissolved in dH_20 up to 1 L]. The prepared denatured protein lysates were loaded in individual wells, along with a molecular weight ladder Prime-Step™ Prestained Broad Range Protein Ladder (Biolegend) loaded into one well in each gel that was run. Once samples were loaded, the gel rig was connected to a power station, and gel electrophoresis was carried out at 80 V for 20 minutes, and then for 140 V for 2 hours, of until the dye reached the bottom of the gel.

After separation of proteins, the transfer of proteins from the gel to the PVDF membrane was done through a "semi-dry" transfer protocol. For each gel, 4 sheets of 10 cm x 7 cm filter paper were soaked in 1X transfer buffer [1.5 g Tris, 7.2 g glycine, 100 mL methanol, brought up to 500 mL with dH_20] and arranged on a transfer rig. Then a 9.5 cm x 6.5 cm PVDF membrane was activated in methanol and then placed on top. The resolving gel with the separated proteins was trimmed and placed in 1X transfer buffer, then placed on top of the membrane, and then 4 more sheets of 10 cm x7 cm filter paper soaked in 1X transfer buffer were placed on top of the gel creating a "sandwich". The rig was sealed and connected to a power station, where the proteins are transferred to the membrane at 12 V for 2 hours.

Next, the membrane underwent blocking and antibody incubations to prepare the blots for visualization of proteins of interest. Before this, ponceau staining was performed to ensure proper transfer of proteins occurred using Ponceau S solution (Sigma Aldrich). Blots were coated with ponceau reagent on an orbital shaker at room temperature for a few minutes, to ensure appearance of properly transferred proteins indicated by pink bands, and then the reagent was washed off of the blots through 3 x 5 minute washes in TBS-T (1X TBS solution with 0.1% Tween) solution on a shaker at room temp. [10X TBS made using 30.2 g Tris, 44 g NaCl, pH=7.4, brought up to 500 mL with dH_20]. Using the aforementioned protein ladder for size reference, the membranes were cut into respective strips based on their respective molecular weight, where each piece would only contain the protein of interest. This was done for efficiency, in order to simultaneously probe for the loading control and the various target

proteins for all of the samples on a single membrane. Membranes were then blocked with 5% dried milk solution in TBS-T at room temperature on shaker for 1 hour. Blots were washed with 3 x 5 minute washes in TBS-T, and then incubated overnight at 4°C on shaker in primary antibody solution. Primary antibody solutions were prepared in 3% BSA in 1X TBS solution at the following dilutions: rabbit anti-ß-actin (Abcam, ab8227) 1:4000, rabbit anti-claudin-5 (Invitrogen, 34-1600) 1:1000, rabbit anti-occludin (Novus Biologicals, NBP-187402) 1:1000, rabbit anti-ZO-1 (Invitrogen, 40-2200) 1:1000, rabbit anti-Bmal1 (Bethyl Laboratories Inc., A302-616A) 1:1000. After this, membranes were washed 3 x 5 minutes with TBS-T on a shaker at room temperature, and then incubated secondary antibody solution- 3% BSA in 1X TBS with secondary antibody goat anti rabbit (IG) horse radish peroxidase (HRP) (Thermo Fisher, 65-6120) 1:3000 dilution for 2 hours at room temperature on shaker. Blots were then washed 3 x 5 minutes with TBS-T on shaker at room temperature to wash off excess solution.

Western blots were then prepared for visualization on the C-DiGit (LI-COR Biosciences) apparatus. Membranes were incubated in 1:1 mixture of ECL WesternBright™ (Advansta) reagent (400 µL of each), for several minutes. Images were acquired on the C-DiGit machine, using the Image Studio™ software (LI-COR Biosciences, U.S.A., https://www.licor.com/bio/image-studio/), on the high sensitivity setting. Images were subsequently analyzed on the Image Studio™ Lite 5.2.5 software. (LI-COR Biosciences, U.S.A., https://www.licor.com/bio/image-studio-lite/).

Serum shock experiments were carried out on cells in 3 independent experiments (n=3), and each biological replicate was analyzed individually in technical replicates (triplicate). Signal intensity for protein of interest in each sample was divided by that of the signal intensity of the respective sample's loading control, thus normalizing it to ß-actin. For the densitometry analysis, to calculate the relative protein expression, the normalized signal intensity was then divided by that of the control, in this case, the pre-serum shock sample. For the technical triplicates, uniform sized small, medium, and large boxes were drawn around each protein band of interest respectively, and the corresponding relative normalized signal intensity was calculated for signal intensity of boxes of the same size respectively. Results were then graphed in GraphPad Prism software for each individual biological replicate separately, and are presented as the mean ± SEM (standard error of the mean), with error bars representing standard deviation of the technical replicates. Statistical analysis was done on each individually analysed biological replicate separately using one-way ANOVA, with a Tukey post-test, specifically looking at significance in protein level changes of samples compared only to the pre-shock control (PS), with *$p<0.05$, **$p<0.01$, ***$p<0.001$. Statistical analysis was

performed using Prism 5.02 for Windows (GraphPad Software Inc., U.S.A., www.graphpad.com).

2.1.5 RNA isolation

In order to extract RNA from cells at the designated time points, RNA was isolated using the E.Z.N.A. Total RNA Kit I (Omega Bio-Lab), according to the manufacturer's instructions. Briefly, cells were washed with 1X PBS and scraped off the plates and resuspended in 350 µL of TRK lysis buffer, and then mixed through vortexing with an equal part of 70% Ethanol in RNAase-free H_20 (350 µL). The homogenized cell solution of each sample was transferred to a HiBind® RNA Mini Column fitted in a collection tube, and centrifuged at 10,000 rpm for 1 minute and filtrate was discarded. 500 µL RNA wash buffer I was added to the column and it was then centrifuged at 10,000 rpm for 30 seconds, and filtrate was discarded from the collection tube. 500 µL of RNA Wash buffer II was added to the column, which was then centrifuged at 10,000 rpm for 1 minute, then the filtrate was discarded, and this step was repeated. The empty column and collection tube were then centrifuged at maximum speed for 2 minutes. The column was transferred to an empty 1.5 mL Eppendorf tube, and approximately 50 µL of DEPC water was added to the column, which was centrifuged at maximum speed for 2 minutes. RNA concentrations were determined using the Nanodrop 1000 (Thermo Scientific). Eluted RNA was then stored at -80°C for long term storage.

2.1.6 cDNA synthesis and Real-Time quantitative Polymerase Chain Reaction (qPCR)

After RNA isolation, RNA was reverse transcribed into cDNA using the High-Capacity cDNA Reverse Transcription Kit (Applied Biosystems), according to the manufacturer's instructions. Briefly, for 1 reaction, 10 µL of mastermix was mixed with a 10 µL total solution of 200 ng RNA and remaining volume RNAase-free H_20. The mastermix for 1 reaction contains 2 µL of 10X RT buffer, 0.8 µL of 25X dNTP mix, 2 µL of 10X RT Random Primers, 1 µL Multiscribe™ Reverse Transcriptase, and 4.2 µL of RNAase-free H_20, and was scaled accordingly to the number of reactions. The cDNA synthesis reactions were carried out on the thermocycler under the following conditions: 25°C for 10 minutes; 37°C for 2 hours; 85°C for 5 minutes; 4°C hold.

The qPCR on the cDNA reverse transcription was carried out as follows, using a SensiFAST SYBR Hi-ROX Kit (Bioline). In a 96 well reaction plate (Applied Biosystems), 5 µL of 1:40 diluted cDNA in RNAase-free H_20, was added, along with 15 µL of mastermix solution. The mastermix of 1 reaction consisted of 10 µL SYBR Green mix, 1 µL of 10 µM

Forward and Reverse Primer Mix, and 4 µL of RNAase-free H_20, and was scaled up as required. The plate was then covered with adhesive film and centrifuged briefly, and then run on the thermocyler Step-One Plus™ Real-Time PCR instrument (Applied Biosystems) under the following conditions: (95°C for 2 minutes, then 95°C for 5 seconds followed by 60°C for 30 seconds for 40 cycles, then a melt curve can be added for 95°C for 15 seconds, then 60°C for 1 minute, then 95°C for 15 seconds), after which, the comparative C_T method (by calculating $2^{-\Delta\Delta Ct}$), normalizing to ß-actin, to compare mRNA levels of the target transcripts. The process of transcript quantification, through qPCR on reverse transcription derived cDNA from isolated RNA, may at times be referred to as RT-qPCR.

For the serum shock experiments, RNA was isolated from bEnd.3 cells (mouse brain endothelial cell line) performed in 3 independent experiments (n=3 biological replicates). The housekeeping gene primers used were ß-actin (universal) :
FP 5' TCACCCACACTGTGCCCATCTACGA 3',
RP 5' CAGCGGAACCGCTCATTGCCAATGG 3', and the primers for the target genes used were mouse claudin-5 FP 5' TTTCTTCTATGCGCAGTTGG 3',
RP 5' GCAGTTTGGTGCCTACTTCA 3', mouse ZO-1
FP 5' CCACCTCTGTCCAGCTCTTC 3', RP 5' CACCGGAGTGATGGTTTTCT 3', mouse Occludin 5' ACAGTCCAATGGCCTACTCC 3', RP 5' ACTTCAGGCACCAGAGGTGT 3', and mouse BMAL1 FP 5' ATCAGCGACTTCATGTCTCC 3',
RP 5' CTCCCTTGCATTCTTGATCC 3'. Samples were pipetted in either duplicate or triplicate for the technical replicates, and averaged to calculate $2^{-\Delta\Delta Ct}$ for each biological replicate, normalized to ß-actin, and the relative mRNA expression of each target was calculated in comparison to that of the pre-serum shock (PS) control. A constant threshold value was maintained at 0.3 for all plates run. Values were graphed in GraphPad Prism, as the mean ± SEM of 3 biological replicates. Statistical analysis used was one-way ANOVA with a Tukey post-test with focus specifically on comparisons only to pre-shock control with *$p<0.05$, **$p<0.01$, ***$p<0.001$. Statistical analysis was performed using Prism 5.02 for Windows (GraphPad Software Inc., U.S.A., www.graphpad.com).

2.2 3'UTR Claudin-5 SNPs

2.2.1 Selection of 3'UTR Claudin-5 SNPs to Screen

SNPs of interest in the 3'UTR region of claudin-5 (CLDN5) to work with and characterize were selected through a series of parameters. In the AURA (Atlas of Regulatory UTR Activity) database (http://aura.science.unitn.it) (Dassi *et al.*, 2014), the 3'UTR region of claudin-5 was selected to generate a list of potential SNPs of interest. After cross-referencing

this information with data from the RBPmap database (http://rbpmap.technion.ac.il) (Paz *et al.*, 2014), where the genetic coordinates of the 3'UTR of claudin-5 and the strand location were input, chr22: 19510547-19511121, - strand, and human/mouse motifs were selected, a list of potential RNA-binding proteins (RBPs) for the 3'UTR region of claudin-5 was generated. The SNPs generated from the AURA search were then compared to the binding sites of potential RBPs generated from RBPmap, looking at RBPs binding directly at or within 5 base pairs of the SNPs. Then the minor allele frequencies of SNPs were also generated using the Ensembl database (https://www.ensembl.org/index.html) (Hunt *et al.*, 2018), and most SNPs were selected that had low minor allele frequencies, in order to select rare polymorphisms to screen. This list was then narrowed down to 7 SNPs [rs200564626, rs45485695, rs1053640, rs1053641, rs11551256, rs111760583, rs1053675].

2.2.2 Generation of 3'UTR Claudin-5 Plasmids through Site-Directed Mutagenesis (SDM)

The plasmid construct expressing the native human cDNA and 3'UTR sequence was previously generated by (Greene *et al.*, 2018), using the pcDNA3-EGFP vector (Addgene, U.S.A., plasmid #13031 from Doug Golenbock's lab). The native human cDNA and 3'UTR of claudin-5 was subcloned into the HindIII/XhoI site of the pcDNA3-EGFP vector by GeneArt (Ireland). Site-directed mutagenesis was then performed on this native plasmid, to express the various 3'UTR SNPs of interest that had been selected for screening, described in section 2.2.1.

Mutagenic primers to conduct site-directed mutagenesis on the native plasmid were generated using the NEBaseChanger webtool v1.2.9 (http://nebasechanger.neb.com) that accompanies the Q5® Site-Directed Mutagenesis Kit (New England Biolabs), where the designated sequence and SNP locations and target base changes were input, and the following primers were generated: rs200564626 FP 5'GGCACGGCCGaGCCCCTCCTG 3',
RP 5' CAGCGCCCGGAGAGAGTTCAAACC 3', rs45485695
FP 5' TGCAGAGCCCgGGGCCCCCAC 3', RP 5' TCCGCCCCTCCGAAGTCAGC 3',
rs1053640 FP 5' CAGGGCCCCCcCCGGAAGATG 3',
RP 5' GGCTCTGCATCCGCCCCT 3', rs1053641
FP 5' CCCACCGGAAaATGTGTACAGC 3', RP 5' GGCCCTGGGCTCTGCATC 3',
rs111760583 FP 5' TTGAACTCTCaCCGGGCGCTG 3',
RP 5' ACCATTTACTAAGCAGATTCTTAGC 3', rs11551256
FP 5' CCCTCCAAGAtGCTGGGGGTC 3',
RP 5' GAAGCGAAATCCTCAGTCTGACAC 3', rs1053675
FP 5' GAGCTTGAGAaAGGGCGGGAG 3', RP 5' CGGTGCCCACAAGCCTTG 3'.

The SDM reactions were carried out using the Q5® Site-Directed Mutagenesis Kit (New England Biolabs), following the manufacturer's instructions, but using half of the specified volume of each reagent. First, the PCR reaction was carried out to amplify the plasmid (linear) with the selected mutation and each reaction was comprised of 6.25 µL Q5® Hotstart High Fidelity 2X Mastermix, 0.625 µL of 10 µM FP, 0.625 µL of 10 µM RP, 25 ng of Template DNA plasmid (native construct), and the remaining reaction was filled with nuclease-free H_20 to get a total reaction volume of 12.5 µL. The reactions for each respective SNP were run under the following thermocycling conditions: [rs200564626, rs45485695, rs1053640: 1 cycle at 98°C for 30 seconds, 25 cycles at 98°C for 10 seconds, 72°C for 30 seconds, 72°C for 4 minutes, followed by 1 cycle at 72°C for 2 minutes followed by 4°C hold indefinitely], [rs11551256: 1 cycle at 98°C for 30 seconds, 25 cycles at 98°C for 10 seconds, 68°C for 30 seconds, 72°C for 4 minutes, followed by 1 cycle at 72°C for 2 minutes followed by 4°C hold indefinitely], [rs1053641: 1 cycle at 98°C for 30 seconds, 25 cycles at 98°C for 10 seconds, 70°C for 30 seconds, 72°C for 4 minutes, followed by 1 cycle at 72°C for 2 minutes followed by 4°C hold indefinitely], [rs111760583: 1 cycle at 98°C for 30 seconds, 25 cycles at 98°C for 10 seconds, 64°C for 30 seconds, 72°C for 4 minutes, followed by 1 cycle at 72°C for 2 minutes followed by 4°C hold indefinitely], and [rs1053675: 1 cycle at 98°C for 30 seconds, 25 cycles at 98°C for 10 seconds, 71°C for 30 seconds, 72°C for 4 minutes, followed by 1 cycle at 72°C for 2 minutes followed by 4°C hold indefinitely].

Next, the amplified mutated linear plasmids were re-circularized and the old template was degraded through DpnI treatment as follows for each individual plasmid: 0.5 µL of PCR product, 2.5 µL of 2X KLD Reaction Buffer, 0.5 µL of 10X KLD Enzyme Mix, and fill up the rest of the reaction with nuclease-free H_20 for a total reaction volume of 5 µL. Reactions were mixed well up and down and incubated at room temperature for 5 minutes.

The plasmids were then transformed using 2.5 µL of the incubated mixture described in the previous step for the site-directed mutagenesis derived plasmids, along with 25 µL of competent 5-alpha E.Coli cells provided with the kit that were thawed on ice. Standard transformation protocol was followed. For plasmids of known concentration that are required to transform, such as the native plasmid, 50 ng can be used. Prior to transformation the required solution was made as follows: LB-Agar-Ampicillin selection plates were made using 10 g NaCl, 10 g tryptone, 5 g yeast extract, 15 g Agar, dissolved in up to 1 L dH_2O, autoclaved at 121°C for 20 minutes, after cooling to approx. 50-60°C, 1000 µL of 100 mg/mL stock Ampicillin solution was added for a final working concentration of 100 µg/mL, and the solution was then poured into petri dished in a sterile laminar flow cabinet and then cooled for approximately 30 minutes to 1 hour. Briefly, the incubated mix of competent cells and mutated

plasmid were incubated on ice for 30 minutes, then heat shocked at 42°C for 30 seconds, and then immediately kept back on ice for 2 minutes. 970 µL of pre-warmed SOC outgrowth media was pipetted into each reaction and incubated at 37°C for 1 hour. Finally, approximately 100-200 µL of this mixture was plated on LB-Agar-Ampicillin selection plates overnight at 37°C, and appearance of colonies was observed the next day. Plates can be stored at 4°C until further use. Colonies were selected for sequencing analysis to confirm presence of SNP (see section 2.2.4).

2.2.3 Inoculation of Plasmids for Miniprep/Maxipreps

Prior to inoculation, the required media was prepared as follows: LB media- 10 g NaCl, 10 g tryptone, 5 g yeast extract, dissolved in up to 1 L of dH_2O, and was autoclaved at 120°C for 20 minutes. Plasmids that has been transformed on the colonies on the agar selection plates described in the previous step were inoculated overnight in a 37°C orbital shaker, with a final working concentration of 100 µg/mL Ampicillin in either 5 mL or 250 mL LB media, depending on whether a lower quantity miniprep, or a higher quantity maxiprep was required to grow up the plasmid. The miniprep kit used was GeneJet Plasmid Miniprep Kit (ThermoScientific), according to the manufacturer's instructions, and the maxiprep used was the QIAGEN Plasmid Maxi kit, according to the manufacturer's instructions.

2.2.4 Sequencing of Plasmids and BLAST Alignment to Confirm SNP Generation

Sequencing primers were designed using Primer Blast (https://www.ncbi.nlm.nih.gov/tools/primer-blast/) (Ye *et al.*, 2012) in order to amplify the sequences including the SNPs of interest generated in the 3'UTR as follows: [rs45485695, rs1053640, rs1053641, rs11551256, rs11760583, rs1053675
FP 5' AAGAAGAACTACGTCTGAGGGC 3'], and [rs200564626
RP 5' AAGTAAGGCAGCAGCCAAGA 3']. In order to sequence the plasmids, 500 ng of plasmid was sent in a total volume of 5 µl with nuclease-free H_20, along with 3.2 pmol/µL in 5 µL of the respective primer with nuclease-free H_20, was sent to Source Biosciences (Ireland) for sequencing. The generated sequences (query sequence) were then compared to the native plasmid sequence (subject sequence) using the BLASTn suite (Altschul *et al.*, 1990), and presence of the single base change between the two sequences at the desired location confirmed the successful generation of 3'UTR CLDN5 plasmid constructs through site-directed mutagenesis.

2.2.5 HeLa Cell Culture

HeLa cells (Sigma Aldrich), an epithelial cervix carcinoma cell line, were subcultured in t-75 flasks with growth media consisting of DMEM(1X) GlutaMAX™ media (Gibco™), supplemented with 10% FBS. Cells were maintained and plated for experiments using the same procedure as described in section 2.1.1. Briefly, cells were maintained in a humidified sterile cycle CO_2 incubator (Hepa Class 100, Thermo Scientific™) at 37°C with 5% CO_2 and cell culture work was performed in a laminar flow cabinet. Cells were washed with 1X PBS and gently aspirated, trypsinized with 0.25% trypsin-EDTA (Gibco™) in the incubator at 37°C with 5% CO_2 for several minutes until cells detached from the flask, then neutralized in growth medium, centrifuged at 1000 rpm for 5 minutes, and resuspended in 1 mL fresh growth media. Cells were counted and plated as required.

2.2.6 Transfection of 3'UTR CLDN5 Plasmid Constructs in Cell Culture

Transfection of 3'UTR CLDN5 native and SNP expressing constructs was conducted in HeLa cells using Lipofectamine® 2000 transfection reagent (ThermoFisher Scientific). 100,000 cells per well were seeded in 12-well plates overnight to obtain a subconfluent layer of cells. Then 500 ng of each plasmid for Empty Vector (pcDNA3-EGFP) (Addgene), pcDNA3-EGFP native human claudin-5 plasmid, rs200564626, rs45485695, rs1053640, rs1053641, rs111760583, rs11551256, and rs1053675 (described in section 2.2.2) was transfected into respective wells at a ratio of 1 µg of plasmid DNA to 3 µL Lipofectamine® 2000. There was also an untransfected control sample. For transfection, the 500 ng of plasmid DNA was incubated at room temperature in 100 µL of OptiMEM reduced serum media (ThermoFisher Scientific) for 5 minutes, and simultaneously but separately, the corresponding amount of Lipofectamine® 2000 transfection reagent was incubated at room temperature in 100 µL of OptiMEM reduced serum media. Then both incubated solutions were incubated together at room temperature for 20 minutes to form a complex. 800 µL of fresh growth media was added to cells, and then the 200 µL mixture described in the previous step was added dropwise to cells, and then cells were incubated at 37°C with 5% CO_2 for either 24 or 48 hours.

2.2.7 Western Blot for 3'UTR CLDN5 SNP Transfected Cells

Protein isolation on transfected cells was done 24 and 48 hours after transfection, and the protein estimation using a BCA assay was performed as described in section 2.1.3. Protein sample preparation using 10 µg of protein lysate and Western blotting for claudin-5 was performed as described in section 2.1.4, with ß-actin as the loading control. Similarly, using the aforementioned protein ladder for size reference, the membranes were cut into respective strips

based on their respective molecular weight, where each piece would only contain the protein of interest. This was done for efficiency, in order to simultaneously probe for the loading control and the target protein for all of the samples on a single membrane. Transfection experiments were carried out on cells in 3 independent experiments (n=3), and each biological replicate was analyzed individually in technical replicates (triplicate). To normalize the signal intensities for each sample, the signal intensity for the protein of interest was divided by the signal intensity for the respective samples ß-actin loading control protein expression. For the densitometry analysis, to calculate the relative claudin-5 protein expression, the normalized signal intensity for each sample was then divided by that of the control, in this case, the native human claudin-5 transfected sample. For the technical triplicates, uniform sized small, medium, and large boxes were drawn around each protein band of interest respectively, and the corresponding relative normalized signal intensity was calculated for signal intensity of boxes of the same size respectively. Results were then graphed in GraphPad Prism software for the combined triplicate analysis of all 3 biological replicates, and are presented as the Mean± SEM (standard error of the mean), with error bars representing standard deviation of the technical replicates and biological replicates combined. Statistical analysis was done on the combined data set using one-way ANOVA, with a Dunnett's post-test, comparing significance in protein level changes of samples compared only to the native human claudin-5 transfected control with *$p<0.05$, **$p<0.01$, ***$p<0.001$. Statistical analysis was performed using Prism 5.02 for Windows (GraphPad Software Inc., U.S.A., www.graphpad.com).

2.2.8 Immunocytochemistry

To perform immunocytochemistry staining glass coverslips 12 mm x 12 mm (Sigma Aldrich) were placed in 12-well plates, and then coated with 1:40 dilution of Collagen I (rat tail) (Sigma Aldrich) in 1X PBS for 3 hours at 37°C (kept in sterile conditions), and were then washed 3x with 1X PBS. Then, approximately 100,000 HeLa cells per coverslip (subconfluent layer) were subcultured according to the previously established protocol, and seeded overnight and incubated at 37°C with 5% CO_2. Cells were then transfected according to the protocol outlined in section 2.2.6. After 24 and 48 hours post transfections, cells were washed with 1X PBS and fixed in ice-cold methanol for 15 minutes and then washed with 1X PBS again. Next, fixed cells were incubated in blocking buffer (5% normal goat serum (NGS) (BioLegend), 0.1% triton X-100 in PBS) for 1 hour at room temperature. Then solution was removed and cells were incubated in primary antibody solution overnight (1:200 rabbit anti-claudin-5 antibody (Invitrogen, 34-1600) in 1% normal goat serum in 1X PBS. The next day, cells were washed 3x in 1X PBS and then the secondary antibody solution (1:500 goat anti-rabbit AlexaFluor® 488 (Abcam, ab150077) in PBS) at room temperature for 2 hours, and was

protected from light from this step forward. Then, cells were washed 3x in 1X PBS and incubated with 1:10,000 DAPI solution (Thermo Fisher) diluted in PBS for 30 seconds to stain cell nuclei. Then cells were washed 2x with 1X PBS and were mounted on glass coverslips using one drop of Aqua polymount (Polysciences, Inc) per coverslip on the cell coated side. Coverslips were dried overnight. Images were then taken on a Zeiss LSM 710 confocal laser scanning microscope with uniform parameters to visualize each component at a 20X magnification (Green=claudin-5, Blue=DAPI stained nuclei).

Chapter 3: Results for Circadian Modeling Experiments and 3'UTR Claudin-5 SNP Characterization

3.1 Circadian Rhythm Modeling in *in vitro* Conditions for Extended Periods Results in Temporal Expression Changes for Various TJ and Clock Components

Initial experiments were performed with the intention to characterize the expression patterns of various tight junction (claudin-5, ZO-1, occludin) and clock genes (Bmal1) when circadian rhythms are recapitulated in *in vitro* conditions over an extended period of time in bEnd.3 cells, which model mouse brain endothelial cells and can mimic the BBB. Cells were subjected to "serum shock" as described by Balsalobre *et al.*, 1998 to model the circadian rhythm. Claudin-5 expression patterns were shown previously to be associated with Bmal1 and cycle in a circadian dependent manner in various tissues, (Hudson *et al.*, 2019). In this study, we wanted to expand on this research and performed Western blots on protein extracts taken every 4 hours for 72 hours post-serum shock, and results are depicted in Fig. 3.1.1.

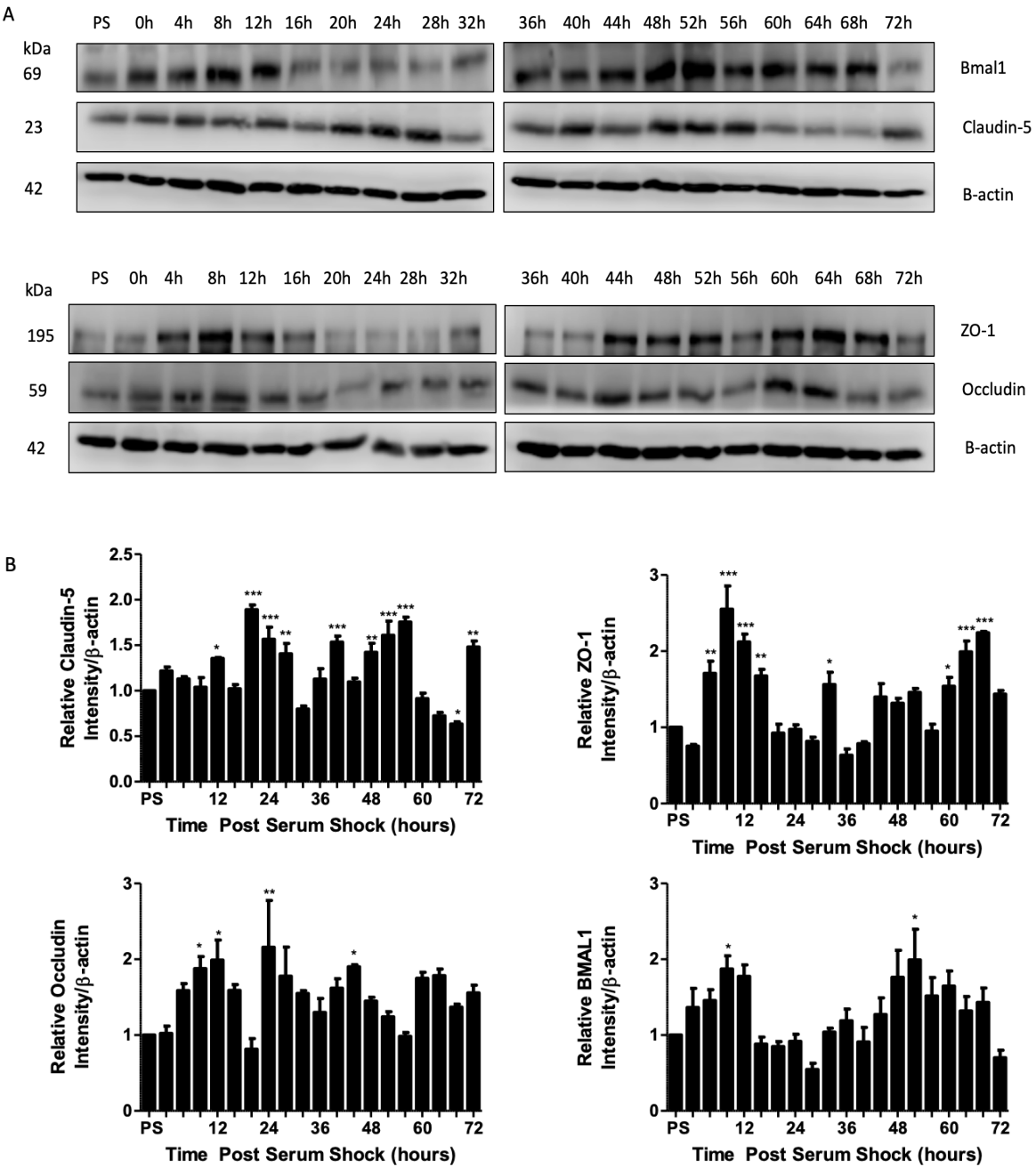

Fig. 3.1.1. **A)** Representative Western Blot Image of serum shock of confluent bEnd.3 cells (mouse origin). Cells were grown to confluency in normal 10% FBS in DMEM media, then underwent serum shock for 2 hours in 50% FBS in DMEM media, after which cells were washed 2x with PBS and media was changed to serum-free DMEM only media. Protein extracts were taken pre-serum shock (PS), immediately after serum shock (0h), and every 4 hours afterwards for 72 hours. Immunoblotting was performed for claudin-5, ZO-1, occludin, Bmal1, with ß-actin loading control. **B)** Densitometry analysis of the individually analyzed representative blot is shown, and are presented as the Mean± SEM (standard error of the mean), with error bars representing standard deviation of the technical replicates. Statistical analysis was done on each individually analyzed biological replicate separately using one-way ANOVA, with a Tukey post-test, specifically looking at comparing significance in protein level changes (normalized to ß-actin) of samples relative to the pre-shock control (PS), with *$p<0.05$, **$p<0.01$, ***$p<0.001$. X-axis labels start with pre-shock control (PS), and each subsequent interval represents every 4 hours for 72 hours post-serum shock, including the 0 hour timepoint, with all 12 hour intervals labeled on the graphs.

It is known that claudin-5 is associated with Bmal1, and together cycle throughout tissues in a circadian manner, and that other TJ proteins cycle in a temporal manner (Hudson *et al.*, 2019). The results from the Western blots reveal that that tight junction and clock component levels do change dynamically over an extended period of time. The pre-shock control expresses protein levels as would be expressed in normal cell culture conditions, without the recapitulation of circadian rhythms after serum shock. For claudin-5, the results show that at 12 and 68 hours post serum shock, there is significant change (*$p<0.05$) in relative protein expression levels compared to that of the pre-shock control, as well as for 28, 48, and 72 hours post-serum shock (**$p<0.01$), and for 20, 24, 40, 52, and 56 hours post-serum shock (***$p<0.001$). For ZO-1, the results show that relative protein expression compared to pre-shock control is significantly different at 32 and 60 hours post shock (*$p<0.05$), for 4 and 16 hours post shock (**$p<0.01$), and for 8, 12, 64, and 68 hours post shock (***$p<0.001$). For occludin, the results show that relative protein expression compared to pre-shock control is significantly different at 8, 12, and 44 hours (*$p<0.05$), and for 24 hours post shock (**$p<0.01$). For Bmal1, the results show that relative protein expression compared to pre-shock control is significantly different at 8 and 52 hours post shock (*$p<0.05$). The data shown reveals that while levels are dynamic over the extended period of circadian rhythm modeling, the changes in protein expression levels can not necessarily be proved to change in relation to each other.

The RT-qPCR analysis of RNA isolated from bEnd.3 cells that have undergone serum shock for an extended period of time (every 4 hours for 72 hours) is shown in Fig 3.1.2. For claudin-5 and ZO-1, the mRNA expression patterns reveal a trend that shows varying levels of mRNA expression relative to the pre-shock control, over the extended 72 hour period of circadian rhythm modeling in bEnd.3 cells. While statistically significant changes in claudin-5 and ZO-1 transcript were not found in bEnd.3 cells which had undergone serum shock, there is clearly a depicted trend of dynamic changes in claudin-5 and ZO-1 transcript expression levels over time. Claudin-5 transcript levels were also shown to cycle in a circadian manner in various neural tissues in Hudson *et al.*, 2019. Occludin shows dynamic changes in mRNA levels over time, with transcript levels showing significant change compared to the pre-shock control 52, 60, and 68 hours post serum shock (*$p<0.05$), and 56 and 64 hours post serum shock (**$p<0.01$). Finally, Bmal1 shows dynamic cycling of transcript levels over the duration of the serum shock mediated circadian modeling in cells, with significant differences in transcript levels apparent at 8 hours post shock (*$p<0.05$), 20 hours post shock (**$p<0.01$), and 4 hours post shock (***$p<0.001$). The RT-qPCR data taken together with the Western blotting data can indicate that there is dynamic cycling of protein and transcript of various key tight junction (claudin-5, ZO-1, occludin) and clock components (Bmal1).

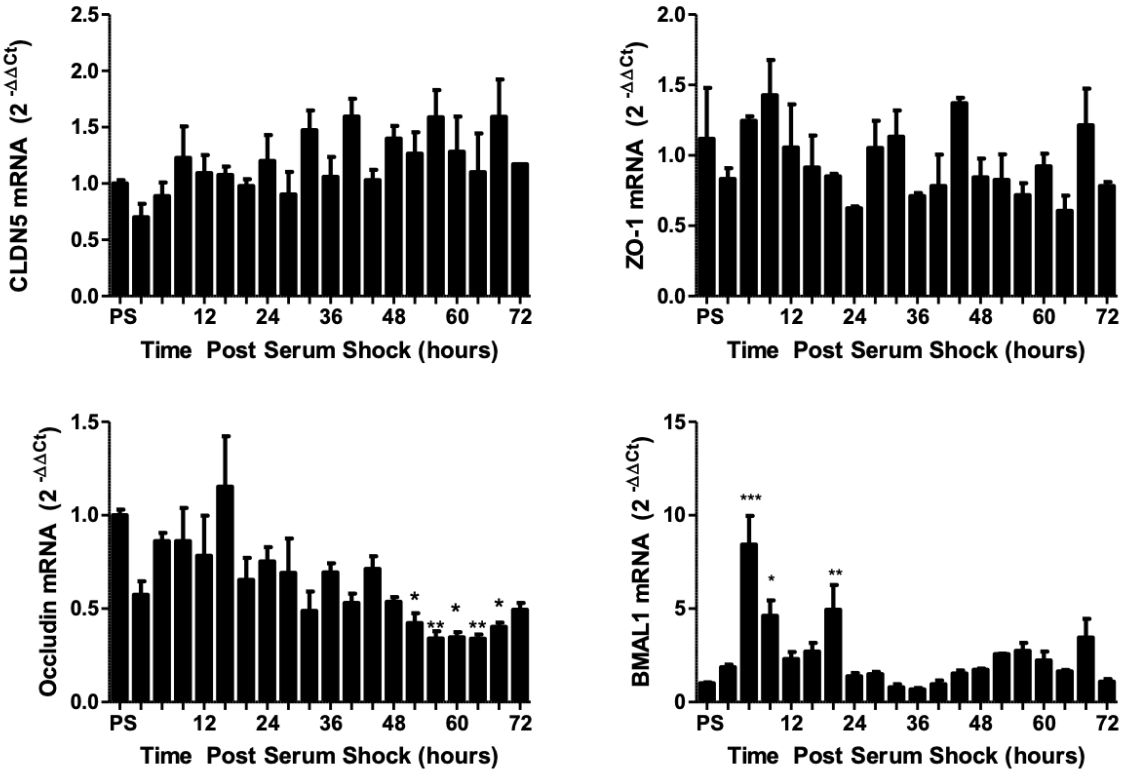

Figure 3.1.2: RT-qPCR Analysis of bEnd.3 cells (mouse origin): Cells were grown to confluency in 10% FBS in DMEM media, then underwent serum shock for 2 hours in 50% FBS in DMEM media, then cells were washed 2x with PBS and media was changed to serum-free DMEM only media. RNA was taken pre-serum shock (PS), immediately after serum shock (0 h), and every 4 hrs afterwards for 72 hours and reverse transcribed into cDNA. RT-qPCR for mouse CLDN5, mouse ZO-1, mouse Occludin, and mouse BMAL1 mRNA levels were compared using the $2^{-\Delta\Delta Ct}$ method, normalizing to ß-actin (n=3). Statistical analysis was done using one-way ANOVA with a Tukey post-test, with specific focus on comparison to the pre-shock control (PS), *p<0.05, **p<0.01, ***p<0.001. All graphs Mean± SEM, with error bars indicating variation among 3 biological replicates. X-axis labels start with pre-shock control (PS), and each subsequent interval represents every 4 hours for 72 hours post-serum shock, including the 0 hour timepoint, with all 12 hour intervals labeled on the graphs.

These dynamic changes could have an impact on BBB integrity and organization. As claudin-5 has previously been shown to be the dominant tight junction protein at the BBB (Ohtsuki *et al.*, 2007), the effect of changes in claudin-5 organization and restructuring at tight junctions throughout the circadian cycle, could potentially have an effect on BBB integrity.

3.2 Generation and Screening of 3'UTR Claudin-5 SNP Plasmids Results in Differences in Claudin-5 Protein Expression

As it was previously shown in other studies associating the 3'UTR claudin-5 variant rs10314 to schizophrenia (Sun *et al.*, 2004; Omidinia *et al,.* 2014) as well as the work done by Greene *et al.*, 2018 which shows significant downregulation of claudin-5 protein expression of

the rs10314 single nucleotide polymorphism, we wanted to screen other variants in the 3'UTR of claudin-5 region to see if they would have an effect on claudin-5 expression, due to its importance as a key mediator of the BBB at tight junctions. The first step in the process was to identify key SNPs of interest to screen in this region. This process is highlighted in Fig. 3.2.1. First, a list of SNPs present in the 3'UTR of claudin-5 was generated using the AURA database. This list was then narrowed down by cross-referenced with the RBPmap database which generated a list of RNA-binding proteins (RBPs) that occur at the 3'UTR region of claudin-5 [chr22: 19510547-19511121, - strand, and human/mouse motifs were selected], and SNPs that occurred either directly at or within 5 base pairs of RBPs were selected. The selected list of 3'UTR claudin-5 SNPs was narrowed down to the following: rs200564626, rs45485695, rs1053640, rs1053641, rs11551256, rs111760583, rs1053675, as shown in Fig. 3.2.1.A. Importantly, the SNPs are dispersed throughout the 3'UTR region of claudin-5, not just clustered around the variant rs10314 which has been shown to decrease claudin-5 expression. These scattered SNPs will provide a more holistic idea of the pathologies of various claudin-5 3'UTR associated SNPs, for the entire region. Also, the minor allele frequencies (MAF) of the selected SNPs were obtained from the Ensembl database, and are given in Fig. 3.2.1.B as percentages expressed as decimals. Compared to rs10314, which has a higher MAF, the SNPs that have been selected for this study have lower MAFs, occurring mostly in under 1% of the general population. The screening results would offer insight regarding the phenotype of claudin-5 expression for rarer polymorphisms, which have not been fully explored as of yet, due to the low occurrence of these SNPs in the general population. The overall flow chart of the selection parameters and protocol is outlined in Fig. 3.2.1.C, as described previously.

A

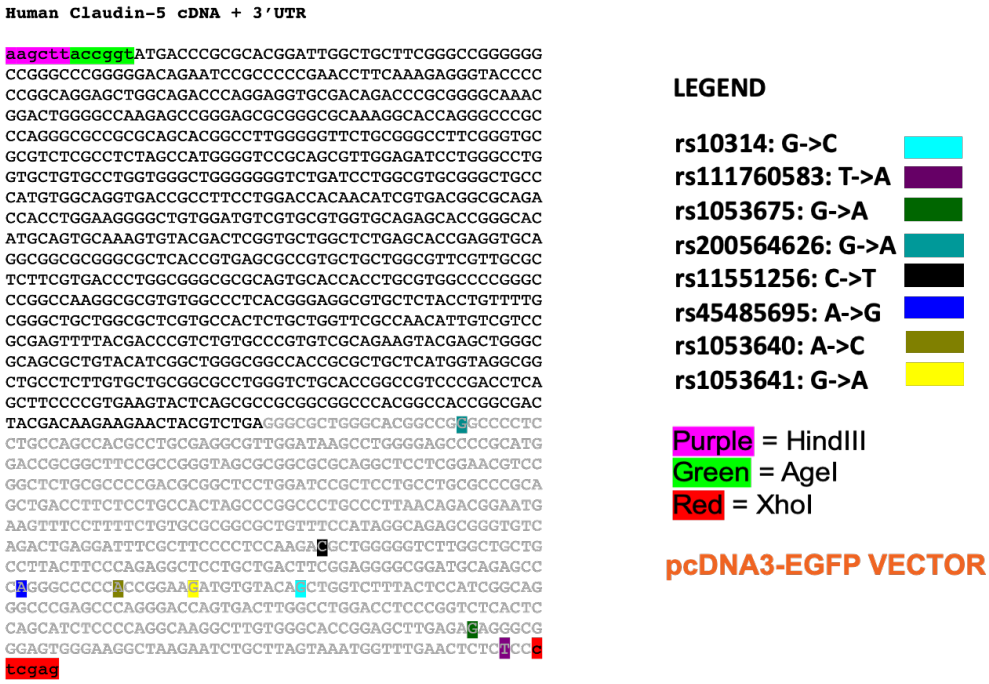

B

From Ensembl (Human GRCh38.12)

rs200564626: **C/T**|Ancestral: **C**|MAF: **< 0.01** (T)|Highest population MAF: **0.01**

rs45485695: **T/C**|Ancestral: **T**|MAF: **0.03** (C)|Highest population MAF: **0.11**

rs1053640: **T/G**|Ancestral: **T**|Highest population MAF: **< 0.01**

rs1053641: **C/T**|Ancestral: **C**|Highest population MAF: **< 0.01**

rs11551256: **G/A**|Ancestral: **G**|MAF: **< 0.01** (A)|Highest population MAF: **0.04**

rs111760583: **A/T**|Ancestral: **A | No Frequency Data**

rs1053675: **C/T**|Ancestral: **C**|Highest population MAF: **< 0.01**

rs10314: **C/G**|Ancestral: **C**|MAF: **0.17** (G)|Highest population MAF: **0.36**

C

UTR: hg19_uc010grr.2_3UTR

Organism: Homo sapiens, assembly hg19.
Gene name: CLDN5
Location: chr22: 19510547-19511121, strand -
Length: 575 bases
Average sequence conservation: 0.0536665553739

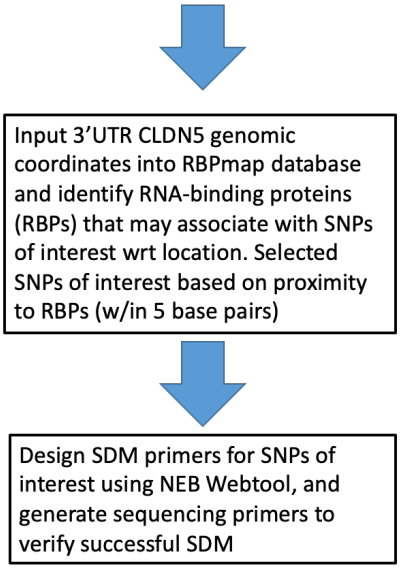

Site-Directed Mutagenesis Primers

	FP 5'->3'	RP 5'->3'	Annealing Temp. (°C)
rs111760583	TTGAACTCTCaC CGGGCGCTG	ACCATTTACTAA GCAGATTCTTAG C	64
rs1053675	GAGCTTGAGAa AGGGCGGGAG	CGGTGCCCACAA GCCTTG	71
rs200564626	GGCACGGCCGa GCCCCTCCTG	CAGCGCCCGGA GAGAGTTCAAA CC	72
rs11551256	CCCTCCAAGAt GCTGGGGGTC	GAAGCGAAATCC TCAGTCTGACAC	68
rs45485695	TGCAGAGCCCg GGGCCCCCAC	TCCGCCCCTCCG AAGTCAGC	72
rs1053640	CAGGGCCCCCc CCGGAAGATG	GGCTCTGCATCC GCCCCT	72
rs1053641	CCCACCGGAAa ATGTGTACAGC	GGCCCTGGGCTC TGCATC	70

Sequencing Primers

SNPs covered	FP 5'->3'	RP 5' ->3'	Annealing Temp (°C)	Amplicon Size (bp)
rs11551256 rs45485695 rs1053640 rs1053641 rs11760583 rs1053675	AAGAAG AACTACG TCTGAG GGC		Approx. 60	80
rs200564626		AAGTAAG GCAGCAG CCAAGA	Approx. 60	53

Fig 3.2.1: The selection of various 3'UTR CLDN5 SNPs and the flowchart for generation of these constructs is detailed **A)** Schematic of the native human CLDN5 cDNA (black text) + 3'UTR sequence (gray text), which was cloned in the HINDIII/XhoI site of the pcDNA3-EGFP plasmid (Addgene), with the location of the SNPs of interested highlighted throughout the 3'UTR region to be generated via site-directed mutagenesis **B)** Data obtained from the Ensembl database, showing the available data for minor allele frequency (given as percentages expressed as decimals) of SNPs of interest **C)** Flowchart of the screening method used to select the key 3'UTR claudin-5 SNPs of interest using the AURA database to generate a list of SNPs in the 3'UTR region of claudin-5, the RBPmap database to generate a list of RNA-binding protein (RBP) in the respective 3'UTR, with SNPs that occur within 5 base pairs or directly at RBP sites selected. Site directed mutagenesis primers were designed using the NEB Webtool (https://nebasechanger.neb.com), and sequencing primers were used to amplify the region of interest to verify if successful mutagenesis has occurred, generating the correct construct.

The selected SNPs and the associated RBPs generated using RBPmap database are highlighted in Table 3.2.2. The in silico generation of putative RBPs that associate with the 3'UTR claudin-5 SNPs of interest is given. Over 18 unique RBPs have been given, which would indicate that there ae various regulatory and mechanistic pathways involved at the

3'UTR, so each SNP could potentially promote dysfunction in different pathways, and are not all involved in the same signal transduction pathways. Some RBPs are common between SNPs though, such as SRSF3 between rs10314 and 1053640, PTBP1 between rs10314 and rs111760583, HNRNPL between rs1053641 and rs1053640, PABPC3 between rs1053641 and rs1053640, SRSF1 between rs1053641 and rs200564626, YBX1 between rs1053640 and rs45485695, YBX2 between rs1053640 and rs45485695, DUG-BP between rs11551256, rs200564626, and rs1053675, MBNL1 between rs200564626 and rs1053675, which may indicate some shared pathways between 3'UTR claudin-5 SNPs.

RBP: Results for chr22:19510547-19511121: - Strand 575 bp long CLDN5 3'UTR sequence	**UTR**	**SNP**	**SNP Direct Overlap with RBP, or Flanking it (within 5bp)**	**Exact Position of SNP on 3' UTR coding region (cDNA) Position in RBPmap/NCBI Database, and AURA Database**	**Genomic Position (NCBI HGVS)**
N/A	3'	rs10314	Direct Overlap	NCBI/RBPmap, 404; C in the place of G AURA 171	Chr22:19510718
SRSF3(Hs/Mm) ZCRB1(Hs/Mm) PTBP1(Hs/Mm)			Flanking		
SRRM4 (from AURA)	3'	rs1053641	Direct Overlap	NCBI/RBPmap 394: A in the place of G AURA 181	Chr22:19510728
HNRNPA1(Hs/Mm) HNRNPL(Hs/Mm) PABPC3(Hs/Mm) SRSF1(Hs/Mm)			Flanking		
SRSF3 (Hs/Mm) HNRNPL(Hs/Mm)	3'	rs1053640	Direct Overlap	NCBI/RBPmap 387: C in the place of A AURA 188	chr22:19510735
SRSF7(Hs/Mm) YBX1 (Hs/Mm) YBX2 (Hs/Mm) PABPC3(Hs/Mm)			Flanking		
N/A	3'	rs45485695	Direct Overlap	NCBI/RBPmap 378: G in the place of A AURA 197	chr22:19510744
SRSF9(Hs/Mm) YBX1(Hs/Mm) YBX2(Hs/Mm)			Flanking		
N/A	3'	rs11551256	Direct overlap	NCBI/RBPmap, 306: T in the place of C AURA 269	chr22:19510816
RBFOX1(Hs/Mm) CUG-BP(Hs/Mm			Flanking		
CUG-BP(Hs/Mm) MBNL1(Hs/Mm) SRSF1(Hs/Mm) SRSF2(Hs/Mm)	3'	rs200564626	Direct Overlap Flanking	NCBI/RBPmap, 19: A in the place of G AURA 556	chr22:19511103
SRSF2(Hs/Mm) TRA2B(Hs/Mm)					
N/A	3'	rs1053675	Direct Overlap	NCBI/RBPmap, 520: A in the place of G AURA 55	Chr22: 19510602
MBNL1(Hs/Mm) CUG-BP(Hs/Mm)			Flanking *(6 bp away)		
N/A	3'	rs111760583	Direct Overlap	NCBI/RBPmap, 573: A in the place of T AURA 2	Chr22: 19510549
PTBP1(Hs/Mm)			Flanking		

Table 3.2.2: Data obtained from RBPmap database, where the 3'UTR CLDN5 coordinates were input, and a list of RNA-binding proteins were generated. 3'UTR CLDN5 SNPs were selected to generate constructs for based on proximity to various RNA-binding proteins (RBPs) listed in the table above (within 5 base pairs)

Next, the sequencing primers described in Fig 3.2.1.C. were used to amplify the sequence of interest on the generated plasmids that express the human claudin-5 cDNA and 3'UTR sequence, each with one of the seven selected SNPs generated via site-directed mutagenesis on the native construct. The sequences for the generated constructs were then compared to that of the original native construct using BLAST alignment, and the successful single base change expressing the SNP of interest in the claudin-5 3'UTR was observed, shown in Fig 3.2.3. Once the plasmid constructs were generated, screening of claudin-5 expression was carried out.

rs200564626

```
Query  726   GGGCGCTGGGCACGGCCGAGCCCCTCCTGCCAGCCACGCCTGCGAGGCGTTGGATAAGCC  785
              |||||||||||||||||| ||||||||||||||||||||||||||||||||||||||||
Sbjct  1     GGGCGCTGGGCACGGCCGGGCCCCTCCTGCCAGCCACGCCTGCGAGGCGTTGGATAAGCC  60

Query  786   TGGGGAGCCCCGCATGGACCGCGGCTTCCGCCGGGTAGCGCGGCGCGCAGGCTCCTCGGA  845
              ||||||||||||||||||||||||||||||||||||||||||||||||||||||||||||
Sbjct  61    TGGGGAGCCCCGCATGGACCGCGGCTTCCGCCGGGTAGCGCGGCGCGCAGGCTCCTCGGA  120

Query  846   ACGTCCGGCTCTGCGCCCCGACGCGGCTCCTGGATCCGCTCCTGCCTGCGCCCGCAGCTG  905
              ||||||||||||||||||||||||||||||||||||||||||||||||||||||||||||
Sbjct  121   ACGTCCGGCTCTGCGCCCCGACGCGGCTCCTGGATCCGCTCCTGCCTGCGCCCGCAGCTG  180

Query  906   ACCTTCTCCTGCCACTAGCCCGGCCCTGCCCTTAACAGACGGAATGAAGTTTCC-TTTCT  964
              |||||||||||||||||||||||||||||||||||||||||||||||||||| |||||
Sbjct  181   ACCTTCTCCTGCCACTAGCCCGGCCCTGCCCTTAACAGACGGAATGAAGTTTCCTTTTCT  240

Query  965   GTGCGCGGCGCTGTTTCCATAGGCAGAGCGGGNNTCAGACTGAGG  1009
              |||||||||||||||||||||||||||||||  ||||||||||||
Sbjct  241   GTGCGCGGCGCTGTTTCCATAGGCAGAGCGGGTGTCAGACTGAGG  285
```

rs45485695

```
Query  17    GCCACGCCTGCGAGGCGTTGGATAAGCCTGGGGAGCCCCGCATGGACCGCGGCTTCCGCC  76
             ||||||||||||||||||||||||||||||||||||||||||||||||||||||||||||
Sbjct  33    GCCACGCCTGCGAGGCGTTGGATAAGCCTGGGGAGCCCCGCATGGACCGCGGCTTCCGCC  92

Query  77    GGGTAGCGCGGCGCGCAGGCTCCTCGGAACGTCCGGCTCTGCGCCCCGACGCGGCTCCTG  136
             ||||||||||||||||||||||||||||||||||||||||||||||||||||||||||||
Sbjct  93    GGGTAGCGCGGCGCGCAGGCTCCTCGGAACGTCCGGCTCTGCGCCCCGACGCGGCTCCTG  152

Query  137   GATCCGCTCCTGCCTGCGCCCGCAGCTGACCTTCTCCTGCCACTAGCCCGGCCCTGCCCT  196
             ||||||||||||||||||||||||||||||||||||||||||||||||||||||||||||
Sbjct  153   GATCCGCTCCTGCCTGCGCCCGCAGCTGACCTTCTCCTGCCACTAGCCCGGCCCTGCCCT  212

Query  197   TAACAGACGGAATGAAGTTTCCTTTTCTGTGCGCGGCGCTGTTTCCATAGGCAGAGCGGG  256
             ||||||||||||||||||||||||||||||||||||||||||||||||||||||||||||
Sbjct  213   TAACAGACGGAATGAAGTTTCCTTTTCTGTGCGCGGCGCTGTTTCCATAGGCAGAGCGGG  272

Query  257   TGTCAGACTGAGGATTTCGCTTCCCCTCCAAGACGCTGGGGGTCTTGGCTGCTGCCTTAC  316
             ||||||||||||||||||||||||||||||||||||||||||||||||||||||||||||
Sbjct  273   TGTCAGACTGAGGATTTCGCTTCCCCTCCAAGACGCTGGGGGTCTTGGCTGCTGCCTTAC  332

Query  317   TTCCCAGAGGCTCCTGCTGACTTCGGAGGGGCGGATGCAGAGCCCGGGGCCCCCACCGGA  376
             |||||||||||||||||||||||||||||||||||||||||||| ||||||||||||||
Sbjct  333   TTCCCAGAGGCTCCTGCTGACTTCGGAGGGGCGGATGCAGAGCCCAGGGCCCCCACCGGA  392

Query  377   AGATGTGTACAGCTGGTCTTTACTCCATCGGCAGGGCCCGAGCCCAGGGACCAGTGACTT  436
             ||||||||||||||||||||||||||||||||||||||||||||||||||||||||||||
Sbjct  393   AGATGTGTACAGCTGGTCTTTACTCCATCGGCAGGGCCCGAGCCCAGGGACCAGTGACTT  452

Query  437   GGCCTGGACCTCCCGGTCTCACTCCAGCATCTCCCCAGGCAAGGCTTGTGGGCACCGGAG  496
             ||||||||||||||||||||||||||||||||||||||||||||||||||||||||||||
Sbjct  453   GGCCTGGACCTCCCGGTCTCACTCCAGCATCTCCCCAGGCAAGGCTTGTGGGCACCGGAG  512

Query  497   CTTGAGAGAGGGCGGGAGTGGGAAGGCTAAGAATCTGCTTAGTAAATGGTTTGAACTCTC  556
             ||||||||||||||||||||||||||||||||||||||||||||||||||||||||||||
Sbjct  513   CTTGAGAGAGGGCGGGAGTGGGAAGGCTAAGAATCTGCTTAGTAAATGGTTTGAACTCTC  572

Query  557   TCC  559
             |||
Sbjct  573   TCC  575
```

rs1053640

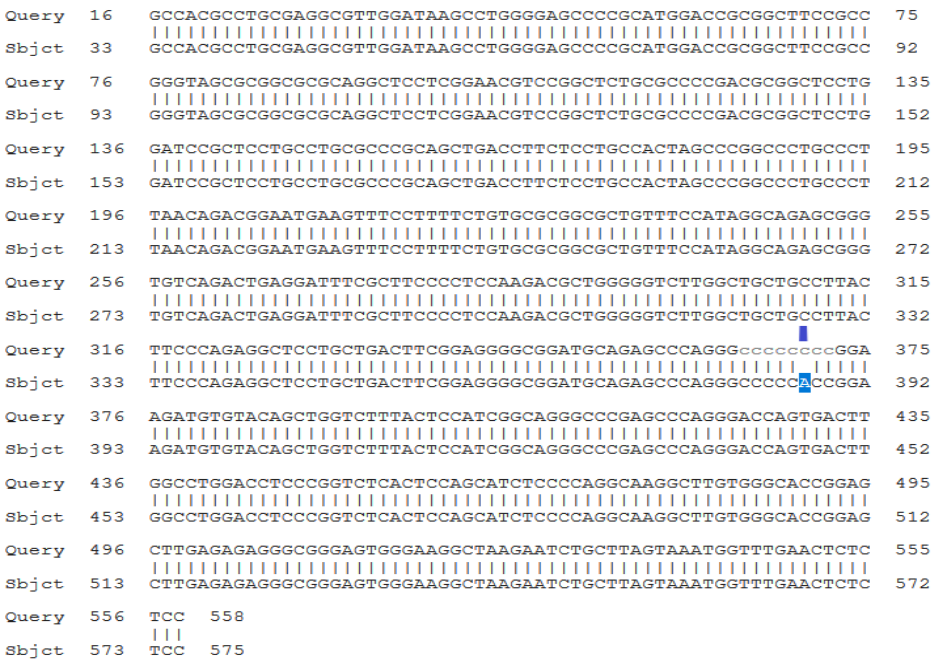

rs1053641

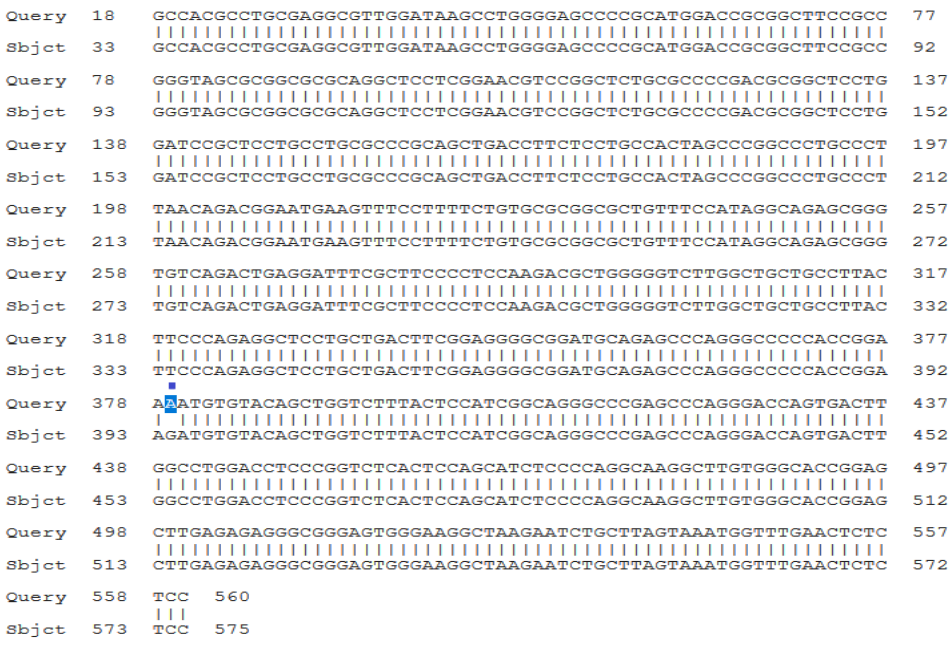

rs11551256

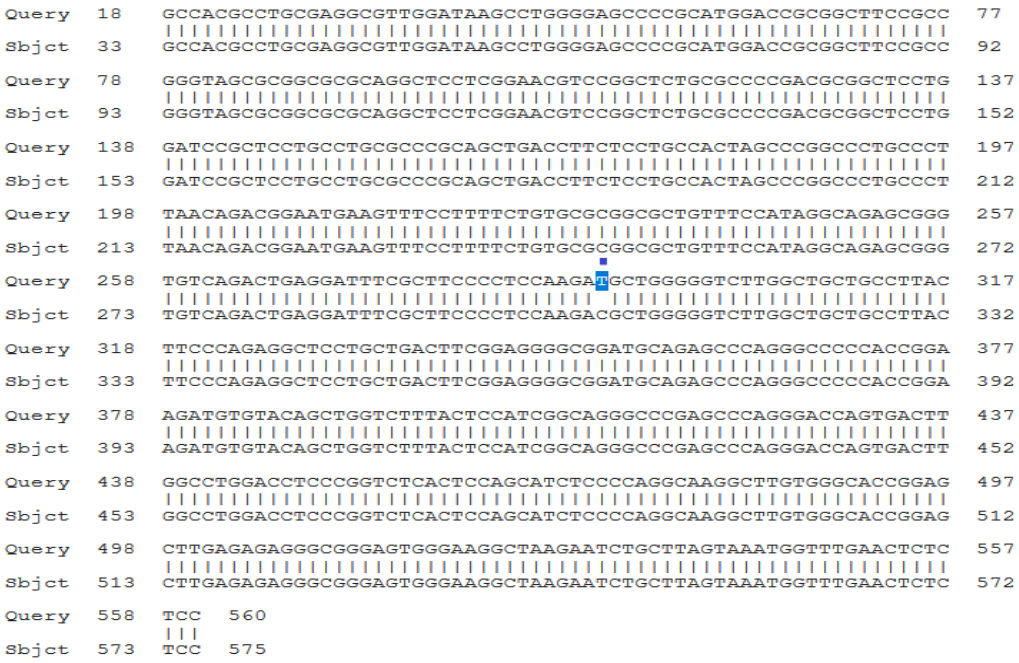

rs111760583

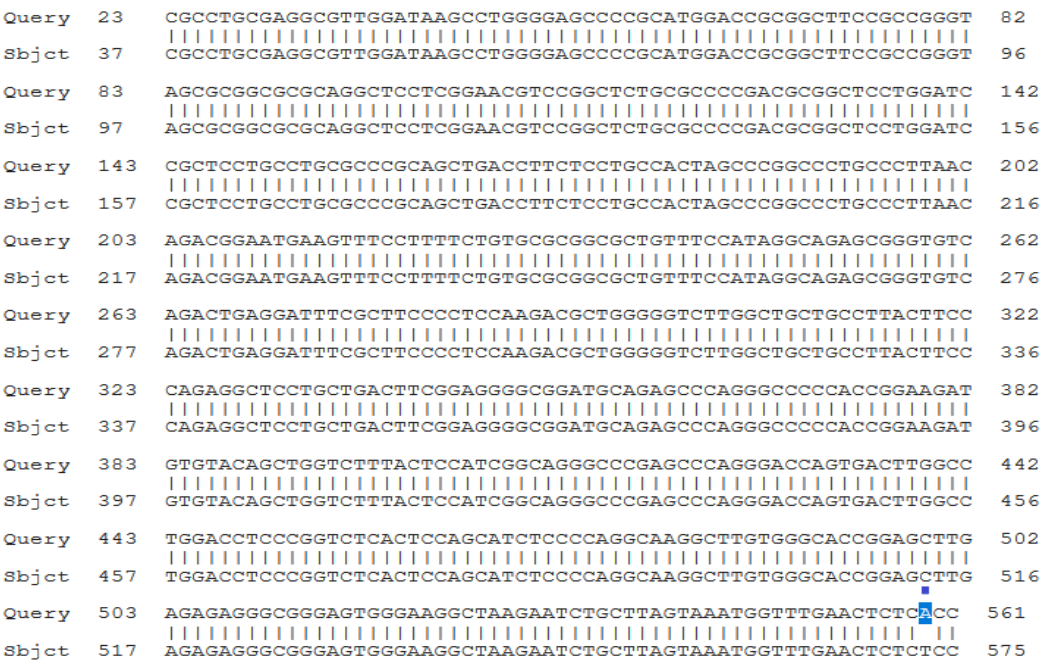

rs1053675

Figure 3.2.3 : BLAST alignments confirming correct 3'UTR CLDN5 SNP constructs have been generated. Original native human CLDN5 construct blasted against the sequenced constructs generated via site-directed mutagenesis on the native construct. Subject= Original native human claudin-5 cDNA+3'UTR sequence, Query=Sequence of site-directed mutagenesis generated human claudin-5 cDNA+3'UTR SNP expressing sequence (sequenced by Source Biosciences, Ireland)

Along with untransfected and pcDNA3-EGFP Empty Vector (Addgene) and native human claudin-5 cDNA+3'UTR (Native) construct controls, HeLa cells were transfected with 500 ng of each plasmid expressing the various 3'UTR claudin-5 single nucleotide polymorphisms, and protein expression was characterized, as shown in Fig 3.2.4. As HeLa cells do not endogenously express claudin-5, this transfection experiment reveals the phenotype of the mutant 3'UTR claudin-5 constructs in the absence of normal tight junction components and wild type claudin-5. Clear differences in claudin-5 protein expression patterns are observed (claudin-5 protein expression is calculated relative to either 24 or 48 hours post transfection relative to the native claudin-5 construct, and normalized to ß-actin). Significant reductions in claudin-5 expression were observed after 24 hours for rs45485695 (*$p<0.05$), for rs111760583 (**$p<0.01$), and for rs1053640 (***$p<0.001$). Also, significant reduction in claudin-5 protein expression was observed after 48 hours for rs200564626 and rs11551256 (*$p<0.05$). There are also reductions in claudin-5 expression levels rs200564626 and rs1053675 after 24 hours, and for rs111760583 after 48 hours. The data reveals that there is abnormal claudin-5 expression for certain selected 3'UTR SNPs in claudin-5 compared to that of native claudin-5 expression.

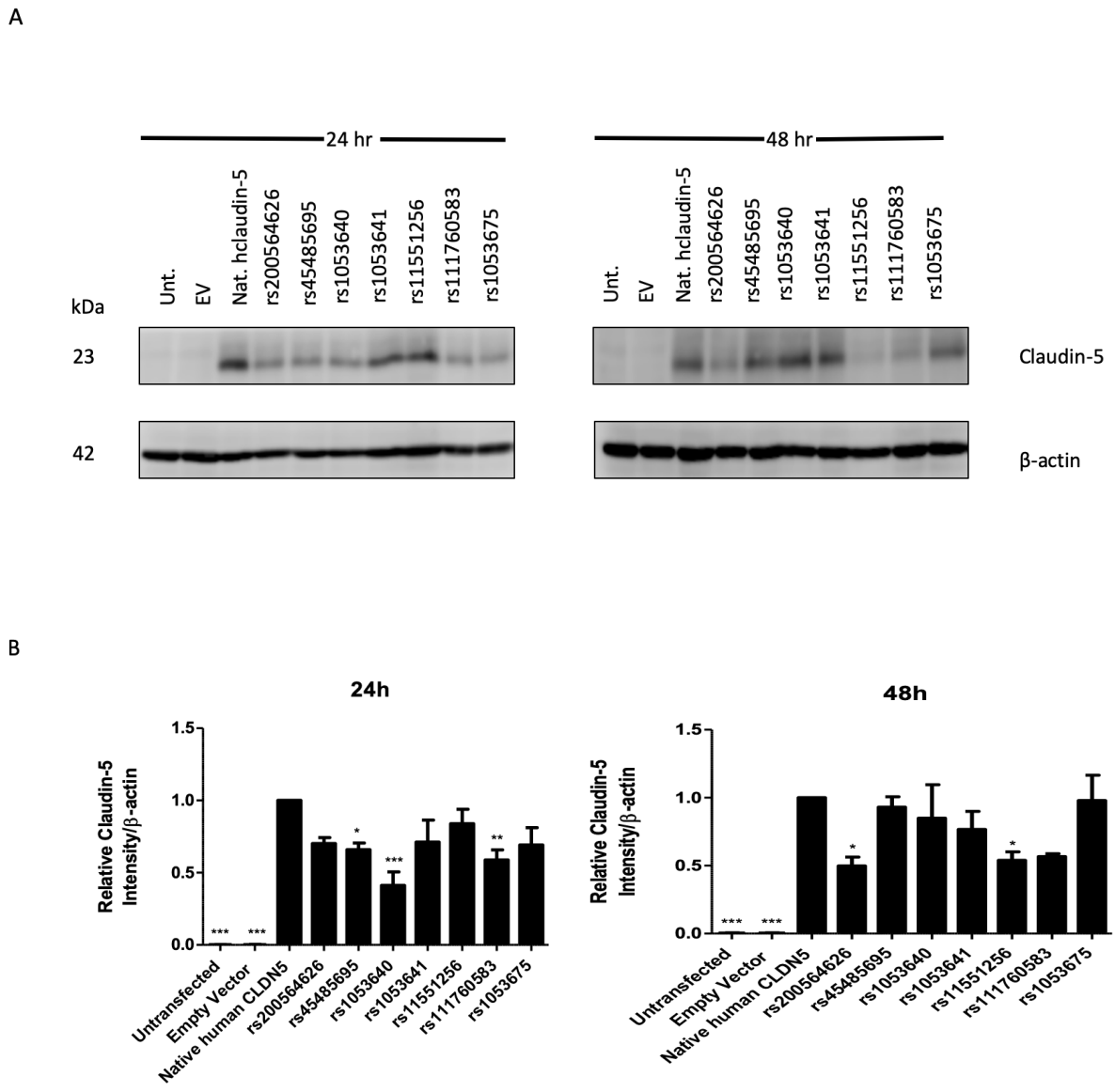

Figure 3.2.4: HeLa cells were transfected when approximately 70% confluent, with 500 ng of each respective plasmid using Lipofectamine® 2000 Reagent for 24 and 48 hours, and show variation in claudin-5 protein expression levels. **A)** Representative Western blot image for 24 and 48 hours post transfection, immunoblotting for claudin-5, with ß-actin loading control. Layout: Untransfected, pcDNA3-EGFP Empty Vector (EV), pcDNA3-EGFP native human claudin-5, rs200564626, rs45485695, rs1053640, rs1053641, rs11551256, rs111760583, rs1053675. **B)** Densitometry analysis: Transfection experiments were repeated in three independent biological replicates (n = 3), and were analysed individually in technical triplicates. Densitometry analysis graphs shown are for the compiled technical triplicate analysis for all 3 individually analysed biological replicates combined. Relative protein intensity is calculated using native human CLDN5 as control, at 24 and 48 hours respectively, and normalized to ß-actin. Statistical analysis was done using one-way ANOVA, with Dunnett's post-test compared to native human CLDN5 transfected control, *$p<0.05$, **$p<0.01$, ***$p<0.001$.

Next, immunocytochemistry staining was performed in order to assess the claudin-5 protein localization for these various SNPs. First, HeLa cells were seeded in a subconfluent monolayer on Collagen I coated glass coverslips, transfected with 500 ng of pcDNA3-EGFP Empty Vector plasmid, and the native human claudin-5 cDNA+3'UTR plasmid, (previously described), as well as untransfected cells, and fixed in methanol. Only the nuclei were stained with DAPI, and it was found that methanol fixation does not preserve the GFP signal in the plasmid backbone in these cells, shown in Appendix A after both 24 and 48 hours post transfection in cells. Thus, this indicates that the claudin-5 protein could be stained with AF488, and the protein and backbone signals would not overlap, as a result only highlighting presence of claudin-5 in these cells. Immunocytochemistry staining in HeLa cells was performed, to show claudin-5 protein localization in cells that do not endogenously express claudin-5, to understand how the mutations in the 3'UTR of claudin-5 may affect it's localization without presence of endogenous tight junction components to affect localization patterns.

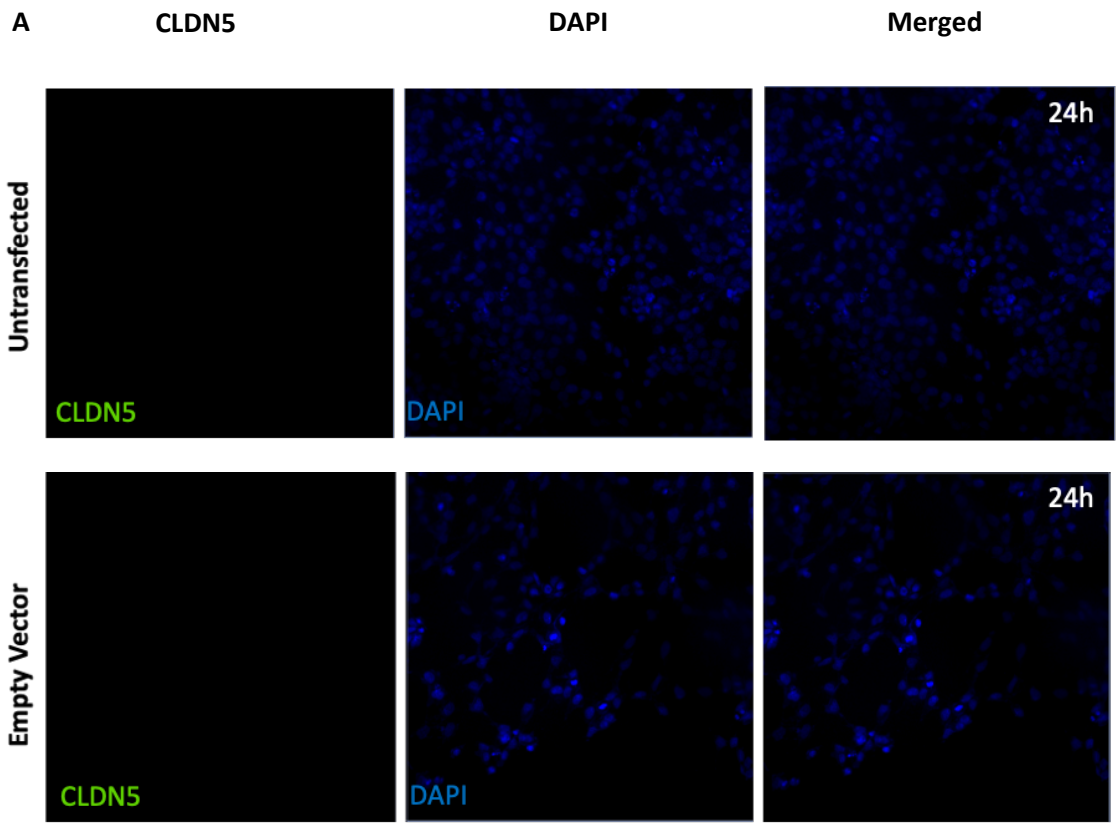

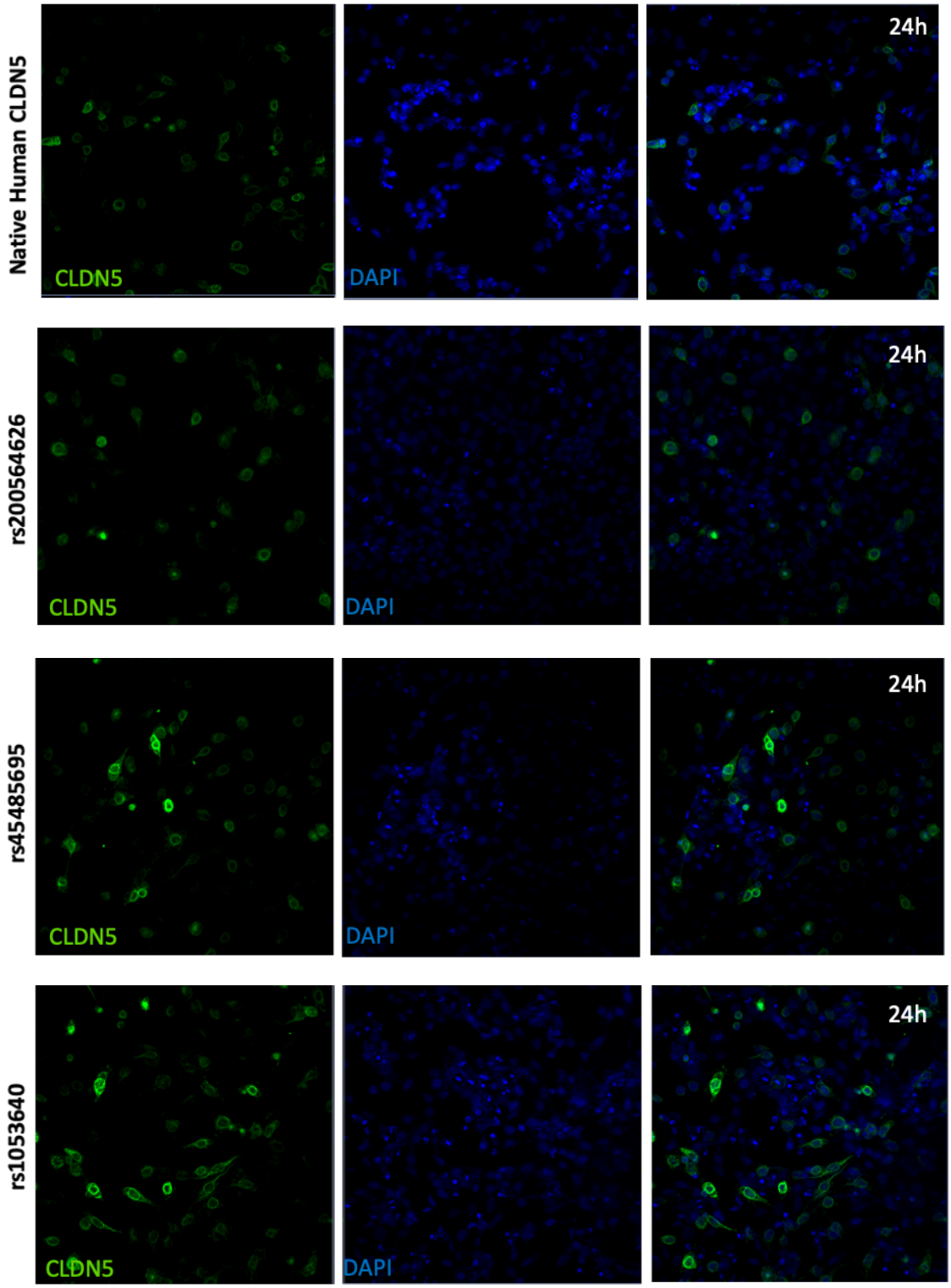
Native Human CLDN5
CLDN5
DAPI
24h
rs200564626
CLDN5
DAPI
24h
rs45485695
CLDN5
DAPI
24h
rs1053640
CLDN5
DAPI
24h

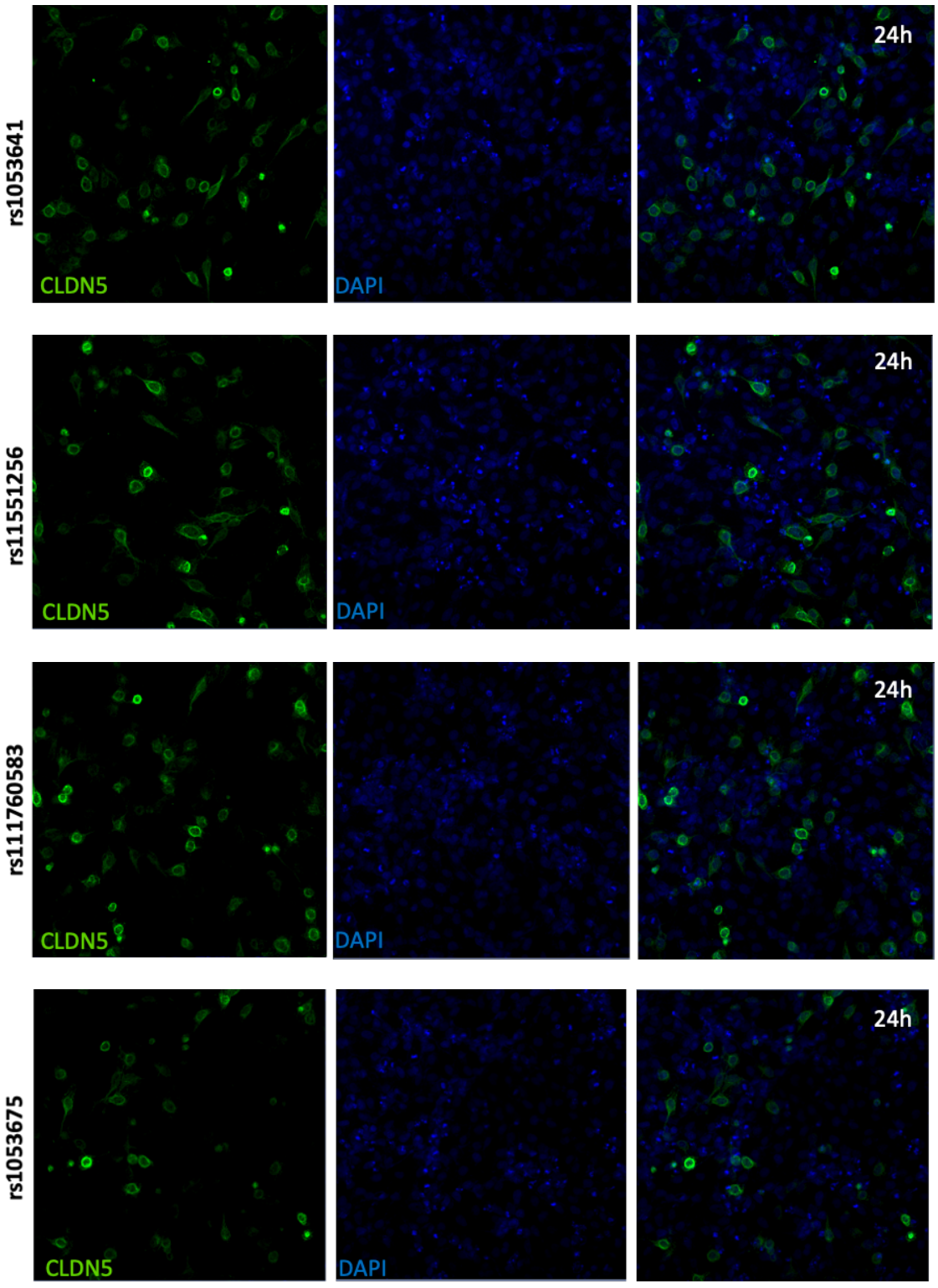
rs1053641
CLDN5
DAPI
24h
rs11551256
CLDN5
DAPI
24h
rs111760583
CLDN5
DAPI
24h
rs1053675
CLDN5
DAPI
24h

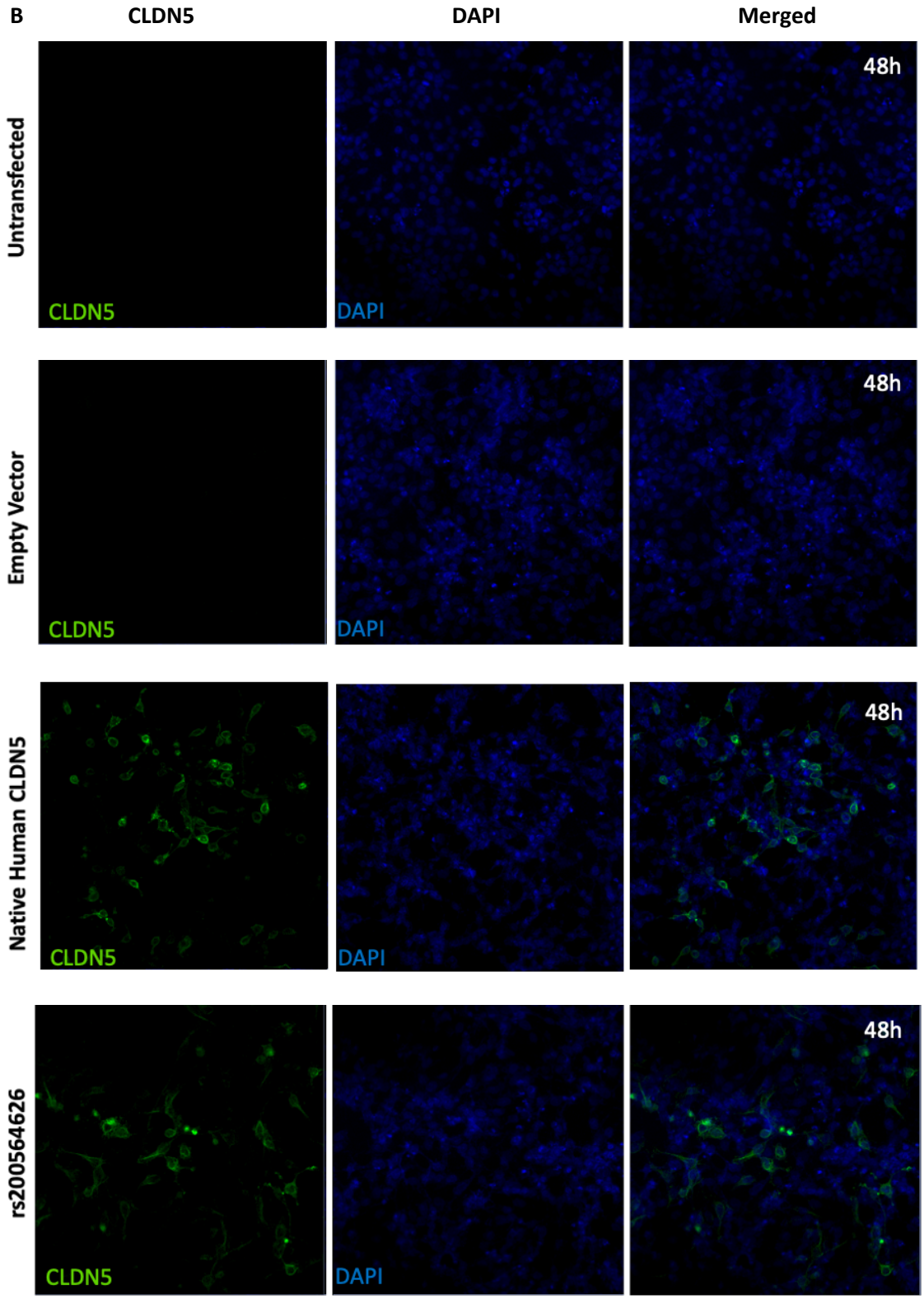
B
CLDN5
DAPI
Merged
Untransfected
Empty Vector
Native Human CLDN5
rs200564626
48h
CLDN5
DAPI

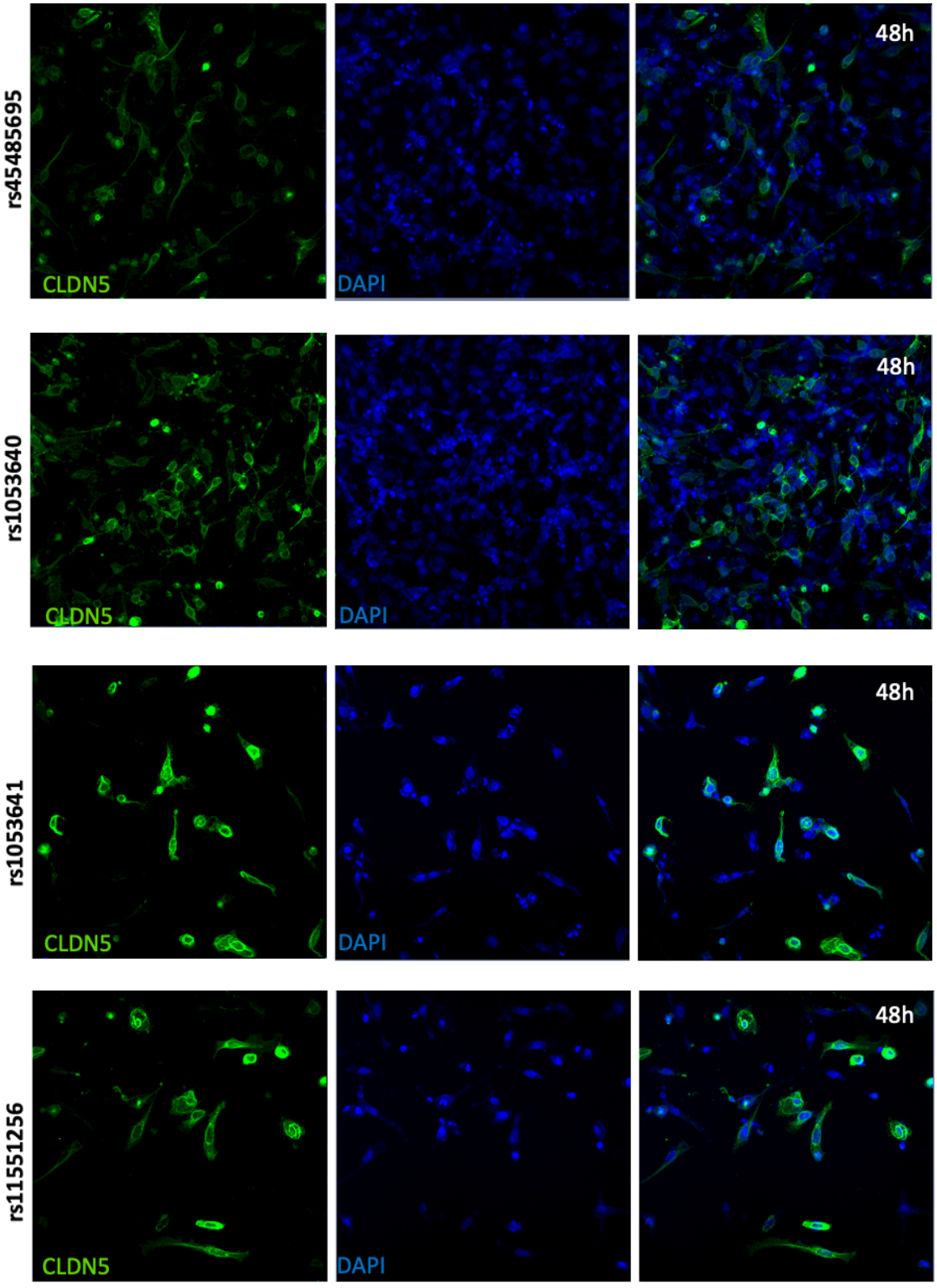
rs45485695
CLDN5
DAPI
48h
rs1053640
CLDN5
DAPI
48h
rs1053641
CLDN5
DAPI
48h
rs11551256
CLDN5
DAPI
48h

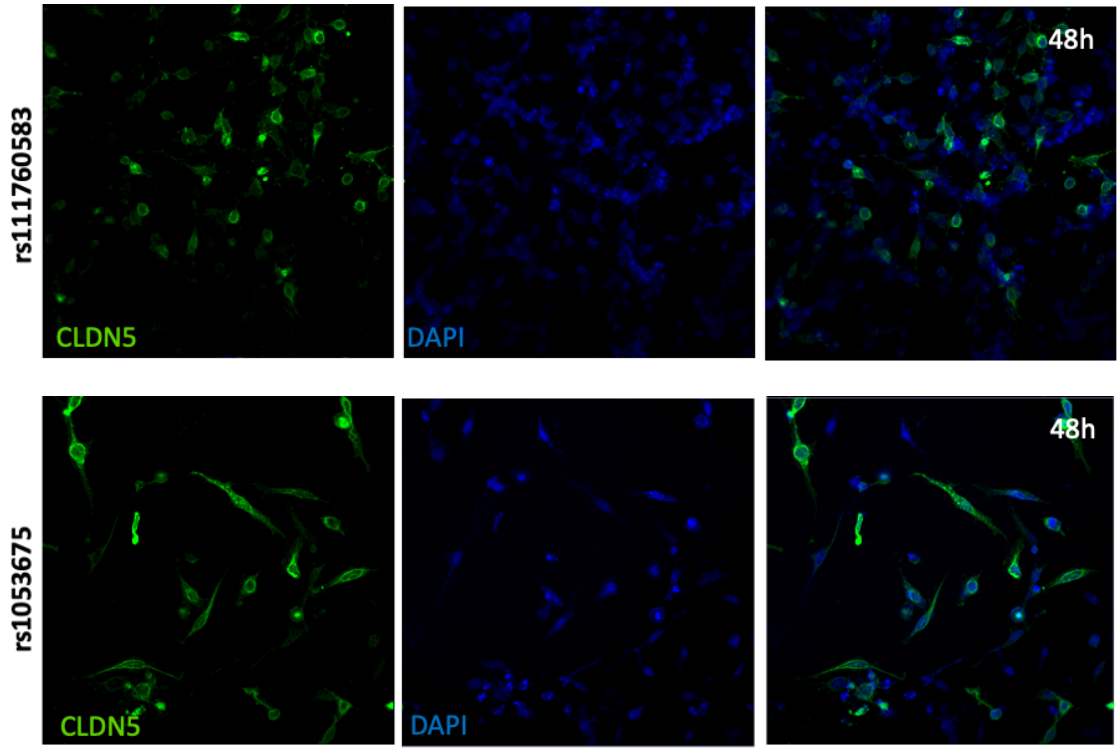

Fig 3.2.5: Immunocytochemistry staining of 3'UTR claudin-5 SNP plasmid transfection in HeLa cells shows claudin-5 protein localization. Representative Image, HeLas were cultured on Collagen I coated coverslips and transfected with 500 ng each of pcDNA3-EGFP Empty Vector, pcDNA3-EGFP human native CLDN5 plasmid, rs200564626, rs45485695, rs1053640, rs1053641, rs11551256, rs111760583, and rs1053675, and untransfected cells for **A)** 24 hours and **B)** 48 hours and fixed ice-cold Methanol, and nuclei were stained with DAPI (Blue), claudin-5 stained with AF488 (Green) and visualized at 20X on a confocal microscope under uniform parameters.

In Figure 3.2.5.A which shows cells 24 hours after transfection, for all of the 3'UTR claudin-5 SNP constructs, much of the protein localization appears to be congregated in the cytoplasm and around the nucleus, instead of at the cell membrane where normally tight junctions are expressed. Although it would be expected that there would be localization at the membrane for native claudin-5 transfected cells, it largely remains localized to the nucleus and cytoplasm as well. This same pattern of claudin-5 localization also appears to be taking place at 48 hours post transfection in HeLa cells, shown in Fig 3.2.5.B. It is also important to note that the transfection efficiency in these cells appears to be low, as even for the native CLDN5 transfected cells, the presence of claudin-5 is not apparent in all cells, as there are plenty of cells where only the stained nuclei is visible, but there is no claudin-5 present; the native CLDN5 transfected cells at 24 and 48 hours reveal approximately 29% and 21% claudin-5 positive stained cells, calculated by counting positive claudin-5 cells and dividing by the total number of DAPI stained cells and averaging 3 technical replicates. This may affect the interpretation of the results, as there is not a high enough transfection efficiency, and proper function of claudin-5 required heterotypic interaction between the extracellular loops of

claudin-5 on opposing plasma membranes (Rossa *et al.*, 2014; Daugherty *et al.*, 2007). There is not a lot of tight junction strand formation in these cells, except for in certain cases like 48 hours after transfection for rs1053675. The levels of claudin-5 protein expression mostly do not appear to change based on the staining data, compared to the Western blot data, but it is important to note that the proteins stained in the immunocytochemistry experiments were not solubilized, whereas the proteins for the Western blot experiment were solubilized and then separated on a gel for visualization; thus, the fixed proteins could be involved in different regulatory processes such as in lysosomes and in proteasomes, and could potentially be why the expression levels do not appear to be changing, as the protein is not present in its final processed form and present at the membrane in tight junctions. Implications of these results will be discussed in the next section**.**

Chapter 4: Discussion

4.1 Implications of Results

The focal point of this investigation was to study the physiology of various tight junction components at the BBB. Ultimately, it is known that claudin-5 is a key tight junction component as it is the most enriched component of endothelial TJs (Ohtsuki *et al.*, 2007), and helps mediate tight junction strand formation at the BBB, along with ZO-1, and occludin (Luissint *et al.*, 2012). Also, downregulation, or relocalization and modification of these components has been known to contribute to disease onset, through subsequent dysregulation of the BBB at endothelial TJs; for example, cerebral ischemia results in downregulation of claudin-5, occludin, and ZO-1 at various time points post injury, and results in an increase in BBB permeability (Jiao *et al.*, 2011), and have been found to be downregulated in other instances as well, such as with interaction with reactive oxygen species, and disruption through retroviral infection (Schreibelt *et al.* 2007; Afonso *et al,.* 2007; Luissint *et al.*, 2012). The size selective discrimination of tight junctions through paracellular pathways, allows the BBB to protect the CNS from harmful pathogens and maintain a homeostatic environment through its dynamic nature (Nitta *et al,.* 2003; Pardridge, 2005). BBB dysfunction is also a hallmark of various other neurodegenerative diseases such as Alzheimer's, multiple sclerosis Parkinson's, and schizophrenia (Luissint *et al.*, 2012; Najjar *et al.*, 2017). Evidence indicates that changes in expression in TJ complexes affect BBB permeability and integrity (Luissint et al., 2012). Overall, the aim was to investigate various aspects of tight junction protein regulation, including both circadian regulation, and 3'UTR mediated post-transcriptional and post-translational regulation of claudin-5.

With respect to circadian regulation and the BBB, it has previously been found that claudin-5 is regulated by Bmal1 and the circadian clock, and claudin-5 has also been found to circulate in tissues in a circadian dependent manner, and that this can be recapitulated *in vitro* (Hudson *et al.*, 2019). The goal of this study was to expand on this work and model the circadian rhythm in *in vitro* conditions for an extended period of time (72 hours) using the serum shock protocol outlined by Balsalobre *et al,.* 1998, in order to study the physiology of important tight junction proteins like claudin-5, occludin, and ZO-1, and clock components like Bmal1 at various points in the circadian rhythm. The results showed that the tight junction and clock components analyzed did in fact change expression levels of protein and transcript throughout the assayed period of time in a cyclical manner. This could potentially affect BBB permeability changes in a temporal manner. As the nature of the BBB is dynamic, this provides useful information, as BBB permeability which is modulated by tight junctions is known to

change over time, and our findings confirmed that TJ component expression changes over time (Zhang *et al.*, 2018; Erdő *et al.*, 2017; Hudson *et al.*, 2019).

Future experiments will be beneficial to expanding on the findings of this study. It would be valuable to repeat the extended serum shock experiments, assessing the protein and mRNA expression patterns as well as permeability in hCMEC/D3 cell lines, as these cells model the human endothelial cell lines which comprise the BBB, and would help supplement the data generated from bEnd.3 mouse endothelial cell lines. It has been shown that disruption of circadian elements like Bmal1 in other cell types that interact with the BBB such as pericytes leads to a disruption in BBB integrity (Nakazato *et al.*, 2017). Thus, it would also be valuable to carry out serum shock experiments in the various cell types that make up the NVU, like pericytes, astrocytes, microglia, etc., to understand how circadian rhythms regulate BBB integrity via crosstalk between all of the cell types, and go beyond our understanding of the BBB integrity mediated in endothelial cells via tight junctions. Serum shock is and effective method of inducing the circadian rhythm in cell lines, as cells *in vitro* do not exhibit a circadian rhythm on their own, serum shock has been shown to recapitulate circadian rhythms in a wide variety of cell lines such as endothelial cells (Hudson et al., 2019), human breast epithelial and breast cancer cells (Xiang *et al.*, 2012), fibroblasts (Balsalobre *et al*., 1998), to name a few. Transcripts that do not show circadian regulation do not cycle *in vitro* after induction of circadian rhythm through serum shock, and only components that cycle *in vivo* in circadian rhythms oscillate after serum shock is undergone in cells *in vitro* (Balsalobre *et al.*, 1998). Also, it would be important to perform permeability (flux) assays to characterize BBB permeability at various points in the circadian rhythm modeled by serum shock experiments in different endothelial cell lines. This can be done by culturing cells on Transwell® inserts, and measuring the passage of FITC-dextran tracer molecules across the cell monolayer, at various points after serum shock, to see how BBB permeability corresponds with varying levels of TJ protein expression that has been shown to occur. Particular focus should be placed on studying BBB permeability at both high and low points of claudin-5 expression in the circadian rhythm. Another beneficial dataset to generate would be to perform chromatin immunoprecipitation (CHIP) assays in endothelial cell lines at various points in the circadian rhythm post-serum shock, in order understand the mechanisms involving TJ regulation, and to see if, and how, tight junction components interact with circadian clock components and how this corresponds to BBB permeability. This will prove useful when designing appropriate drug delivery methods that are normally prevented from crossing the BBB tight junctions when its integrity is intact (Chen and Liu, 2012). Instead, points in the circadian rhythm when BBB permeability is increased due to variable TJ protein expression levels can be taken advantage of for drug delivery.

The sleep-wake cycle has also been found to disrupt circadian rhythms, and are affected by many people's lifestyles (He *et al.*, 2014), and sleep disruption is also known to play a role in schizophrenia pathogenesis (Wilson and Argyopoulos, 2012). Incidentally, the next topic of interest after studying circadian and temporal regulation was to study 3'UTR mediated regulation of post-transcriptional and post-translational activity. Functional polymorphisms in the 3'UTR are known to be implicated in schizophrenia pathogenesis (Mohamed *et al.*, 2018), and was an interesting phenomenon to begin exploring as our research transitioned from exploring circadian cycles, to understanding that 3'UTR mediated regulation can have an effect on BBB integrity.

The overall goal of this study is to investigate BBB dysregulation with respect to tight junctions, as this phenomenon of aberrant TJ phenotypes is a distinctive feature of neurological diseases. Recent studies show that the rs10314 3'UTR single nucleotide polymorphism in claudin-5 is associated weakly with schizophrenia in Han Chinese and Iranian populations (Sun *et al.*, 2004) (Omidinia *et al.*, 2014). Further work by Greene *et al.*, 2018 revealed that presence of this polymorphism reduces claudin-5 expression by up to 50%, and when this SNP is present in patients that also have 22q11 deletion syndrome, claudin-5 expression can be downregulated by up to 75%. Given this information regarding the link between the 3'UTR polymorphisms and neurological disease pathogenesis of diseases like schizophrenia, and the significant effect that rs10314 has on claudin-5 expression which is a key TJ component that mediates BBB integrity, the goal of the investigation was to screen the claudin-5 phenotype of various other SNPs in the 3'UTR claudin-5 region to determine whether they also contribute to abrogated claudin-5 expression. We selected SNPs of interest in the claudin-5 3'UTR through cross-referencing them with prospective RNA-binding proteins (RBPs) through *in silico* analysis that may potentially interact with the 3'UTR *cis* elements, and lead to post-transcriptional and post-translational modifications. The results revealed that after transfection of plasmids expressing various 3'UTR claudin-5 SNPs, protein expression levels differed significantly for several SNPs when transfected in HeLa cells, which do not express endogenous claudin-5. This suggests that further exploration of the 3'UTR of claudin-5 would yield valuable information about the nature of the *cis*-elements in the 3'UTR, regarding these polymorphisms, and the post-transcriptional and post-translational mechanisms in which they affect claudin-5 expression, especially through interactions with RBPs.

An interesting pattern emerged with the Lipofectamine® 2000 mediated transfection of 3'UTR claudin-5 SNP expression plasmids in HeLa cells, which revealed decreases in protein expression patterns for various SNPs. However, often the level of expression differed between 24 hours and 48 hours post transfection in these cells. The reason may be due to the fact that

there are changes in the rates of translation over time, as the nature of the BBB is dynamic. Also, as the nature of this transfection is transient, and differences in cellular metabolism and processing of the introduced plasmids could also be why expression patterns of claudin-5 change over time; overall, reduction in expression was observed in the Western blots for various SNPs compared to native claudin-5 expression. Also, it is important to note that the immunocytochemistry studies did not reveal much change in claudin-5 expression levels, as compared with the Western blotting data. However, the transfection efficiency appeared to be very low, as claudin-5 was not present in a majority of the cells, including both for 3'UTR claudin-5 SNP transfected cells, as well as native claudin-5 plasmid transfected cells. The majority of cells expressed only the stained nuclei signal, with a fewer number of cells expressing claudin-5, largely in the cytoplasm. The resulting low transfection efficiencies can be a result of several factors. The Lipofectamine® 2000 reagent used for transfections has been shown to result in cytotoxicity, particularly when used in high amounts, while lower amounts of this reagent result in lower transfection efficiencies (Avci-Adali *et al.*, 2014). Incubating endothelial cells along with Lipofectamine® 2000 has also been shown to reduce cell viability for longer periods of time such as 48 hours compared with 24 hours, even though longer periods of incubation time can increase transfection efficiency (Hunt *et al.*, 2010). Reproducible transfection efficiency of up to 19 ± 9% for Lipofectamine® 2000 was shown in endothelial cells (Hunt *et al.*, 2010), which can explain the lower transfection efficiencies observed in this study. Other factors relevant to this study that affect transfection efficiencies are cell type, confluence of cells, size of vector, the ratio of DNA to transfection reagent when forming complexes, and incubation time of complex with cells (Hunt *et al.*, 2010) (Colosimo *et al.*, 2000); dosage curves have been successfully employed as a means of optimizing the transfection of the foreign component into the cells of interest (Avci-Adali *et al.*, 2014). Optimization experiments can be conducted by testing various transfection conditions described above with the desired conditions to improve the efficiency for each cell type. As claudin-5 is known to require heterotypic interactions between the extracellular loops of claudin-5 on opposing plasma membrane to form appropriate tight junction strands and contribute to BBB integrity (Rossa *et al.*, 2014; Daugherty *et al.*, 2007; Piontek *et al.*, 2008), this low transfection efficiency and resulting dearth of claudin-5 might have prevented proper claudin-5 interactions and aggregation at the plasma membrane, and could be the reason that much of the claudin-5 localization is limited to the cytosol and nuclei in these cells. Claudin-5 would not be available to aggregate at the BBB and promote proper TJ strand formation, making this difficult to model and study. It is clear that this is a limitation in the transfection model of claudin-5 3'UTR SNP plasmid phenotype assessment, and a better model can be developed.

Rather than use HeLa cells which do not express endogenous tight junction components such as claudin-5 in order to assess the differences in claudin-5 protein expression of 3'UTR SNPs in claudin-5, it would be better to study hCMEC/D3 or bEnd.3 cell lines which model the human and mouse endothelial cell lines at the BBB respectively. It is important to note that the hCMEC/D3 cell line expresses low TEER values, and transcriptomic profiling of these cells lower expression levels of key tight junction genes such as claudin-5 and occludin compared to mouse cells (Urich *et al.*, 2012). However, optimized co-culture conditions with glial cells in various *in vitro* models has been shown to increase claudin-5 levels in hCMEC/D3 cells to overcome these limitations (Cooper *et al.*, 2011). It has been revealed that the 3'UTR isoform expression is cell-type specific in nature, and it is actually recommended that cell sorting into pure populations before profiling would lead better quantification of the target phenotype of interest than using mixed populations (Lianoglou *et al.*, 2013; Mayr, 2018). Thus, it would be a better assessment model to use CRISPR mediated base pair editing to introduce the desired SNP into the genome in the 3'UTR region of claudin-5, and Cas9/gRNA complexes can be efficiently introduced to cells using lipofectamine (Yu *et al.*, 2016), and then use a technique like limited dilution in order to isolate single cell clones expressing the desired mutation, and expand these clones into stable cell lines after the sequence has been verified. Then, using these uniform populations, where all of the cells permanently express the desired 3'UTR SNP in claudin-5, between Western blots and immunocytochemistry studies, the data will provide a more realistic and holistic picture of the effect of the polymorphisms on protein expression, localization, and BBB physiology, as theoretically, every cell would contain claudin-5, and would be available to interact across membranes, and more accurately model BBB function as it exists *in vivo*. These single cell clone populations can also be made for other 3'UTR TJ components in the future, like occludin, and ZO-1. It will also be important to repeat Western blotting protein characterization experiments with the generated cell lines, in order to reduce the error bars among the biological replicates that was observed.

Some other useful experiments to perform will be to perform qPCR analysis on reverse transcription derived cDNA, in order to assess the level of claudin-5 transcript, and determine whether the 3'UTR polymorphisms affect post-transcriptional changes in expression. It will also be important to perform polysome analysis to identify mRNA complexes that are undergoing translation, and the effect that 3'UTR SNPs have on this process (Chassé *et al.*, 2017). It will also be imperative to perform RNA/protein pulldown assays (Panda *et al.*, 2016), preferably in the generated cell lines each expressing different 3'UTR SNPs in claudin-5, in order to identify RNA-mediated protein complex formation with RNA-binding proteins, and also to compare the results to our *in silico* analysis that identified putative RBPs that bind to the SNP sites in the 3'UTR, which will give us a better idea as to how the transcriptional and

translational regulatory machinery is impacted by these *cis* elements on the 3'UTR. Finally, it will also be necessary to compare the *in vitro* data obtained from these experiments, and compare it to the observed trends gleaned from patient data, and determine how the physiology of these SNPs is manifested in the general population. This will help determine the overall mechanisms involved in 3'UTR post-transcriptional and post-translational regulation of claudin-5, a key TJ component of the BBB.

Overall, the conclusions that can be made from this investigation are that **1)** tight junction and clock components cycle in a time-dependent manner, and levels vary throughout the day, which can conceivably affect BBB permeability and **2)** various single nucleotide polymorphisms at the 3'UTR of claudin-5 can abrogate its expression and potentially contribute to disease pathogenesis. The interface of temporal regulation and post-transcriptional and post-translational regulation mediated by circadian rhythms and 3'UTR, involving key tight junction proteins, can have an overall effect on BBB integrity, which is dynamic, and this information can potentially be taken advantage of to dispense neurotherapeutics across the BBB.

APPENDIX A

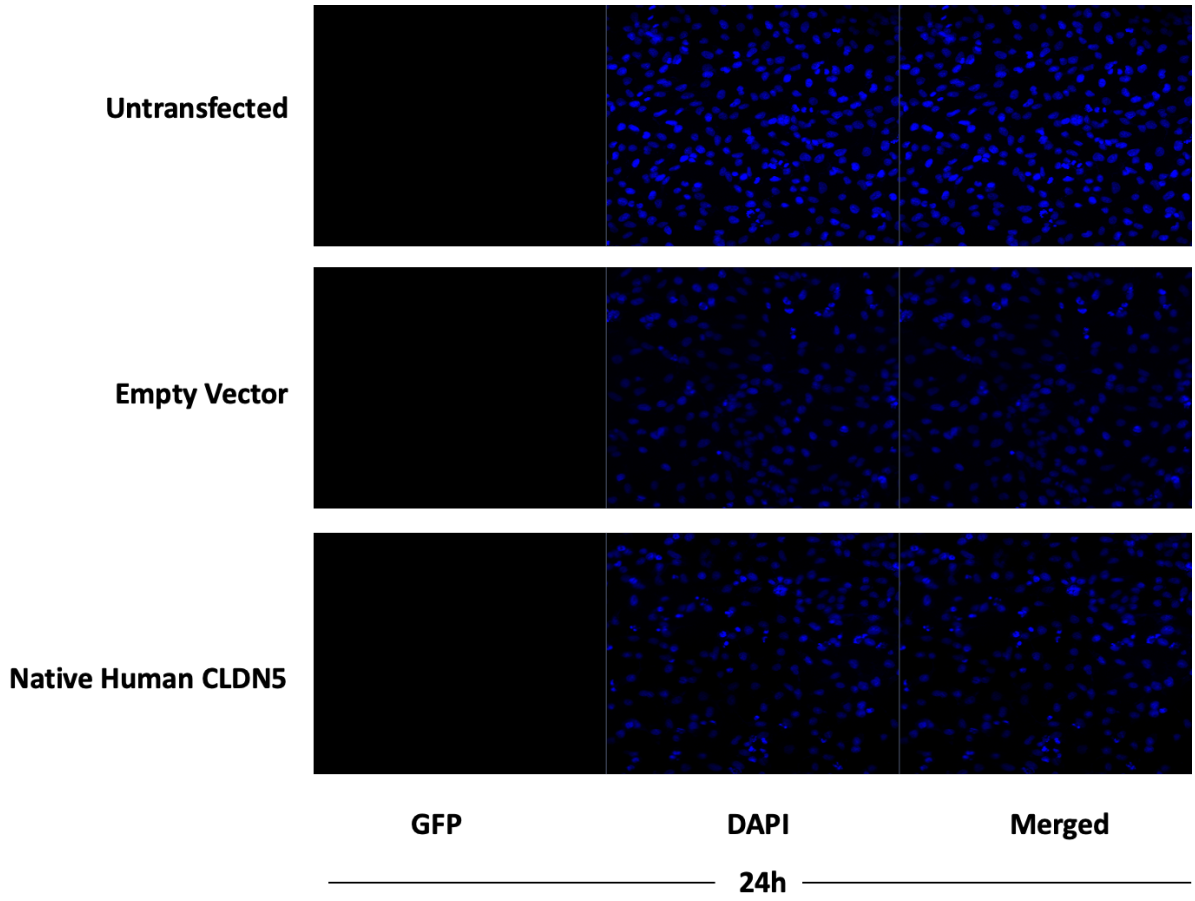
Untransfected
Empty Vector
Native Human CLDN5
GFP
DAPI
Merged
24h

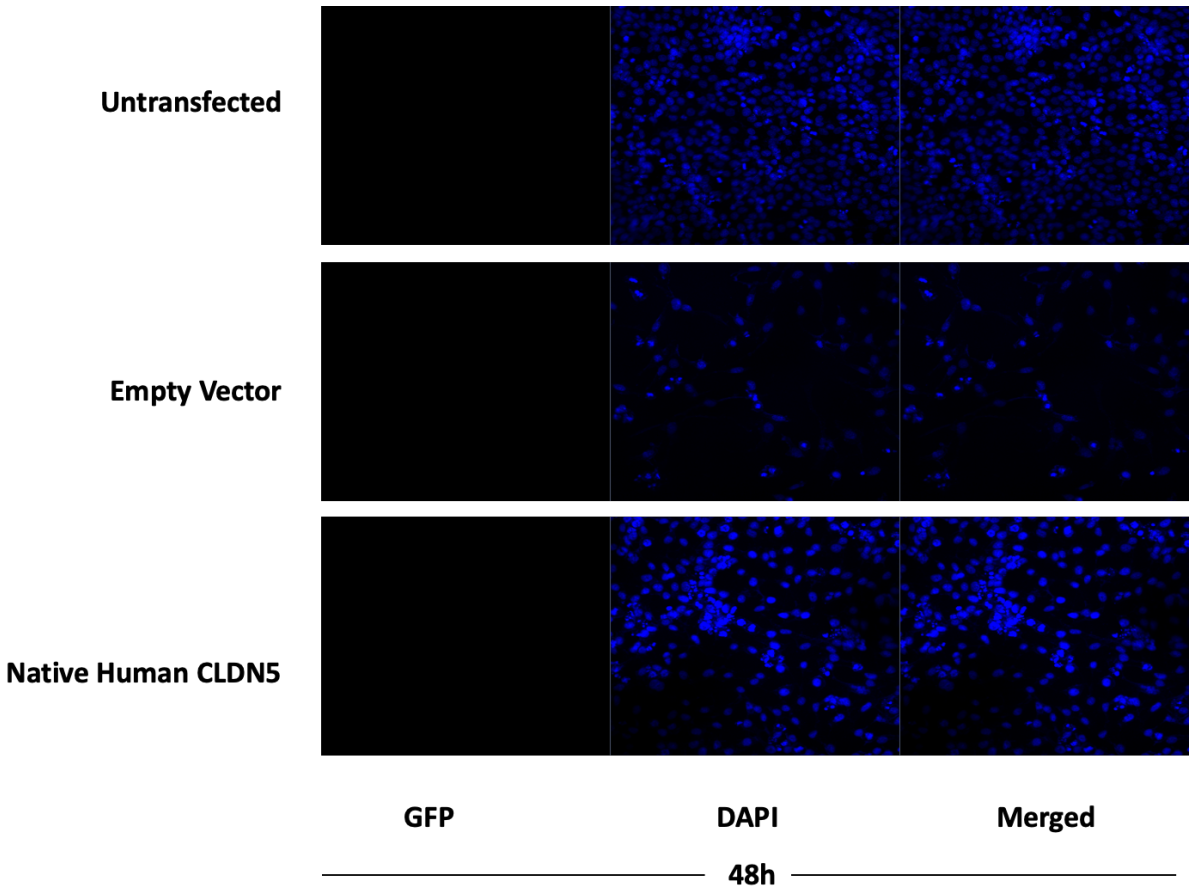

Representative Image: Immunocytochemistry staining of HeLas transfected with 500 ng pcDNA3-EGFP Empty Vector and 500 ng of pcDNA3-EGFP native human claudin-5 cDNA+3'UTR plasmid using Lipofectamine 2000 ® and fixed in ice-cold Methanol at 24 and 48 hours post-transfection, shows that the endogenous GFP signal present in the backbone of these plasmids is not preserved after Methanol fixation. Nuclei were stained with DAPI (blue), GFP (green, not visible).

References:

Abbott, N.J., Patabendige, A.A.K., Dolman, D.E.M., Yusof, S.R., Begley, D.J. (2010). Structure and function of the blood-brain barrier. *Neurobiology of Disease*, 37(1), 13-25. https://doi.org/10.1016/j.nbd.2009.07.030

Abbott, N.J., Ronnback, L., Hansson, E. (2006). Astrocyte – endothelial interactions at the blood–brain barrier. *Nature Reviews Neuroscience,* 7, 41–53. https://doi.org/10.1038/nrn1824

Afonso, P.V., Ozden, S., Prevost, M.-C., Schmitt, C., Seilhean, D., Weksler, B., Couraud, P.-O., Gessain, A., Romero, I.A., Ceccaldi, P.-E. (2007). Human blood–brain barrier disruption by retroviral-infected lymphocytes: role of myosin light chain kinase in endothelial tight-junction disorganization. *The Journal of Immunology,* 179(4), 2576–2583. https://doi.org/10.4049/jimmunol.179.4.2576

Altschul, S.F., Gish, W., Miller, W., Myers, E.W. & Lipman, D.J. (1990). Basic local alignment search tool. *Journal of Molecular Biology*, 215(3), 403-410. https://doi.org/10.1016/s0022-2836(05)80360-2

Anderson, J. M., Fanning, A.S., Lapierre, L., & Van Itallie, C.M. (1995). Zonula occludens (ZO)-1 and ZO-2, Membrane-associated guanylate kinase homologues (MAGUKs) of the tight junction. *Biochemical. Society Transactions,* 23(3), 470–475. https://doi.org/10.1042/bst0230470

Anderson, J. M., & Van Itallie, C. M. (2009). Physiology and function of the tight junction. *Cold Spring Harbor Perspectives in Biology,* 1(2). https://doi.org/10.1101/cshperspect.a002584

Armulik, A., Abramsson, A., & Betsholtz, C. (2005). Endothelial/pericyte interactions. *Circulation Research,* 97(6), 512–523. https://doi.org/10.1161/01.RES.0000182903.16652.d7

Attwell, D., Buchan, A. M., Charpak, S., Lauritzen, M., Macvicar, B. A., & Newman, E. A. (2010). Glial and neuronal control of brain blood flow. *Nature*, 468(7321), 232–243. https://doi.org/10.1038/nature09613

Avci-Adali, M., Behring, A., Keller, T., Krajewski, S., Schlensak, C., Wendel, H. P. (2014). Optimized conditions for successful transfection of human endothelial cells with in vitro synthesized and modified mRNA for induction of protein expression. *Journal of Biological Engineering*, 8(1), 8. https://doi.org/10.1186/1754-1611-8-8

Ayloo, S., & Gu, C. (2019). Transcytosis at the blood-brain barrier. Transcytosis at the Blood-Brain Barrier. *Current Opinion in Neurobiolgy*, 57, 32–38. https://doi.org/10.1016/j.conb.2018.12.014

Bake, S., Friedman, J. A., & Sohrabji, F. (2009). Reproductive age-related changes in the blood brain barrier: Expression of IgG and tight junction proteins. *Microvascular Research*, 78(3), 413–424. https://doi.org/10.1016/j.mvr.2009.06.009

Balsalobre, A., Damiola, F., & Schibler, U. (1998). A Serum Shock Induces Circadian Gene Expression in Mammalian Tissue Culture Cells. *Cell*, 93(6), 929–937. https://doi.org/10.1016/s0092-8674(00)81199-x

Bamforth, S.D., Kniesel, U., Wolburg, H., Engelhardt, B., & Risau, W. (1999). A dominant mutant of occludin disrupts tight junction structure and function. *Journal of Cell Science,* 112(Pt 12), 1879–1888.

Başkaya, M. K., Rao, A. M., Doğan, A., Donaldson, D., & Dempsey, R. J. (1997). The biphasic opening of the blood–brain barrier in the cortex and hippocampus after traumatic brain injury in rats. *Neuroscience Letters*, 226(1), 33–36. https://doi.org/10.1016/s0304-3940(97)00239-5

Bauer, H., Zweimueller-Mayer, J., Steinbacher, P., Lametschwandtner, A., & Bauer, H. C. (2010). The dual role of zonula occludens (ZO) proteins. *Journal of Biomedicine & Biotechnology*, 2010, 402593. https://doi.org/10.1155/2010/402593

Bazzoni, G., & Dejana, E. (2004). Endothelial Cell-to-Cell Junctions: Molecular Organization and Role in Vascular Homeostasis. *Physiological Reviews*, 84(3), 869–901. https://doi.org/10.1152/physrev.00035.2003

Bazzoni, G., Tonetti, P., Manzi, L., Cera, M.R., Balconi, G., & Dejana, E. (2005). Expression of junctional adhesion molecule-A prevents spontaneous and random motility. *Journal of Cell Science,* 118(Pt 3), 623–632. https://doi.org/10.1242/jcs.01661

Begley, D.J., & Brightman, M.W. (2003). Structural and functional aspects of the blood–brain barrier. *Progress in Drug Res*earch, 61, 39–78. https://doi.org/10.1007/978-3-0348-8049-7_2

Berkovits, B. D., & Mayr, C. (2015). Alternative 3' UTRs act as scaffolds to regulate membrane protein localization. *Nature*, 522(7556), 363–367. https://doi.org/10.1038/nature14321

Blanchette, M., & Daneman, R. (2015). Formation and maintenance of the BBB. *Mechanisms of Development*, 138, 8–16. https://doi.org/10.1016/j.mod.2015.07.007

Bors, L., & Erdő, F. (2019). Overcoming the Blood–Brain Barrier. Challenges and Tricks for CNS Drug Delivery. *Scientia Pharmaceutica*, *87*(1), 6. https://doi.org/10.3390/scipharm87010006

Brightman, M.W., & Reese, T.S. (1969). Junctions between intimately apposed cell membranes in the vertebrate brain. *The Journal of Cell Biol*gy, 40(3), 648–677. https://doi.org/10.1083/jcb.40.3.648

Brown, A. S., Mohanty, B. K., & Howe, P. H. (2015). Computational Identification of Post Translational Modification Regulated RNA Binding Protein Motifs. *Plos One*, 10(9). https://doi.org/10.1371/journal.pone.0137696

Butt, A.M., Jones, H.C., Abbott, N.J. (1990) Electrical-Resistance Across the Blood-Brain-Barrier in Anesthetized Rats - A Developmental-Study. *The Journal of Physiology*, 429, 47–62. https://doi.org/10.1113/jphysiol.1990.sp018243

Campbell, M., Kiang, A.-S., Kenna, P. F., Kerskens, C., Blau, C., Odwyer, L., Tivnan, A., Kelly, JA., Brankin, B., Farrar GJ., Humphries, P. (2008). RNAi-mediated reversible opening of the blood-brain barrier. *The Journal of Gene Medicine*, 10(8), 930–947. https://doi.org/10.1002/jgm.1211

Chassé, H., Boulben, S., Costache, V., Cormier, P., & Morales, J. (2017). Analysis of translation using polysome profiling. *Nucleic Acids Research*, 45(3), e15. https://doi.org/10.1093/nar/gkw907

Chen, Y., & Liu, L. (2012). Modern methods for delivery of drugs across the blood–brain barrier. *Advanced Drug Delivery Reviews*, 64(7), 640–665. https://doi.org/10.1016/j.addr.2011.11.010

Chiba, H., Osanai, M., Murata, M., Kojima, T., & Sawada, N. (2008). Transmembrane proteins of tight junctions. *Biochimica Et Biophysica Acta (BBA) - Biomembranes*, 1778(3), 588–600. https://doi.org/10.1016/j.bbamem.2007.08.017

Cipolla, M.J. (2009). Chapter 2, Anatomy and Ultrastructure. *The Cerebral Circulation*. San Rafael (CA): Morgan & Claypool Life Sciences; Available from: https://www.ncbi.nlm.nih.gov/books/NBK53086/

Clarke, D.D. & Sokoloff, L. (1999). Chapter 31, Circulation and Energy Metabolism of the Brain. In: Siegel, G.J., Agranoff, B.W., Albers, R.W., et al., editors. *Basic Neurochemistry: Molecular, Cellular and Medical Aspects. 6th edition.* Philadelphia: Lippincott-Raven. Available from: https://www.ncbi.nlm.nih.gov/books/NBK20413/

Colosimo, A., Goncz, K., Holmes, A., Kunzelmann, K., Novelli, G., Malone, R., Bennett, M.J., Gruenert, D. (2000). Transfer and Expression of Foreign Genes in Mammalian Cells. *BioTechniques,* 29(2), 314-331. https://doi.org/10.2144/00292rv01

Cook, B. D., Ferrari, G., Pintucci, G., & Mignatti, P. (2008). TGF-β1 induces rearrangement of FLK-1-VE-cadherin-β-catenin complex at the adherens junction through VEGF-mediated signaling. *Journal of Cellular Biochemistry*, 105(6), 1367–1373. https://doi.org/10.1002/jcb.21935

Coomber, BL., & Stewart, PA. (1985). Morphometric analysis of CNS microvascular endothelium. *Microvascular Research*, 30 (1), 99-115. https://doi.org/10.1016/0026-2862(85)90042-1

Cooper, I., Cohen-Kashi-Malina, K., & Teichberg, V. I. (2011). Claudin-5 Expression in In Vitro Models of the Blood–Brain Barrier. *Methods in Molecular Biology Claudins,* 347-354. https://doi.org/10.1007/978-1-61779-185-7_25

Crick FH. (1958) On protein synthesis. *Symposia of the Society for Experimental Biology,* 12, 138–163.

Crone, C., Christensen, O. Electrical Resistance of a Capillary Endothelium. *The Journal of General Physiology*, 77(4), 349–71. https://doi.org/10.1085/jgp.77.4.349

Cummins, P.M. (2012). Occludin: one protein, many forms. *Molecular and Cellular Biology,* 32(2), 242-50. https://doi.org/10.1128/MCB.06029-11

Daneman, R., & Prat, A. (2015). The Blood–Brain Barrier. *Cold Spring Harbor Perspectives in Biology,* 7(1), a020412. https://doi.org/10.1101/cshperspect.a020412

Daneman, R., Zhou, L., Agalliu, D., Cahoy, J.D., Kaushal, A., Barres, B.A. (2010). The mouse blood-brain barrier trancriptome: a new resource for understanding the development and function of brain endothelial cells. *PloS One,* 5(10), e13741. https://doi.org/10.1371/journal.pone.0013741

Dassi, E., Re, A., Leo, S., Tebaldi, T., Pasini, L., Peroni, D., & Quattrone, A. (2014) .AURA 2: Empowering discovery of post-transcriptional networks. *Translation,* 2(1), e27738. https://doi.org/10.4161/trla.27738

Daugherty, B. L., Ward, C., Smith, T., Ritzenthaler, J. D., & Koval M. (2007). Regulation of heterotypic claudin compatibility. *The Journal of Biological Chemistry,* 282(41), 30005–30013. https://doi.org/10.1074/jbc.M703547200

Dias, M. C., Coisne, C., Baden, P., Enzmann, G., Garrett, L., Becker, L., Hölter, S.M., German Mouse Clinic Consortium, de Angelis, M.F., Deutsch, R., Engelhardt, B. (2019).

Claudin-12 is not required for blood–brain barrier tight junction function. *Fluids and Barriers of the CNS,* 16(1), 30. https://doi.org/10.1186/s12987-019-0150-9

Dithmer, S., Staat, C., Müller, C., Ku, M.-C., Pohlmann, A., Niendorf, T., Gehne, N, Fallier-Becker, P., Kittel, A., Walter, F.R., Veszelka, S., Deli, M.A., Blasig, R., Haseloff, R.F., Blasig, I.E., Winkler, L. (2017). Claudin peptidomimetics modulate tissue barriers for enhanced drug delivery. *Annals of the New York Academy of Sciences*, 1397(1), 169–184. https://doi.org/10.1111/nyas.13359

Dong X. (2018). Current Strategies for Brain Drug Delivery. *Theranostics*, 8(6), 1481–1493. https://doi.org/10.7150/thno.21254

Drouin-Ouellet, J., Sawiak, S.J., Cisbani, G., Lagacé, M., Kuan, W.L, Saint-Pierre, M., Dury, R.J., Alata, W., St-Amour, I., Mason, S.L., Calon, F., Lacroix, S., Gowland, P.A., Francis, S.T., Barker, R.A., & Cicchetti, F. (2015). Cerebrovascular and blood-brain barrier impairments in Huntington's disease: Potential implications for its pathophysiology. *Annals of Neurol*ogy, 78(2), 160–177. https://doi.org/10.1002/ana.24406

Engelhardt, B., & Liebner, S. (2014). Novel insights into the development and maintenance of the blood-brain barrier. *Cell Tissue Research,* 355(3), 687-699. https://doi.org/10.1007/s00441-014-1811-2

Erdő, F., Denes, L., & de Lange, E. (2017). Age-associated physiological and pathological changes at the blood-brain barrier: A review. *Journal of cerebral blood flow and metabolism : official journal of the International Society of Cerebral Blood Flow and Metabolism*, 37(1), 4–24. https://doi.org/10.1177/0271678X16679420

Fanning, A. S., Little, B. P., Rahner, C., Utepbergenov, D., Walther, Z., & Anderson, J. M. (2007). The Unique-5 and -6 Motifs of ZO-1 Regulate Tight Junction Strand Localization and Scaffolding Properties. *Molecular Biology of the Cell*, 18(3), 721–731. https://doi.org/10.1091/mbc.e06-08-0764

Furuse, M. (2010). Molecular basis of the core structure of tight junctions. *Cold Spring Harbor Perspectives in Biology*, 2(1), a002907. https://doi.org/10.1101/cshperspect.a002907

Furuse, M., Fujimoto, K., Sato, N., Hirase, T., Tsukita, S., Tsukita, S. (1996). Overexpression of occludin, a tight junction-associated integral membrane protein, induces the formation of intracellular multilamellar bodies bearing tight junction-like structures. *Journal of Cell Sci*ence, 109(Pt 2), 429-35.

Furuse, M., Hirase, T., Itoh, M., Nagafuchi, A., Yonemura, S., Tsukita, S., Tsukita, S. (1993). Occludin: a novel integral membrane protein localizing at tight junctions. *Journal of Cell Biology,* 123(6 Pt 2), 1777-88. https://doi.org/10.1083/jcb.123.6.1777

Furuse, M., Sasaki, H., Fujimoto, K., Tsukita, S. (1998). A single gene product, claudin-1 or -2, reconstitutes tight junction strands and recruits occludin in fibroblasts. *Journal of Cell Biology, 143(2)*, 391–401. https://doi.org/10.1083/jcb.143.2.391

Furuse, M., Sasaki, H., Tsukita ,S. (1999). Manner of interaction of heterogeneous claudin species within and between tight junction strands. *Journal of Cell Biology,* 147(4), 891–903. https://doi.org/10.1083/jcb.147.4.891

Gekakis, N., Staknis, D., Nguyen, H.B., Davis, F.C., Wilsbacher, L.D., King, D.P., Takahashi, J.S., &Weitz, C.J. (1998). Role of the CLOCK Protein in the Mammalian Circadian Mechanism. *Science (New York, N.Y.)*, 280 (5369), 1564–1569. https://doi.org/10.1126/science.280.5369.1564

Goldmann, E.E. (1909). Die äussere und innere Sekretion des gesunden und kranken Organismus im Lichte der 'vitalen Farbung'. *Beiträg Klinische Chirurgie,* 64, 192–265.

Goldmann, E.E. (1913). Vitalfarbung am Zentralnervensystem. Abh. preuss. *Akad. Wiss Phys.-Math K1*, 1, 1–60.

Gonschior, H., Haucke, V., & Lehmann, M. (2020). Super-Resolution Imaging of Tight and Adherens Junctions: Challenges and Open Questions. *International Journal of Molecular Sciences*, 21(3), 744. https://doi.org/10.3390/ijms21030744

Gordon, G.R., Howarth, C., & MacVicar, B.A. (2011). Bidirectional control of arteriole diameter by astrocytes. *Experimental Physiol*ogy, 96(4), 393–399. https://doi.org/10.1113/expphysiol.2010.053132

Greene, C., & Campbell, M. (2016). Tight junction modulation of the blood brain barrier: CNS delivery of small molecules. *Tissue Barriers*, 4(1), e1138017. https://doi.org/10.1080/21688370.2015.1138017

Greene, C., Kealy, J., Humphries, M. M., Gong, Y., Hou, J., Hudson, N., Cassidy, L.M., Martiniano, R., Shashi, V., Hooper, S.R., Grant, G.A., Kenna, P.F., Norris, K., Callaghan, C.K., Islam, M.D., O''Mara, S.M., Najda, Z., Campbell, S.G., Pachter, J.S., Thomas, J., Williams , N.M., Humphries, P., Murphy, K.C., Campbell, M. (2018).

Dose-dependent expression of claudin-5 is a modifying factor in schizophrenia. *Molecular Psychiatry*, 23(11), 2156–2166. https://doi.org/10.1038/mp.2017.156

Habgood, M. D., Bye, N., Dziegielewska, K. M., Ek, C. J., Lane, M. A., Potter, A., Morganti-Kossman, C., Saunders, N. R. (2007). Changes in blood-brain barrier permeability to large and small molecules following traumatic brain injury in mice. *The European Journal of Neuroscience*, 25(1), 231–238. https://doi.org/10.1111/j.1460-9568.2006.05275.x

Hartsock, A., & Nelson, W. J. (2008). Adherens and tight junctions: Structure, function and connections to the actin cytoskeleton. *Biochimica Et Biophysica Acta (BBA) - Biomembranes*, 1778(3), 660–669. https://doi.org/10.1016/j.bbamem.2007.07.012

Hastings M. (1997). Central clocking. *Trends in Neurosciences,* 20(10), 459-64. https://doi.org/10.1016/s0166-2236(97)01087-4

Hastings, M. (1998). The brain, circadian rhythms, and clock genes. *BMJ (Clinical research ed.)*, 317(7174), 1704–1707. https://doi.org/10.1136/bmj.317.7174.1704

Hawkins, B.T., & Davis, T.P. (2005). The blood-brain barrier neurovascular unit in health and disease. *Pharmacological Reviews,* 57*(2)*, 173–185. https://doi.org/10.1124/pr.57.2.4

He, J., Hsuchou, H., He, Y., Kastin, A. J., Wang, Y., & Pan, W. (2014). Sleep restriction impairs blood-brain barrier function. *The Journal of neuroscience : the official journal of the Society for Neuroscience*, 34(44), 14697–14706. https://doi.org/10.1523/JNEUROSCI.2111-14.2014

Heinemann, U., & Schuetz, A. (2019). Structural Features of Tight-Junction Proteins. *International journal of molecular sciences*, 20(23), 6020. https://doi.org/10.3390/ijms20236020

Hersh, D. S., Wadajkar, A. S., Roberts, N., Perez, J. G., Connolly, N. P., Frenkel, V., Winkles, J. A., Woodworth, G. F., & Kim, A. J. (2016). Evolving Drug Delivery Strategies to Overcome the Blood Brain Barrier. *Current pharmaceutical design*, *22*(9), 1177–1193. https://doi.org/10.2174/1381612822666151221150733

Hervé, F., Ghinea, N., & Scherrmann, J.-M. (2008). CNS Delivery Via Adsorptive Transcytosis. *The AAPS Journal*, *10*(3), 455–472. https://doi.org/10.1208/s12248-008-9055-2

Hirase, T., Staddon, J.M., Saitou, M., Ando-Akatsuka, Y., Itoh, M., Furuse, M., Fujimoto, K., & Rubin, L.L. (1997). Occludin as a possible determinant of tight junction permeability in endothelial cells. *Journal of Cell Science,* 110, 1603– 1613.

Hudson, N., Celkova, L., Hopkins, A., Greene, C., Storti, F., Ozaki, E., Fahey, E., Theodoropoulou, S., Kenna, P. F., Humphries, M. M., Curtis, A. M., Demmons, E., Browne, A., Liddie, S., Lawrence, M. S., Grimm, C., Cahill, M. T., Humphries, P., Doyle, S. L., & Campbell, M. (2019). Dysregulated claudin-5 cycling in the inner retina causes retinal pigment epithelial cell atrophy. *JCI insight*, 4(15), e130273. https://doi.org/10.1172/jci.insight.130273

Hunt, M. A., Currie, M. J., Robinson, B. A., & Dachs, G. U. (2010). Optimizing transfection of primary human umbilical vein endothelial cells using commercially available chemical transfection reagents. *Journal of biomolecular techniques : JBT*, 21(2), 66–72.

Hunt, S. E., McLaren, W., Gil, L., Thormann, A., Schuilenburg, H., Sheppard, D., Parton, A., Armean, I. M., Trevanion, S. J., Flicek, P., & Cunningham, F. (2018). Ensembl variation resources. *Database : the journal of biological databases and curation*, *2018*, bay119. https://doi.org/10.1093/database/bay119

Hurtado-Alvarado, G., Velázquez-Moctezuma, J., & Gómez-González, B. (2017). Chronic sleep restriction disrupts interendothelial junctions in the hippocampus and increases blood-brain barrier permeability. *Journal of Microscopy*, 268(1), 28–38. https://doi.org/10.1111/jmi.12583

Itoh, M., Furuse, M., Morita, K., Kubota, K., Saitou, M., & Tsukita, S. (1999). Direct binding of three tight junction-associated MAGUKs, ZO-1, ZO-2, and ZO-3, with the COOH termini of claudins. *The Journal of cell biology*, *147*(6), 1351–1363. https://doi.org/10.1083/jcb.147.6.1351

Jiao, H., Wang, Z., Liu, Y., Wang, P., & Xue, Y. (2011). Specific Role of Tight Junction Proteins Claudin-5, Occludin, and ZO-1 of the Blood–Brain Barrier in a Focal Cerebral Ischemic Insult. *Journal of Molecular Neuroscience*, 44(2), 130–139. https://doi.org/10.1007/s12031-011-9496-4

Jones, A. R., & Shusta, E. V. (2007). Blood-brain barrier transport of therapeutics via receptor-mediation. *Pharmaceutical research*, 24(9), 1759–1771. https://doi.org/10.1007/s11095-007-9379-0

Karayiorgou, M., Morris, M. A., Morrow, B., Shprintzen, R. J., Goldberg, R., Borrow, J., Gos,A., Nestadt, G., Wolyniec, PS., Lasseter, V. K. (1995). Schizophrenia

susceptibility associated with interstitial deletions of chromosome 22q11. *Proceedings of the National Academy of Sciences of the United States of America*, 92(17), 7612–7616. https://doi.org/10.1073/pnas.92.17.7612

Karayiorgou, M., Simon, T. J., & Gogos, J. A. (2010). 22q11.2 microdeletions: linking DNA structural variation to brain dysfunction and schizophrenia. *Nature reviews. Neuroscience*, 11(6), 402–416. https://doi.org/10.1038/nrn2841

Katsuno, T., Umeda, K., Matsui, T., Hata, M., Tamura, A., Itoh, M., Tekeuchi, K., Fujimori, T., Nabeshima, Y., Noda, T., Tsukita, S., Tsukita, S. (2008). Deficiency of Zonula Occludens-1 Causes Embryonic Lethal Phenotype Associated with Defected Yolk Sac Angiogenesis and Apoptosis of Embryonic Cells. *Molecular Biology of the Cell,* 19(6), 2465–2475. https://doi.org/10.1091/mbc.e07-12-1215

Kealy, J., Greene, C., & Campbell, M., (2018). Blood-brain barrier regulation in psychiatric disorders. *Neuroscience Letters*. https://doi.org/10.1016/j.neulet.2018.06.033

Keaney, J., & Campbell, M. (2015). The dynamic blood-brain barrier. *The FEBS Journal*, 282(21), 4067–4079. https://doi.org/10.1111/febs.13412

Kennedy, C., & Sokoloff, L. (1957). An adaptation of the nitrous oxide method to the study of the cerebral circulation in children; normal values for cerebral blood flow and cerebral metabolic rate in childhood. *The Journal of Clinical Investigation,* 36(7), 1130- 1137. https://doi.org/10.1172/JCI103509

Kim, S., Han, S. C., Gallan, A. J., & Hayes, J. P. (2017). Neurometabolic indicators of mitochondrial dysfunction in repetitive mild traumatic brain injury. *Concussion (London, England)*, *2*(3), CNC48. https://doi.org/10.2217/cnc-2017-0013

Kirk, J., Plumb, J., Mirakhur, M., & Mcquaid, S. (2003). Tight junctional abnormality in multiple sclerosis white matter affects all calibres of vessel and is associated with blood-brain barrier leakage and active demyelination. *The Journal of Pathology*, 201(2), 319–327. https://doi.org/10.1002/path.1434

Klein, D.C., Moore, R.Y., Reppert, S.M. (1991). Suprachiasmatic nucleus: the mind's clock. *New York: Oxford University Press.*

Kowalczyk, A. P., & Nanes, B. A. (2012). Adherens junction turnover: regulating adhesion through cadherin endocytosis, degradation, and recycling. *Sub-cellular biochemistry*, 60, 197–222. https://doi.org/10.1007/978-94-007-4186-7_9

Krause, G., Winkler, L., Mueller, S. L., Haseloff, R. F., Piontek, J., & Blasig, I. E. (2008). Structure and function of claudins. *Biochimica et biophysica acta*, 1778(3), 631–645. https://doi.org/10.1016/j.bbamem.2007.10.018

Krause, G., Winkler, L., Piehl, C., Blasig, I., Piontek, J., & Müller, S. L. (2009). Structure and function of extracellular claudin domains. *Annals of the New York Academy of Sciences*, 1165, 34–43. https://doi.org/10.1111/j.1749-6632.2009.04057.x

Krueger, P. M., & Friedman, E. M. (2009). Sleep duration in the United States: a cross-sectional population-based study. *American journal of epidemiology*, 169(9), 1052–1063. https://doi.org/10.1093/aje/kwp023

Lewandowsky, M. (1900). Zur lehre der cerebrospinalflussigkeit. *Z. Klin. Med*. 40, 480–494.

Li, X., Shi, L., Zhang, K., Wei, W., Liu, Q., Mao, F., Li, J., Cai, W., Chen, H., Teng, H, Li, J., Sun, Z. (2018). CirGRDB: a database for the genome-wide deciphering circadian genes and regulators. *Nucleic acids research*, 46(D1), D64–D70. https://doi.org/10.1093/nar/gkx944

Lianoglou, S., Garg, V., Yang, J.L., Leslie, C.S., & Mayr, C. (2013). Ubiquitously transcribed genes use alternative polyadenylation to achieve tissue- specific expression. *Genes & Development,* 27(21), 2380–2396. https://doi.org/10.1101/gad.229328.113

Liddelow S. A. (2011). Fluids and barriers of the CNS: a historical viewpoint. *Fluids and barriers of the CNS*, 8(1), 2. https://doi.org/10.1186/2045-8118-8-2

Luissint, A. C., Artus, C., Glacial, F., Ganeshamoorthy, K., & Couraud, P. O. (2012). Tight junctions at the blood brain barrier: physiological architecture and disease-associated dysregulation. *Fluids and barriers of the CNS*, 9(1), 23. https://doi.org/10.1186/2045-8118-9-23

Mayr, C. (2018). What Are 3′ UTRs Doing? *Cold Spring Harbor Perspectives in Biology*, *11*(10). https://doi.org/10.1101/cshperspect.a034728

McConnell, H. L., Kersch, C. N., Woltjer, R. L., Neuwelt, E. A. (2017). The Translational Significance of the Neurovascular Unit. *The Journal of biological chemistry*, *292*(3), 762–770. https://doi.org/10.1074/jbc.R116.760215

Merkel, S. F., Andrews, A. M., Lutton, E. M., Mu, D., Hudry, E., Hyman, B. T., Maguire, C.A., & Ramirez, S. H. (2016). Trafficking of adeno-associated virus vectors across a model of the blood-brain barrier; a comparative study of transcytosis and transduction

using primary human brain endothelial cells. *Journal of Neurochemistry*, *140*(2), 216–230. https://doi.org/10.1111/jnc.13861

Mineta, K., Yamamoto, Y., Yamazaki, Y., Tanaka, H., Tada, Y., Saito, K., Tamura, A., Igarashi, M., Endo, T., Takeuchi, K., Tsukita, S. (2011). Predicted expansion of the claudin multigene family. *FEBS Letters*, 585(4), 606–612. https://doi.org/10.1016/j.febslet.2011.01.028

Mohamed, Z. I., Tee, S. F., & Tang, P. Y. (2018). Association of functional polymorphisms in 3′-untranslated regions of COMT, DISC1, and DTNBP1 with schizophrenia. *Psychiatric Genetics*, *28*(6), 110–119. https://doi.org/10.1097/YPG.0000000000000210

Morita, K., Furuse, M., Fujimoto, K., & Tsukita, S. (1999). Claudin multigene family encoding four-transmembrane domain protein components of tight junction strands. *Proceedings of the National Academy of Sciences of the United States of America*, 96(2), 511–516. https://doi.org/10.1073/pnas.96.2.511

Murata, M., Kojima, T., Yamamoto, T., Go, M., Takano, K.-I., Osanai, M., Chiba, H., Sawada, N. (2005). Down-regulation of survival signaling through MAPK and Akt in occludin-deficient mouse hepatocytes in vitro. *Experimental Cell Research*, 310(1), 140–151. https://doi.org/10.1016/j.yexcr.2005.07.017

Najjar, S., Pahlajani, S., De Sanctis, V., Stern, J., Najjar, A., & Chong, D. (2017). Neurovascular Unit Dysfunction and Blood-Brain Barrier Hyperpermeability Contribute to Schizophrenia Neurobiology: A Theoretical Integration of Clinical and Experimental Evidence. *Frontiers in psychiatry*, 8, 83. https://doi.org/10.3389/fpsyt.2017.00083

Najjar, S., Pearlman, D. M., Alper, K., Najjar, A., & Devinsky, O. (2013). Neuroinflammation and psychiatric illness. *Journal of neuroinflammation*, 10(1), https://doi.org/10.1186/1742-2094-10-43

Nakazato, R., Kawabe, K., Yamada, D., Ikeno, S., Mieda, M., Shimba, S., Hinoi, E., Yoneda, Y., Takarada, T. (2017). Disruption of Bmal1 Impairs Blood–Brain Barrier Integrity via Pericyte Dysfunction. *The Journal of Neuroscience*, *37*(42), 10052–10062. https://doi.org/10.1523/JNEUROSCI.3639-16.2017

Nitta, T., Hata, M., Gotoh, S., Seo, Y., Sasaki, H., Hashimoto, N., Furuse, M., & Tsukita, S. (2003). Size-selective loosening of the blood-brain barrier in claudin-5-deficient

mice. *The Journal of Cell Biology*, 161(3), 653–660. https://doi.org/10.1083/jcb.200302070

Nowakowski, R. S. (2006). Stable neuron numbers from cradle to grave. *Proceedings of the National Academy of Sciences,* 103(33), 12219–12220. https://doi.org/10.1073/pnas.0605605103

O'Connor, C., Ramanath, N., & Campbell, M. (2019). Pharmacokinetics of Systemic Drug Delivery. *Nervous System Drug Delivery*, 39–56. https://doi.org/10.1016/B978-0-12-813997-4.00003-7

Ohtsuki S., Sato S., Yamaguchi H., Kamoi M., Asashima T., Terasaki T. (2007). Exogenous expression of claudin-5 induces barrier properties in cultured rat brain capillary endothelial cells. *Journal of cellular physiology*, 210(1), 81–86. https://doi.org/10.1002/jcp.20823

Oldendorf, W. H., Cornford, M. E., & Brown, W. J. (1977). The large apparent work capability of the blood-brain barrier: A study of the mitochondrial content of capillary endothelial cells in brain and other tissues of the rat. *Annals of Neurology*, 1(5), 409–417. https://doi.org/10.1002/ana.410010502

Omidinia, E., Mashayekhi Mazar, F., Shahamati, P., Kianmehr, A., & Shahbaz Mohammadi, H. (2014). Polymorphism of the CLDN5 gene and schizophrenia in an Iranian population. *Iranian Journal of Public Health,* 43(1), 79–83.

Padden, M., Leech, S., Craig, B., Kirk, J., Brankin, B., & McQuaid, S. (2007). Differences in expression of junctional adhesion molecule-A and beta-catenin in multiple sclerosis brain tissue: increasing evidence for the role of tight junction pathology. *Acta Neuropathologica,* 113(2), 177–186. https://doi.org/10.1007/s00401-006-0145-x

Pan, W., & Kastin, A. J. (2016). The Blood-Brain Barrier. *The Neuroscientist*, 23(2), 124–136. https://doi.org/10.1177/1073858416639005

Panda, A. C., Martindale, J. L., & Gorospe, M. (2016). Affinity Pulldown of Biotinylated RNA for Detection of Protein-RNA Complexes. *Bio-protocol*, 6(24), e2062. https://doi.org/10.21769/BioProtoc.2062

Pardridge W. M. (2005). The blood-brain barrier: bottleneck in brain drug development. *NeuroRx : the journal of the American Society for Experimental NeuroTherapeutics*, 2(1), 3–14. https://doi.org/10.1602/neurorx.2.1.3

Pardridge, W. (2006). Molecular Trojan horses for blood–brain barrier drug delivery. *Current Opinion in Pharmacology*, 6(5), 494–500. https://doi.org/10.1016/j.coph.2006.06.001

Pardridge W. M. (2012). Drug transport across the blood-brain barrier. *Journal of cerebral blood flow and metabolism : official journal of the International Society of Cerebral Blood Flow and Metabolism*, 32(11), 1959–1972. https://doi.org/10.1038/jcbfm.2012.126

Pardridge, W. M., Triguero, D., Buciak, J., & Yang, J. (1990). Evaluation of cationized rat albumin as a potential blood-brain barrier drug transport vector. *The Journal of pharmacology and experimental therapeutics*, 255(2), 893–899.

Paz, I., Kosti, I., Ares, M., Jr, Cline, M., & Mandel-Gutfreund, Y. (2014). RBPmap: a web server for mapping binding sites of RNA-binding proteins. Nucleic acids research, 42(Web Server issue), W361–W367. https://doi.org/10.1093/nar/gku406

Piontek, J., Winkler, L., Wolburg, H., Müller, S. L., Zuleger, N., Piehl, C., Weisner, B., Krause, G., Blasig, I. E. (2008). Formation of tight junction: determinants of homophilic interaction between classic claudins. *The FASEB Journal*, 22(1), 146–158. https://doi.org/10.1096/fj.07-8319com

Reese, T.S., & Karnovsky, M.J. (1967). Fine structural localization of a blood- brain barrier to exogenous peroxidase. *The Journal of Cell Biology*, 34(1), 207–217. https://doi.org/10.1083/jcb.34.1.207

Rossa, Jan, Ploeger, C., Vorreiter, F., Saleh, T., Protze, J., Günzel, D., Wolburg, H., Krause, G., & Piontek, J. (2014). Claudin-3 and Claudin-5 Protein Folding and Assembly into the Tight Junction Are Controlled by Non-Conserved Residues in the Transmembrane 3 (TM3) and Extracellular Loop 2 (ECL2) Segments. *The Journal of Biological Chemistry*, 289 (11). 7641–7653. https://doi.org/10.1074/jbc.M113.531012

Saitou, M., Fujimoto, K., Doi, Y., Itoh, M., Fujimoto, T., Furuse, M., Takano, H., Noda, T., & Tsukita, S. (1998). Occludin-deficient embryonic stem cells can differentiate into polarized epithelial cells bearing tight junctions. *The Journal of cell biology*, *141*(2), 397–408. https://doi.org/10.1083/jcb.141.2.397

Saitou, M., Furuse, M., Sasaki, H., Schulzke, J. D., Fromm, M., Takano, H., Noda, T., & Tsukita, S. (2000). Complex phenotype of mice lacking occludin, a component of tight junction strands. *Molecular biology of the cell*, 11(12), 4131–4142. https://doi.org/10.1091/mbc.11.12.4131

Schneeberger, E. E., & Lynch, R. D. (2004). The tight junction: a multifunctional complex. *American journal of physiology. Cell physiology*, 286(6), C1213–C1228. https://doi.org/10.1152/ajpcell.00558.2003

Schreibelt, G., Kooij, G., Reijerkerk, A., van Doorn, R., Gringhuis, S.I., van der Pol, S., Weksler, B.B., Romero, I.A., Couraud, P.O., Piontek, J., Blasig, I.E., Dijkstra, C.D., Ronken, E., & de Vries, H.E. (2007). Reactive oxygen species alter brain endothelial tight junction dynamics via RhoA, PI3 kinase, and PKB signaling. *The FASEB Journal,* 21(13), 3666–3676. https://doi.org/10.1096/fj.07-8329com

Simionescu, M., Simionescu, N., & Palade, G. E. (1975). Segmental differentiations of cell junctions in the vascular endothelium. The microvasculature. *The Journal of cell biology*, *67*(3), 863–885. https://doi.org/10.1083/jcb.67.3.863

Srinivasan, B., Kolli, A. R., Esch, M. B., Abaci, H. E., Shuler, M. L., & Hickman, J. J. (2015). TEER Measurement Techniques for In Vitro Barrier Model Systems. *Journal of Laboratory Automation*, 20(2), 107–126. https://doi.org/10.1177/2211068214561025

Staat, C., Coisne, C., Dabrowski, S., Stamatovic, S. M., Andjelkovic, A. V., Wolburg, H., Engelhardt, B., Blasig, I. E. (2015). Mode of action of claudin peptidomimetics in the transient opening of cellular tight junction barriers. *Biomaterials*, 54, 9–20. https://doi.org/10.1016/j.biomaterials.2015.03.007

Stewart, P. A., & Wiley, M. J. (1981). Developing nervous tissue induces formation of blood-brain barrier characteristics in invading endothelial cells: a study using quail--chick transplantation chimeras. *Developmental biology*, 84(1), 183–192. https://doi.org/10.1016/0012-1606(81)90382-1

Steed, E., Rodrigues, N. T., Balda, M. S., & Matter, K. (2009). Identification of MarvelD3 as a tight junction-associated transmembrane protein of the occludin family. *BMC cell biology*, 10, 95. https://doi.org/10.1186/1471-2121-10-95

Sun, Z.-Y., Wei, J., Xie, L., Shen, Y., Liu, S.-Z., Ju, G.Z., Shi, JP., Yu YQ., Zhang, X. Xu, Q., & Hemmings, G.P. (2004). The CLDN5 locus may be involved in the vulnerability to schizophrenia. *European Psychiatry*, *19*(6), 354–357. https://doi.org/10.1016/j.eurpsy.2004.06.007

Suzuki, H., Tani, K., & Fujiyoshi, Y. (2017). Crystal structures of claudins: insights into their intermolecular interactions. *Annals of the New York Academy of Sciences*, 1397(1), 25–34. https://doi.org/10.1111/nyas.13371

Sweeney, M. D., Zhao, Z., Montagne, A., Nelson, A. R., & Zlokovic, B. V. (2019). Blood-Brain Barrier: From Physiology to Disease and Back. *Physiological reviews*, 99(1), 21–78. https://doi.org/10.1152/physrev.00050.2017

Tornavaca, O., Chia, M., Dufton, N., Almagro, L. O., Conway, D. E., Randi, A. M., Schwartz, M. A., Matter, K., & Balda, M. S. (2015). ZO-1 controls endothelial adherens junctions, cell-cell tension, angiogenesis, and barrier formation. *The Journal of cell biology*, 208(6), 821–838. https://doi.org/10.1083/jcb.201404140

Tsukita, S., Furuse, M., & Itoh, M. (2001). Multifunctional strands in tight junctions. *Nature reviews. Molecular cell biology*, *2*(4), 285–293. https://doi.org/10.1038/35067088

Umeda, K., Ikenouchi, J., Katahira-Tayama, S., Furuse, K., Sasaki, H., Nakayama, M. Matsui, T, Tsukita, M., Furuse, M., Tsukita, S. (2006). ZO-1 and ZO-2 Independently Determine Where Claudins Are Polymerized in Tight-Junction Strand Formation. *Cell*, *126*(4), 741–754. https://doi.org/10.1016/j.cell.2006.06.043

Urich, E., Lazic, S. E., Molnos, J., Wells, I., & Freskgård, P. O. (2012). Transcriptional profiling of human brain endothelial cells reveals key properties crucial for predictive in vitro blood-brain barrier models. *PloS one*, *7*(5), e38149. https://doi.org/10.1371/journal.pone.0038149

Vagner, J., Qu, H., & Hruby, V. J. (2008). Peptidomimetics, a synthetic tool of drug discovery. *Current opinion in chemical biology*, *12*(3), 292–296. https://doi.org/10.1016/j.cbpa.2008.03.009

von Tell, D., Armulik, A., & Betsholtz, C. (2006). Pericytes and vascular stability. *Experimental cell research*, *312*(5), 623–629. https://doi.org/10.1016/j.yexcr.2005.10.019

Vorbrodt, A. W., Li, S., Brown, W. T., & Ramakrishna, N. (2008). Increased expression of β-catenin in brain microvessels of a segmentally trisomic (Ts65Dn) mouse model of Down syndrome. *Brain Cell Biology,* 36(5-6), 203–211. https://doi.org/10.1007/s11068-008-9038-3

Wang, F., Cheng, Y., Mei, J., Song, Y., Yang, Y.-Q., Liu, Y., & Wang, Z. (2009). Focused Ultrasound Microbubble Destruction-Mediated Changes in Blood-Brain Barrier Permeability Assessed by Contrast-Enhanced Magnetic Resonance Imaging. *Journal of Ultrasound in Medicine*, *28*(11), 1501–1509. https://doi.org/10.7863/jum.2009.28.11.1501

Wilson, S., & Argyropoulos, S. (2012). Sleep in schizophrenia: time for closer attention. *The British journal of psychiatry : the journal of mental science*, 200(4), 273–274. https://doi.org/10.1192/bjp.bp.111.104091

Winger, R. C., Koblinski, J. E., Kanda, T., Ransohoff, R. M., & Muller, W. A. (2014). Rapid Remodeling of Tight Junctions during Paracellular Diapedesis in a Human Model of the Blood–Brain Barrier. *The Journal of Immunology*, *193*(5), 2427–2437. https://doi.org/10.4049/jimmunol.1400700

Wolburg, H., & Lippoldt, A. (2002). Tight junctions of the blood-brain barrier: development, composition and regulation. *Vascular pharmacology*, *38*(6), 323–337. https://doi.org/10.1016/s1537-1891(02)00200-8

Winkler, E. A., Nishida, Y., Sagare, A. P., Rege, S. V., Bell, R. D., Perlmutter, D., Sengillo, JD., Hillman,S., Kong, P., Nelson, AR., Sullivan, JS., Zhao, Z., Meiselman, HJ., Wendy, RB., Soto, J., Abel, ED., Makshanoff, J., Zuniga, E., De Vivo, DC., Zlokovic, B. V. (2015). GLUT1 reductions exacerbate Alzheimer's disease vasculo-neuronal dysfunction and degeneration. *Nature Neuroscience*, 18(4), 521–530. https://doi.org/10.1038/nn.3966

Xiang, S., Mao, L., Duplessis, T., Yuan, L., Dauchy, R., Dauchy, E., Blask, D. E., Frasch, T., & Hill, S. M. (2012). Oscillation of clock and clock controlled genes induced by serum shock in human breast epithelial and breast cancer cells: regulation by melatonin. *Breast cancer : basic and clinical research*, *6*, 137–150. https://doi.org/10.4137/BCBCR.S9673

Xu, B., Roos, J. L., Levy, S., Rensburg, E. J. V., Gogos, J. A., & Karayiorgou, M. (2008). Strong association of de novo copy number mutations with sporadic schizophrenia. *Nature Genetics*, *40*(7), 880–885. https://doi.org/10.1038/ng.162

Yang, S., Mei, S., Jin, H., Zhu, B., Tian, Y., Huo, J., Xu, C., Guo, A., & Zhao, Z. (2017). Identification of two immortalized cell lines, ECV304 and bEnd3, for in vitro permeability studies of blood-brain barrier. *Plos One*, *12*(10), e0187017. https://doi.org/10.1371/journal.pone.0187017

Ye, J., Coulouris, G., Zaretskaya, I., Cutcutache, I., Rozen, S., & Madden, T. L. (2012). Primer-BLAST: A tool to design target-specific primers for polymerase chain reaction. *BMC Bioinformatics*, *13*(1). https://doi.org/10.1186/1471-2105-13-134

Yu, X., Liang, X., Xie, H., Kumar, S., Ravinder, N., Potter, J., de Mollerat du Jeu, X., & Chesnut, J. D. (2016). Improved delivery of Cas9 protein/gRNA complexes using

lipofectamine CRISPRMAX. Biotechnology letters, 38(6), 919–929. https://doi.org/10.1007/s10529-016-2064-9

Zhang, S. L., Yue, Z., Arnold, D. M., Artiushin, G., & Sehgal, A. (2018). A Circadian Clock in the Blood-Brain Barrier Regulates Xenobiotic Efflux. *Cell*, *173*(1), 130–139.e10. https://doi.org/10.1016/j.cell.2018.02.017

Zhao, W., Blagev, D., Pollack, J. L., & Erle, D. J. (2011). Toward a systematic understanding of mRNA 3' untranslated regions. *Proceedings of the American Thoracic Society*, *8*(2), 163–166. https://doi.org/10.1513/pats.201007-054MS

Zisapel, N. (2018). New perspectives on the role of melatonin in human sleep, circadian rhythms and their regulation. *British Journal of Pharmacology*, 175(16), 3190–3199. https://doi.org/10.1111/bph.14116

Zlokovic, B. V. (2005). Neurovascular mechanisms of Alzheimer's neurodegeneration. *Trends in Neurosciences*, *28*(4), 202–208. https://doi.org/10.1016/j.tins.2005.02.001

Zlokovic, B. V. (2008). The Blood-Brain Barrier in Health and Chronic Neurodegenerative Disorders. *Neuron*, 57(2), 178–201. https://doi.org/10.1016/j.neuron.2008.01.003